# UNIVERSITY OF GHANA

## VARIABLE DENSITY GROUNDWATER FLOW MODELLING OF THE KETA STRIP, SOUTHEASTERN GHANA – EVALUATING THE IMPACTS OF SALINITY VARIATIONS ON THE VELOCITY FIELD

**BY**

**MEJIDA RICHARD ADAMS**

**(10300874)**

**THIS THESIS IS SUBMITTED TO THE EARTH SCIENCE DEPARTMENT, UNIVERSITY OF GHANA, LEGON IN PARTIAL FULFILMENT OF THE REQUIREMENT FOR THE AWARD OF A MASTER OF PHILOSOPHY DEGREE IN GEOLOGY**

**JULY, 2016**

## DECLARATION

I, Mejida Richard Adams, hereby declare that this is a result of an original research undertaken under supervision of Prof. Sandow Mark Yidana and Dr. Larry-Pax Chegbeleh towards the award of Master of Philosophy in Geology in the Earth Science Department, University of Ghana. And that to the best of my knowledge, it has not been presented elsewhere for another degree except where due acknowledgement has been made in the text.

…… Date……

MEJIDA RICHARD ADAMS

(Student)

…… Date……

PROF. SANDOW MARK YIDANA

(Principal Supervisor)

…… Date……

DR. LARRY PAX CHEGBELEH

(Co-Supervisor)

## ABSTRACT

The impact of density variations on hydraulic head and flow geometry on the shallow unconfined aquifer part of the Keta Strip was investigated using finite element numerical modelling techniques (FEMWATER). A calibrated transient state numerical model shows groundwater flow pattern in the area to be northwest southeast and northeast southwest with some few cases of south to north flow directions. The calibrated transient state model was used to simulate various scenarios of groundwater abstraction in the area. The results suggest that the spatial variations of groundwater velocities range between 0.93 m/day to 8.37 m/day with an average of 4.05 m/day. The spatial variations of groundwater velocities in the area appear to take the trend of variations in the nature of materials in space and density of the water. Locations of high nodal velocities appear to present low TDS contents and vice versa. The TDS concentration in the area ranges between 180 mg/l and 1800 mg/l with an average of 990 mg/l with significant spatial and temporal variability. The temporal variability in TDS suggests the impact of seasonal variations on groundwater salinity variations in the domain. This may be due to increasing salinity arising from evaporative enrichment of residual groundwater as the shallow aquifer system is prone to evaporation especially in the dry season. This is reflected in the variations in the predicted groundwater velocity field and the general groundwater flow pattern in the domain. The predicted flow field and potential distribution appear to be dictated by groundwater density variations and the nature of the material in space. Groundwater Scenario analysis conducted also suggested that, increasing the TDS concentration via surface activities in the area have no direct impact on the hydraulic head except for subtle changes along the boundaries of the study domain. An increased in TDS however reduced the velocity of groundwater in the aquifer drastically.

## DEDICATION

This work is dedicated to my supervisor and mentor; Prof. Sandow Mark Yidana and Dr. Larry-Pax Chegbeleh. To my family; Mr. Musah Abubakar Gbanzaba and especially to my siblings for their prayer; support and contribution to making this work a success. I am very grateful and may God bless you all.

## ACKNOWLEDGEMENT

My sincere gratitude goes to the Almighty God for providing me with the strength and protection throughout this research work. My profound gratitude goes to my supervisors, Prof. Sandow Mark Yidana and Dr. Larry-Pax Chegbeleh, for their immense supervision, hard work, constructive criticisms and support in making this thesis a success. God richly bless them.

I wish to also extend my appreciation to the coordinators of the Capacity Building Project Fund, Prof. Daniel Aseidu and Prof. Prosper Nude for the financial support. I want to say thank you to Dr. Francis Achaempong and Mr. Agyemang for their wonderful assistance.

To all my colleagues who have contributed in one way or the other to the success of this project, I say God mightily bless you all.

# TABLE OF CONTENT

## LIST OF FIGURES

# LIST OF TABLES

## LIST OF APPENDICES

# CHAPTER ONE

# INTRODUCTION

## 1.1 BACKGROUND AND JUSTIFICATION

In recent times, there has been an increase in demand for groundwater leading to an immense rise in exploration for aquifers. Groundwater serves as a main source of potable water supply for over 1.5 billion people worldwide (Wilhelm, 2005). It provides secure, sufficient and cost effective water supply which is often more reliable than surface water which is seasonal, prone to contamination, and needs to be piped to the points of demand. It is generally of excellent quality, requiring less or no prior treatment and can be developed incrementally and often accessed cheaply. Technologically, it is often amenable to community operation and management (Mygatt, 2006 and Hiscock, 2011). The use of groundwater for irrigation, industrialization and domestic activities has gained a lot of attention in recent years. The competition amongst these users for groundwater deliveries is a compelling issue for economic growth in nations with limited water resources. These constraining factors are predicted to become more severe as climatic changes cause more desertification, greater erosion in watersheds, and sea level elevation in coastal regions (Rouaida et al., 2007)

In Ghana, groundwater plays a key role in the water delivery systems as well as the promotion of economic growth and poverty eradication (Yidana et al., 2008). The demand for groundwater is increasing rapidly in the country. Most urban communities depend on water from river basins which are developed and distributed through a pipe system. Whereas rural communities which are at a distant from the urban centers often rely on groundwater for their water needs. Due to the overwhelming interest in

groundwater resource in the country, it is being developed at various aquifer depths for domestic water supply in rural communities nationwide. The Community Water and Sanitation Agency (CWSA) in Ghana has been mandated to explore and develop prolific groundwater aquifers to meet the increasing water need of rural folks. In addition to that, various governments have made efforts to address the millennium development goals by choosing to use groundwater as a pivot for agricultural development to reduce poverty in rural communities (Yidana et al., 2012). These efforts are however being hampered by the several issues facing groundwater development in the country. The factors include but not limited to; inadequate knowledge on aquifer geometry nationwide, lack of information regarding aquifer yields and scarcity of information to resolve problems related to groundwater quality in most parts of the country.

Another emerging issue threating the development of groundwater in Ghana is saline water intrusion in coastal areas. One such coastal area in the country is the Keta strip where there has been reported incidence of salinity intrusion into the shallow unconfined aquifer in the area. The influx of saline water creates density variations which in turn influences the flow geometry of the aquifer. This challenge requires proper understanding in terms of exploration and development of the resources in order for it to be sustained. A lack of proper understanding of the groundwater system is a major problem to the effective management of the resources, especially in coastal areas in the country. However, solutions to the effective management of groundwater resource in coastal areas have been achieved through the use of numerical modeling techniques worldwide (Zhou and Wenpeng, 2011).

Even though the importance of groundwater models cannot be underestimated, they are not widely used in Ghana particularly in terms of decision making due to insufficient data and expertise required for modeling (Yidana et al., 2010). Groundwater modeling is necessary because it provides comprehensive and thorough knowledge about groundwater recharge zones which can be useful in protecting the aquifers system. This study is undertaken to investigate the impact of density variations on the simulation of groundwater flow and the prediction of optimal safe yield in the shallow unconfined aquifer part of the Keta strip. The study is designed to determine whether or not the incorporation of salinity variations in the modelling of the groundwater in the basin makes any significant differences in the predictions, especially since the aquifer is amenable to the impact of seawater intrusion.

The domain had earlier been modeled using a constant water density numerical code, MODFLOW-2000 (Harbaugh et al., 2000). The results of this current investigation will be compared with earlier finding to determine the appropriateness of using a finite difference model which assumes constant water density over an entire domain, to simulate groundwater conditions in a coastal aquifer system. This study will also suggest an approximate interface between the saline and fresh water. Thus, in addition to highlighting variations in hydraulic potential, a density dependent flow model will also suggest areas of significantly high salinities which may render the water unsuitable for use.

The area forms a coastal setting and offers a serene environment where most people prefer to settle for both pleasure and economic activities. This has led to rapid growth in population in the coastal region creating additional demand of crop productivity and infrastructural development per unit of groundwater available. Mechanization of groundwater for irrigation schemes coupled with erratic rainfall patterns in the wake of

climate change/variability has also led to increased abstraction of the groundwater in the Keta Strip. About 35% of the populations in the area are into crop production all year round and these activities are dependent mostly on abstraction of water from the shallow unconfined aquifer (GSS, 2013). The increased abstractions of freshwater from aquifers and the application of chemicals to crops during farming contribute to variations in density of the groundwater resources in the area.

## 1.2 RESEARCH OBJECTIVES

The main objective of the study is to investigate the impact of density variations on the simulation of groundwater flow and the prediction of optimal safe yield in the shallow unconfined aquifer of the Keta strip through model calibration. The specific objectives include to;

- Investigate the impact of density variations on the hydraulic head
- Examine the effect of density variations on groundwater flow geometry in the study area
- Delineate the approximate interface between the saline water and freshwater
- Highlight high groundwater salinity zones in addition to potential areas through model calibration
- Assess groundwater abstraction scenarios

## 1.3 STUDY AREA

### 1.3.1 Location and Accessibility

The study area forms part of the Keta municipality, with Keta as the administrative and political capital. It was carved out of the former Anlo District, which also comprised Akatsi and Ketu Districts and is one of the twenty-five (25) municipalities and districts in the Volta Region of Ghana. It shares boundaries with Akatsi South District to the north, Ketu South District to the east, South Tongu District to the west and the Gulf of Guinea to the south. Whutti-Anloga is the precise location where this study was conducted, and is along the Strip of Keta at the southeastern part of Ghana. It falls roughly between latitudes $5^0$46'N and $5^0$50'N and longitudes $0^0$49'E and $0^0$57'E. According to 2010 population and housing census, the population of the municipality stood at 147,618 with 68,556 males and 79,062 females. Transportation in the area is a combination of roads and water. The roads network has over 74.8 km of first class, 30.05 km second class and 46.50 km of third class road. Water transportation though essential is poorly developed. None motorized local canoes are used mostly to transport goods and people across the lagoons (Banoeng-Yakubo et al., 2005).

### 1.3.2 Climate and Vegetation

The study area, which forms part of the Keta strip falls within the arid climatic zone of the country (Dickson and Benneh, 1995; Yidana and Chegbeleh, 2013). There are two seasons which are defined in the study area: the raining and dry seasons. The raining season occur in two folds: the major raining season starts from April to July, whilst the minor starts from September to October each year. The study area usually experience heavy down pour around June. Relative humidity which ranges from 60% to 75% in

the study area is normally high in the mornings and at night but lowest at mid-days. The area experience an average monthly temperature of about 30 $^0$C in the hottest month (March) and about 26$^0$ C in August which is the coldest month (Dickson and Benneh, 1995). The recorded relative humidity in the study area is as high as 'nighty-six' percent in the morning and as low as 'sixty-three' percent in the afternoon (Yidana and Chegbeleh, 2013). From data collected in the area for the period between 1913 and 1992, the mean yearly rainfall is about 800.8 mm. The highest monthly mean value of 187.5 mm occurs in June whilst the mean minimum value of 10.6 mm occurs in January (Yidana and Chegbeleh, 2013).

Annual evapotranspiration of water is about 1785 mm. This value compared to the yearly rainfall value in the area is quite high. In the entire year, only the rainfall in June surpasses the potential evapotranspiration in the area (Yidana and Chegbeleh, 2013).The movement and location of the Inter Tropical Continental Zone within the sub region control the climate of the area (Dickson and Benneh, 1995). The Inter Tropical Continental Zone occurs between two overriding air masses namely the Southwest Monsoon winds and the Northeast Trade winds in the sub region. The Northeast Trade winds also known as the harmattan which starts from November to February each year, gives rise to the long dry season in the area.

### 1.3.3 Topography and Drainage

The Keta Municipality is a low-lying coastal plain with the highest point of elevation being only 53 meters above sea level around Abor in the north and the lowest point is approximately 1-3.5 m below sea level along the coast. Three main geographic belts are identified within the municipality; the Narrow Coastal Strip, the Lagoon Basin of

the middle belt and the Plains of the North. The study area is part of the Coastal Strip which is marked by sand bars with a few sea cliffs bordering the coast. Although the coastal strip is severely affected by sea erosion, there was no erosion channels observed within the catchment of this research. In terms of drainage system in the study area, the Keta lagoon is the only visible drainage located north to west of the area (Banoeng-Yakubo et al., 2005).

### 1.3.4 Soil

There are three different kinds of soils identified in the area based on major geographic units. The Oyibi-Muni and Keta associates occurring along the coastal strip and composed mostly of sandy soils which is often devoid of a top layer. This type of soil in its natural state support only coconut cultivation. However, when manured, it can support cultivation of vegetables such as okro, pepper, carrot, tomatoes and shallot. Although the soil along the coastal strip covers only about elven percent of the municipality (excluding lagoon), it serves as the leading shallot producing area in Ghana. The Ada-Oyibi associations of soil occur at the lagoon basin. It consists of a very shallow, hard and compact clay formation which is alkaline and supports mostly mangrove vegetation, sugarcane and grass for pasture. Due to the underlying clay, this area is liable to flood and not suitable for arable farming (Banoeng-Yakubo et al., 2005).

### 1.3.5 Geology

The geology of the study area (Keta basin) is fault-controlled Mesozoic/Tertiary sedimentary basin along the shore of the Gulf of Guinea (Akpati, 1978; Yidana and Chegbeleh, 2013). The basement complex comprises of early Precambrian Dahomeyan gneisses, migmatites, and schists. The Pan-African orogeny affected the rocks which

outcrop along the borders of the basin to the north (Yidana and Chegbeleh, 2013). The basal sedimentary sequence in the basin consist of lower to Middle Devonian marine shale, siltstones, and sandstone, which are overlain by sills and dolerites (Yidana and Chegbeleh, 2013). A sequence of Cretaceous–Eocene marine sediments consisting of shales, limestones, and sandstone outcrops along the eastern margins of the basin close to the Ghana-Togo border (Jorgensen and Banoeng-Yakubo, 2001; Yidana and Chegbeleh, 2013). Lithologies such the limestones and sandstones in the area are highly consolidated and coagulate near the shore in the southwest of the basin. Overlying unconformably on the limestones and sandstones at the northeastern section of the basin are scattered deposits of Neogene continental sediments. These materials are composed of unconsolidated to semi-consolidated limonitic argillaceous sands with gravelly beds at the base. The center of the basin is dominated by Quaternary unconsolidated coastal sediments, marine sands, and gravels, which are 30 m thick on the average, around Keta, though they thicken toward the Volta River estuary (Yidana and Chegbeleh, 2013).

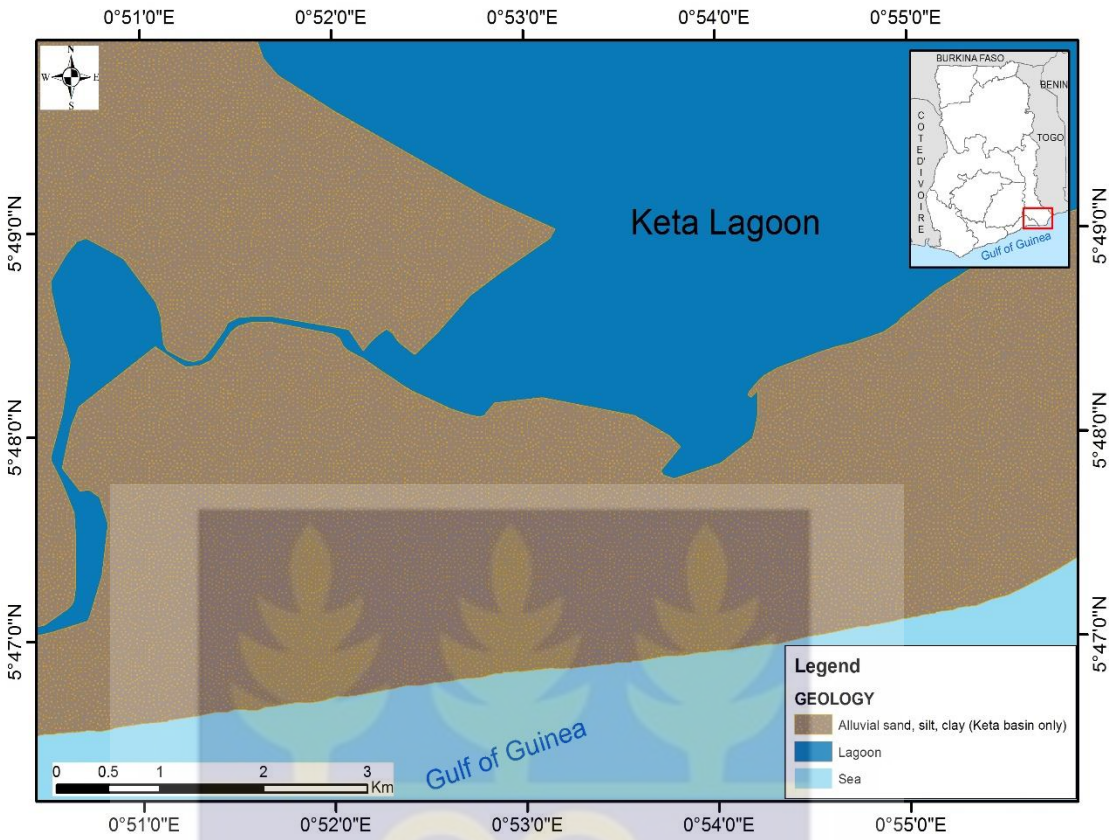


Figure 1.1 Geological map of the study area

### 1.3.6 Hydrogeology

The Keta basin according to Nerquaye-Tetteh (1993) has four main aquifer units which he identified based on the geography and geological setting of the area. These aquifer units include; the Weathered Dahomeyan gneiss, the shallow unconsolidated to semi consolidated limonitic argillaceous sand, the coastal marine sand and gravel and the limestones and sandstone aquifer units. The weathered Dahomeyan gneiss aquifer unit can be found at the northeastern parts of the basin whilst the shallow unconsolidated to semi consolidated limonitic argillaceous sand aquifer is found around the northeastern and central portions of the basin. The third unit is the coastal marine sands and gravels in the Keta Lagoon area and estuary of the Volta River. The unconsolidated sands and gravels are usually characterized with high groundwater recharge. The marine

limestones and sandstone aquifer units serve as sources of drinking water in the central and southeastern portions of the strip; this aquifer forms the main and most important deeper aquifer in the Keta basin (Yidana and Chegbeleh, 2013). The shallow unconfined aquifer serves as the most important of all the aquifers in the area relatively due to its easy access. With a drilling depth of about one meter, this aquifer is encountered and has a prolific yield. It also forms the basis of this research work.

### 1.3.7 Socio Economic Activities in the Study Area

Farming and fishing are the main occupation of residents in the study area. The farmers produce different variety of crops and food items including; fresh vegetables (shallot, cabbage, tomatoes, peppers, carrot, lettuce, onions etc.). They also cultivate food items such as cassava both for food and for commercial purposes. Due to the relatively easy access to the shallow unconfined aquifer in the area, farming activities continuous all year around and depended mostly on irrigation. It is a common phenomenon to see residence busily engaging in their irrigation activities upon a visit to the area.

The irrigation activity in the area has provided a lot of job opportunity for the youth in the area and it is becoming the main stay of livelihood for residence along the strip since fishing is no longer yielding the much-desired results. The aquifer therefore is worth protecting in order to enhance the living standard of the people in the area. Some residences are also into mining of salt in the area. The area stretches between the sea and the Keta lagoon providing residences the opportunity to mine salt during the dry season.

# CHAPTER TWO

# LITERETURE REVIEW

## 2.1 GROUNDWATER RESOURCE DEVELOPMENT AND SALINITY INTRUSION

Density variations influence the flow rate of groundwater and thereby reducing the availability and supply of fresh groundwater in coastal areas. The density of groundwater is a function of its concentration and is defined as the mass per unit volume of groundwater (Fetter, 2001 and Naderi et al., 2013). Maintaining same volume of groundwater while increasing the mass increases the density hence density and mass are directly related. The mass of groundwater is influenced by the amount of total dissolved solids (TDS) in the water which can easily be measured on the field using a conductivity meter. The total dissolved solids (TDS) vary marginally in space from one aquifer to another or even within same aquifer in any hydrogeological setup.

These variations are more severe in coastal aquifers where freshwater is in direct contact with saline water. Differences in TDS cause variations in density of groundwater which in return affects the mass flow rate due to the direct relationship between the mass and density of the water. In coastal regions, the trend is more prevalent in that almost all life activities in such area hinge on the groundwater resource from costal aquifers leading to over pumping of the groundwater resource. One notable cause of density variation in littoral areas is intrusion of saline water into the freshwater aquifer (Essink, 2001 and Bithin et al., 2009).

Saline water intrusions lead to contamination of fresh water resources increasing salinities beyond tolerable limits (Meier et al., 2007 and Bear, 2010). Adequate knowledge about the spatial distribution of fresh and saline groundwater and the processes that determine their evolution would help in proper management of the available groundwater reserves in coastal areas (Glynn and Plummer 2005). Understanding the spatial variations in chemical composition of groundwater resulting from diverse sources is extremely difficult, especially if concentrations have differed over time or if boundary conditions have changed (Hussein, 2004). Descriptions of the processes and factors that control saline water evolution over time is an academic challenge, but of important practical use for water resource evaluation and seawater intrusion studies (Post 2004).

According to Hutchings and David (2003), the freshwater- seawater interface is affected by groundwater extraction by public supply, irrigation activities, industrial activities and domestic wells in coastal communities. The position of the interface is controlled by several factors including precipitation, recharge, evapotranspiration, hydraulic conductivity, hydraulic head, etc. Landward migration of the interface often results in a significant decrease in the water resources available to coastal communities (Basack, 2012). Modeling density variable flow in coastal area enables the evaluation of the potential for seawater intrusion into surficial and confined aquifers as a result of artificial extraction of groundwater. When carefully done, the process leads to the definition of the interface between fresh water and saline water (Sherif et al., 2006).

The intrusion of seawater in coastal aquifer has long been widely attracting an attention among researchers for the management of coastal water resource and environment protection (Bear et al., 1999; Giada et al., 2013). It is worthwhile to note that human water use patterns are the most important factors causing seawater intrusion. Seawater intrusion is practically density dependent problem. Owing to the density difference, the seawater intrusion into freshwater aquifer would usually happen in both vertical and lateral direction if groundwater were excessively pumped in the sensitive portions of the freshwater aquifer (Barlow et al., 2006). This problem, therefore, has become an important factor that affects decisions related to exploitation strategies of freshwater resources (Ying et al., 2001).

In general, two kinds of approaches have usually been used to analyze density dependent flows (seawater intrusion) in coastal aquifers: the dispersed interface and the sharp interface (Gaalou et al., 2012). In the dispersed interface research, one of the principal complexities in modeling is how to simulate accurately the movement of the transition zone between fresh/saltwater (density variations) generated by hydrodynamic dispersion. Numerous researchers have made quantitative analyses system in an attempt to describe mathematically the physical system and its important mechanisms (Bear et al., 2010; Desechaine, 2013).

Over the past 100 years, two different groups of investigators who worked independently along the European shore established that seawater occurred underground below sea level at a depth of about 40 times the height of the fresh water above sea level. This was attributed to a hydrostatic equilibrium existing between the two fluids of different densities. An equation derived to explain this phenomenon is generally referred to as the Ghyben-Herzberg relation, after its originators (Vacher,1988; Weingchanda, 2010).

The hydrostatic balance between fresh and saline water can be illustrated by the U-tube (Todd and Mays, 2005) shown in Figure 2.1. Pressures on each side of the tube must be equal; therefore,

$$\boldsymbol{\rho_s g z_s = \rho_f g (z + h_f)} \qquad \textbf{2.1}$$

Where $\rho_s$ is the density of the saline water, $\rho_f$ is the density of the fresh water, g is the acceleration of gravity, and z and $h_f$ are as shown in Figure 2.1. Solving for z yields;

$$\boldsymbol{Z = \frac{\rho_f}{\rho_{s-\rho_f}} h_f} \qquad \textbf{2.2}$$

Which is the Ghyben-Herzberg relation for typical seawater conditions, let $\rho_s$ = 1.025 g/cm and $\rho_f$= 1.000 g/cm so that

$$\boldsymbol{z = 40hf} \qquad \textbf{2.3}$$

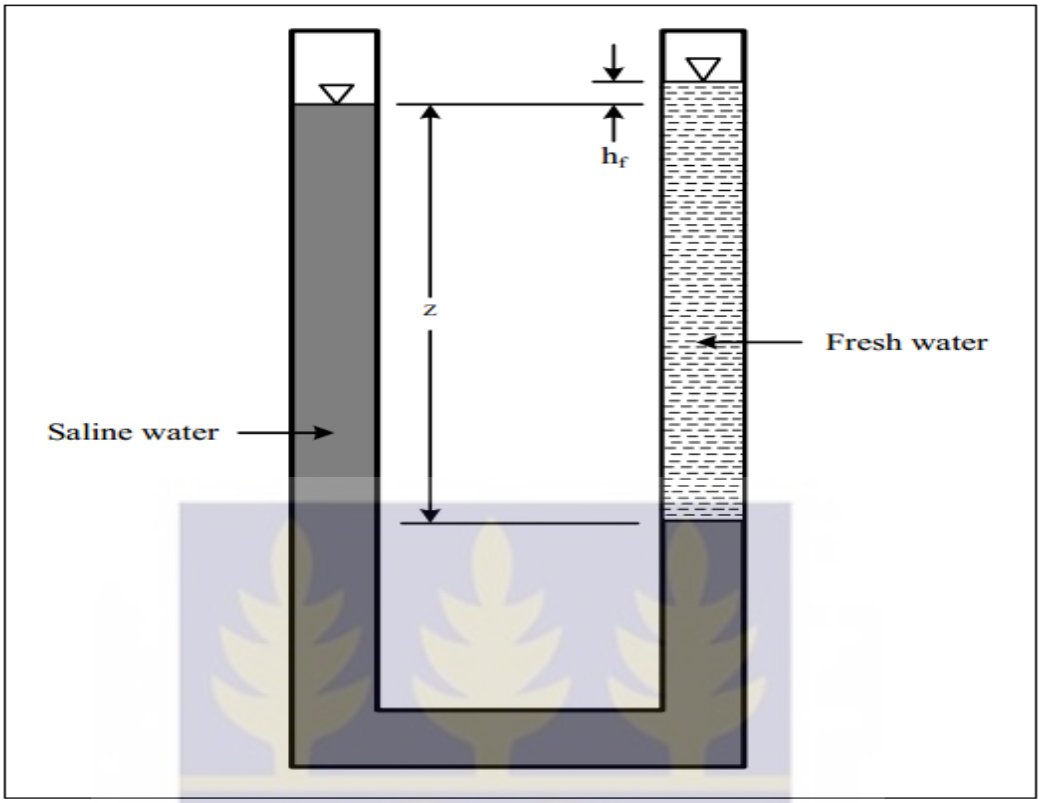


Figure 2.1 Hydrostatic balances between fresh water and saline water illustrated by a U- tube. (After Todd and Mays, 2005)

Translating the U-tube to a littoral situation, as shown in Figure 2.2, $h_f$ becomes the elevation of the water table above sea level and z is the depth to the fresh-saline interface below sea level. This situation is a hydrodynamic rather than a hydrostatic balance because fresh water is moving toward the ocean. Considering density alone, deprived of flow, a horizontal interface would develop with fresh water everywhere floating above saline water. Ghyben-Herzberg relation produces satisfactory results where the flow is nearly horizontal (Mondal et al., 2011). But near the coastline, where vertical flow components become distinct (see Fig 2.2) considerable errors do occur in the location of the interface (Todd and Mays, 2005).

The theories as outlined by Todd and Mays do not reflect reality to some extent. Their analyses of both the hydrostatic and the steady-state suggested that the interface separating fresh water and seawater in a coastal aquifer is a sharp boundary. However, in reality they tend to be a mixing of seawater and fresh water in a zone of diffusion around the interface. The process of mixing leads to increases in the amount of TDS in the freshwater aquifer (Gounaric et al., 1999). The extent of the zone is controlled by the dispersive features of the geologic strata. The method give satisfactory predictions of the fresh water flow patterns where the zone is narrow but an extensive zone of diffusion can change the flow pattern and the position of the interface, and must be taken into account. Henry (1960) was the first to present a mathematical solution for the steady state case that includes consideration of dispersion. Cooper et al. (1964) provided a summary of the various analytical solutions. Density dependent flow can be induced in both unconfined and confined aquifers.

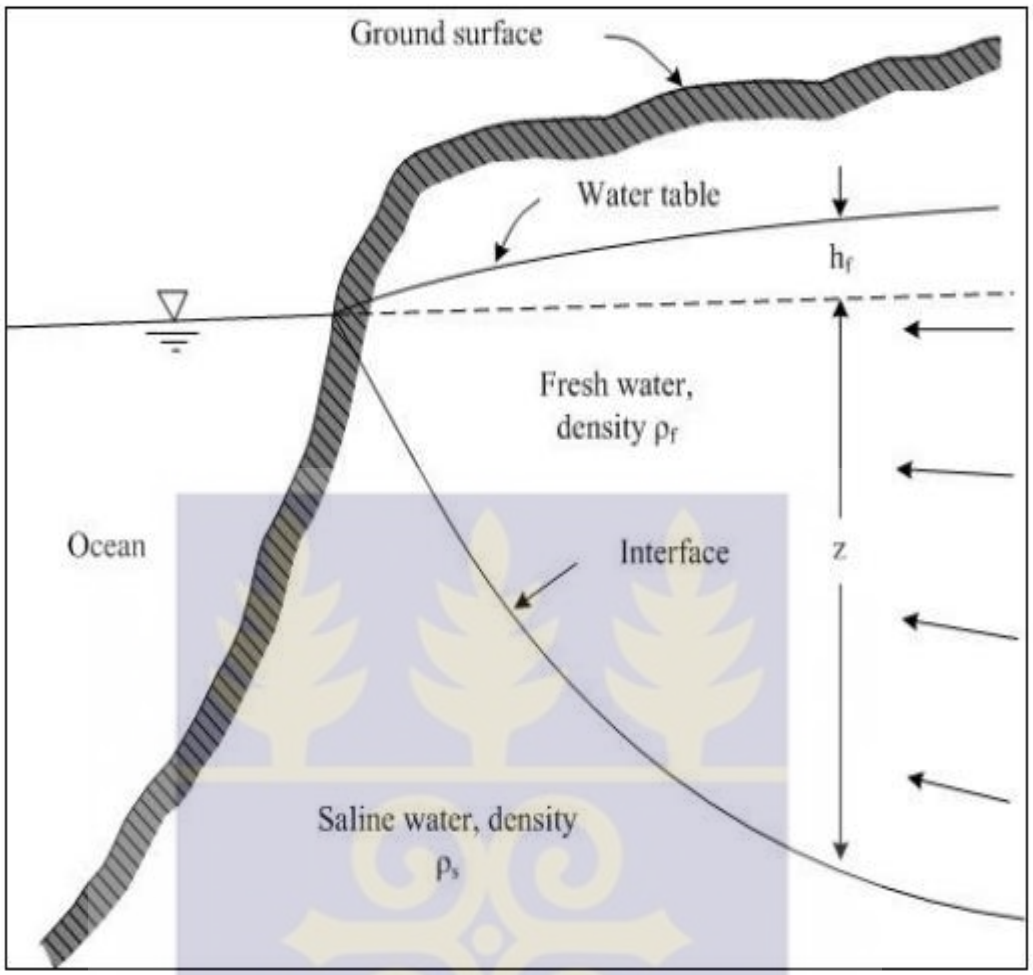


Figure 2.2 Idealized sketch of the occurrence of fresh and saline groundwater in an unconfined coastal aquifer resulting from density difference (Todd and Mays, 2005).

Figure 2.3 provides a schematic representation of the seawater wedge that would exist in a confined aquifer under conditions of natural steady state outflow. Beginning of pumping (Fig. 2.4) sets up a transient flow pattern that leads to declines in the potentiometric surface on the confined aquifer and inland movement of the seawater interface. Pinder and Cooper (1970) presented a numerical mathematical method for the calculation of the transient position of the seawater front in a confined aquifer. Their solution includes consideration of dispersion.

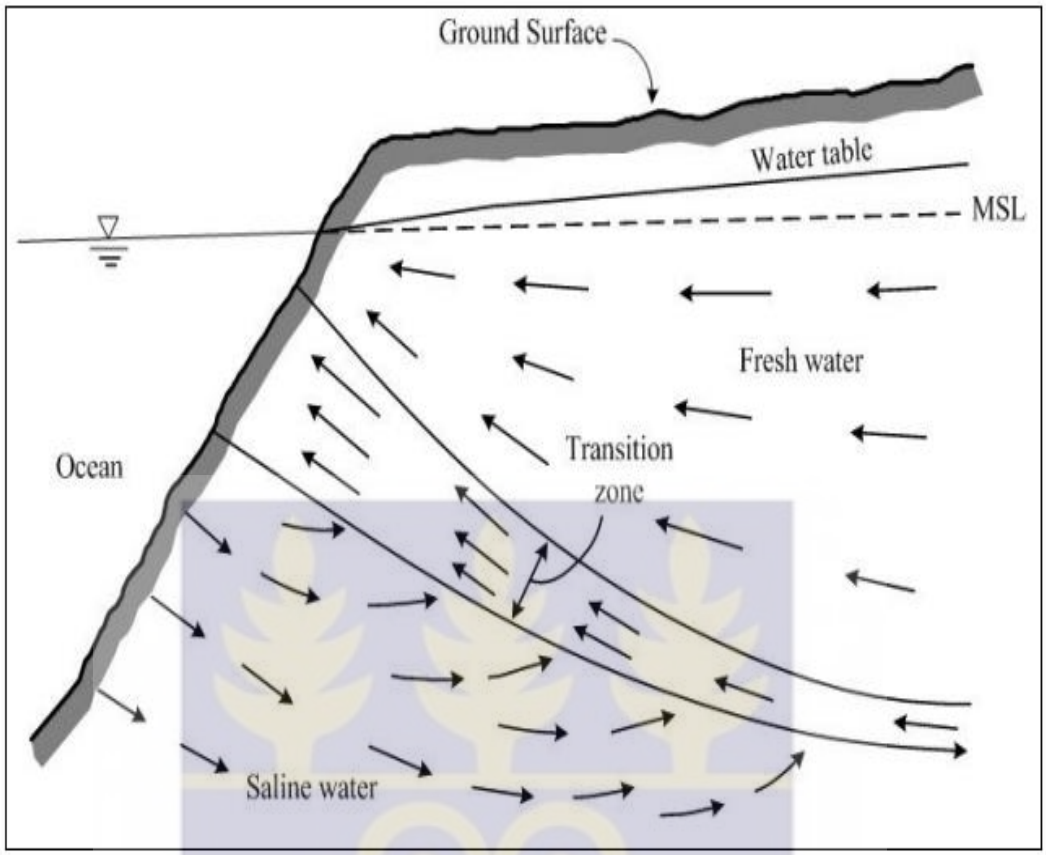


Figure 2.3 Vertical cross section showing flow patterns of fresh and saline water in an unconfined coastal aquifer (Todd and Mays, 2005).

The Biscayne aquifer located at southeastern Florida in North America is one of the most intensively studied coastal aquifers (Kohout, 1960). The aquifer is unconfined consisting of lithologies such as limestone and calcareous sandstone which extend to an average depth of 30 m below sea level. Field data indicate that the seawater front undergoes transient changes in position under the influence of seasonal recharge patterns and the resulting water-table fluctuations. Lee and Cheng (1974) and Segol and Pinder (1976) have simulated transient conditions in the Biscayne aquifer with finite-element numerical models. Both the field evidence and the numerical modeling confirm the necessity of considering dispersion in the steady-state and transient analyses (Freeze and Cherry, 1979).

One important consequence of the transition zone and its seaward movement is the transport of saline water to the sea. The water comes from the underlying saline water; hence, from continuity considerations, there must exits a small landward flow in the saline water region. Figure 2.2 illustrates the flow patterns in the three subsurface zones. Experimental studies and field measurement at Miami have confirmed the landward movement of the seawater body. Where tidal action is the predominant mixing mechanism, fluctuations of groundwater and hence the thickness of the transition zone become greatest near the shoreline.

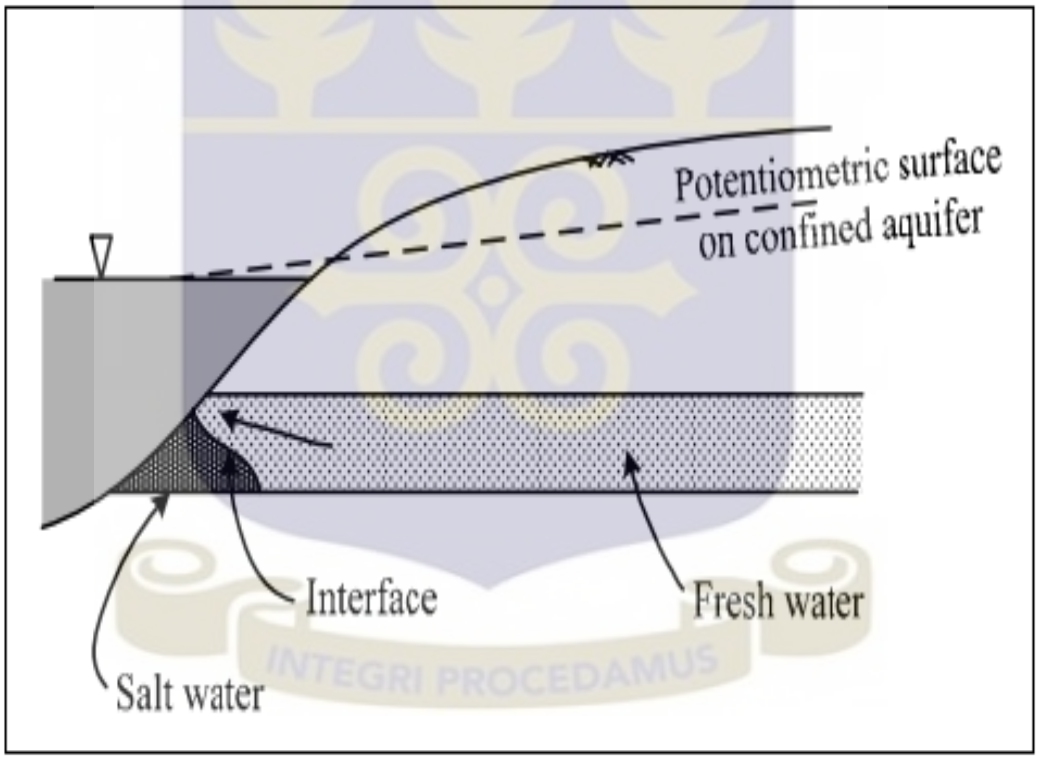


Figure 2.4 Saltwater-freshwater interfaces in a confined coastal aquifer under conditions of steady-state seaward flow (After Freeze and Cherry, 1979).

According to Javadi et al., (2011) seawater intrusion results from the density disparity between fresh groundwater and saline water and is one of the major problems in coastal aquifers. The problem is more serious in dry areas where the groundwater abstractions rates surpass the natural recharge from precipitation events. Saline water intrusion is influenced by a number of factors including, the type of aquifer, geological setting of the system, geometry of the aquifer hydrogeological factors, recharges rates and abstraction. Groundwater normally flows towards the sea under natural conditions and without any human interference activities. This trend however is reversed, when groundwater is pumped excessively from the aquifers causing saline water to flow towards the freshwater aquifer.

Saline water intrusion into coastal aquifers is considered a special kind of contamination that threatens the freshwater resources, because mixing a very little volume (2-3 percent) of seawater with fresh groundwater makes it unpleasant for human consumption and could lead to desertion of the freshwater aquifers (Thomas et al., 1994). The peril of seawater invasion obviously restricts the degrees at which coastline aquifers are developed for water supply. The strategy to managing this challenge is to ensure a good balance between the amount of water recharging the aquifer and water being pumped from the aquifer. Continuous monitoring of the saline water freshwater boundary through groundwater modelling is essential in defining adequate control measures (Javadi et al., 2011; Ralph et al., 2012).

## 2.2 APPLICATIONS OF NUMERICAL TECHNIQUES IN HYDROGEOLOGICAL INVESTIGATIONS

Modelling the density variations in littoral aquifers enables the valuation of the possibility of saline water incursion and allows for the proper management of groundwater withdrawals and recharge rates for the aquifer. The numerical modelling of saline water intrusion epitomizes a complex challenge as the invasion may vary from one aquifer to another (Sherif et al., 1988).

Several of numerical models have been deployed to evaluate density driven flow based on sharp interface or diffusive (dispersive) interface assumptions. The application of the sharp interface is required when the width of the transition zone is comparably smaller to that of the thickness of the aquifer. The dispersive interface model that accounts for the effects of hydrodynamic dispersion may be more practical because it provides more details concerning the transition zone (Chan-Hee; 2004).

Diersch, (2002) used application of numerical modeling to jointly assess seawater intrusion and the remediation strategy for a coastal aquifer. A 3D density-dependent flow and transport model was implemented using the finite element code FEFLOW. Based on the model results, a coupled pumping injection barrier was the best remediation strategy. This solution allows the effective containment of the groundwater contamination and controls the intrusion of saline water. Diersch (2002) concluded that, installing a vertical barrier would actually increase seawater intrusion at the site. The consequence would be a worsening of groundwater quality in the shallow aquifer in the area between the site and the coast line.

Elhassadi (2007) stated that the city of Derna, in Libya which is located on the Green Mountain Coastal area is bedeviled with a severe water shortage problem due to

exposure of the water resource to sea water intrusion. This frightening phenomenon is being persistent with several cities in the coast. The paper considers the evaluation of this problem and suggests proper means to resolving it, including desalination.

Demirel (2003) describes the Mersin–Kazanli province as a heavily industrialized region. The industrial unit and municipalities satisfy their water demand by pumping from groundwater resource available. The excessive groundwater demand has setup density variations in the aquifer. He monitored chloride concentration of the water in the aquifer by periodically sampling from some wells for analyses. The results of these analyses and electrical conductivity measurements were used to show the history and development of saltwater intrusion up to the year 2000. The chloride concentration of the water within the alluvial aquifer increased to over 3000 mg/l in 1999 and the wells were closed completely.

Narayan et al. (2007) studied the Burdekin Delta which is a major irrigation area situated in the dry tropics of North Queensland, using variable density flow and solute transport model, SUTRA, to define the current and potential extent of density variations in the Burdekin Delta under various pumping and recharge conditions. A two-dimensional vertical cross-section model, which accounts for groundwater abstraction and recharge, was developed for the area. The Burdekin Delta aquifer comprises primarily of sand and clay lenses with granitic bedrock. The model domain uses vertical cross-sections along the path of groundwater flow. The initial conditions used in the conceptualization of model are based on land use prior to agricultural development when the seawater wedge was in its assumed natural state. The findings of this study show the effects of variations in groundwater abstraction and net recharge rates on the subtleties of seawater intrusion.

Simulations have been carried out for a range of recharge, abstraction rates and hydraulic conductivity values. Modeling results show that seawater intrusion is far more sensitive to abstraction rates and recharge than to aquifer properties such as hydraulic conductivity. The analysis also reveals that the effect of tidal oscillations on groundwater levels is restricted to areas very close to the coast. Tidal influences on saltwater intrusion therefore can be neglected when compared with the effects due to groundwater abstraction. The impacts of various management options on groundwater quality were also discussed.

According to Kouzana et al. (2007), intensive irrigation activities frequently increase the menace of groundwater quality degradation through high groundwater abstraction rates. The uninhibited groundwater abstraction causes an alteration of natural flow systems and induces saline water intrusion from the ocean and causes groundwater quality deterioration. The main aim of the study was to characterize the hydrochemistry of the coastal aquifer, identifying the key processes that occur in the system, and to define the degree of oceanic intrusion in the aquifer. In order to attain this aim, geophysical and chemical parameters measurement such as vertical electrical soundings (VES), electrical conductivity, pH, temperature, anions and cations concentrations were taken. The results obtained after the analysis of the hydrochemistry in the study area were interpreted using ion correlations with chloride and $SO4^{2-}/Cl$ and $Mg^{2+}/Ca^{2+}$ ratios, in conjunction with calculations of the ionic deviations and the saturation indexes. Saturation indexes are calculated with the PHREEQC 2.8 software used for mineral saturation modeling of the aquifer seawater-freshwater mixture. The high groundwater salinity anomaly observed in some sections in the area was explained by the presence of seawater intrusion in these areas.

Milnes and Renard (2003) carried out a study in coastal aquifers which are been exploited for irrigation purposes. The principal objective of their research was to examine and quantify the impact of solute recycling from agriculture relative to seawater intrusion. Salinization by salt recycling from irrigation is superimposed on the effects of seawater intrusion. Water quality degradation of irrigation pumping wells caused by seawater intrusion further augments salinization by irrigation, as the extracted solute mass is recycled and is not withdrawn from the system.

Lookjan et al. (2009) conducted a study on the concentration of chloride of groundwater from the major aquifer Hat Yai and found that the chloride concentrations were higher than standard and acceptable values. They developed a 3D density-dependent salinity intrusion model for the Hat Yai aquifer in order to evaluate saline water intrusion from the Songkhla Lake and the Gulf of Thailand and to predict the effect of various scenarios for future increase of groundwater abstraction in the next 20 years. Density-dependent groundwater flow and mass transport modeling code SEAWAT-2000 was used for the study. The developed model was calibrated using hydraulic heads and chloride concentrations from 47 observation wells. The results from the calibrated model indicated that for the Hat Yai basin which have annual groundwater abstraction rate of about 25 million cubic meter per year, when the pumping rate was increased 5% annually for the next 20 years, average groundwater declined by 2 meters. For Hat Yai city, groundwater drawdown was about 3.5-10 m. In additions, seawater intrusion area was widely spread toward Hat Yai basin.

For the past two decades, seawater intrusion has become one of the most prevalent forms of groundwater contaminations causing stern environmental problems globally. The problem is particularly serious in littoral areas, where rigorous commercial activity

has amplified the necessity for freshwater provisions. The need is mostly gratified by abstracting groundwater from littoral aquifer systems. Many problems such as well field salinization, crop damage, and surface water quality deterioration are often associated with pollution of fresh water resources by saltwater in littoral areas (Gorgij et al. 2012). The precise management of available groundwater reserves is difficult without understanding of the spatial distribution of freshwater and saline groundwater and the processes that govern their evolution (Rouaida et al., 2007). It is often difficult to understand the spatial variations of groundwater that is coming from various kinds of input, especially if concentrations have differed over time or if boundary conditions have changed. The determination of the procedures and dynamics that regulate seawater evolution over time is an academic challenge, but of important practical use for water resource evaluation and saline water intrusion studies (Rouaida et al., 2007).

Solutions to the complex groundwater density dependent flow problems in coastal regions have been achieved with the help of groundwater numerical models (Zhou and Wenpeng, 2011). In conventional hydrogeological practice and groundwater resource assessment, numerical groundwater models have been deployed and have been found to yield satisfactory results throughout the world. The models are relevant in performing complex analyses and making informed predictions. Several numerical models are available to solve the groundwater equation upon definition of boundary and initial conditions (Anderson and Woessner, 2002). The two most commonly used ones include finite difference and finite element methods. Many researchers such as Rushton and Redshaw (1979), Guiguer and Franz (1996), GHP (2001), McDonald and Harbaugh (2003), Bakker et al., (2004), Huysmans et al., (2006) and Post et al., (2007) have used different numerical techniques to solve complex hydrogeological problems. Although

there are some errors and uncertainties in any modeling study with respect to hydrogeological understanding, the conceptual model design, calibration and predictions simulations as well as evapotranspiration estimation, numerical modelling is one of the best approaches to simulate and predict aquifer conditions. According to Anderson and Woessner (2002), groundwater models represent the best available tools for hydrogeologist to meet the challenge of predicting aquifer conditions. Groundwater models have limitations in that they are based on the simplified assumptions of the physical system and not the exact replica of the physical hydrogeology of the basin. Like all other numerical models, groundwater models cannot predict the future with outright certainty.

Several research works has been conducted in the Keta Strip particularly on the shallow unconfined aquifer. Kortatsi et al., (2005) investigated the impact of large scale abstraction of groundwater on the shallow unconfined aquifer using techniques such as geophysics and hydrogeological data from the strip to analyzed groundwater quality. Their assessment shows that the quality of the water in the area is only good enough for salt tolerant crops such as shallot and onions which are currently being cultivated in the area. They concluded that the large-scale abstractions of water from the aquifer will result in drastic decline of water level of about one meter per year and subsequently cause up coning of the fresh/saline water wedge in the area.

Yidana and Chegbeleh, (2013) used a calibrated steady-state finite difference numerical code MODFLOW-2000 (Harbaugh et al., 2000), to characterize the spatial distribution hydraulic conductivity field in the area. Their study suggested that hydraulic conductivity ranges between 2.0 m/d to 20 m/d with an average of 15 m/d. They also indicated that the hydraulic conductivity in the area is controlled by the percentage of finer materials as well as the degree of sorting of sedimentary materials in the area. The

conductivity map was the first of its kind to be produce in the area and is therefore vital for the characterization of other hydrogeological parameters of the aquifer system in the area. The finite difference codes however consider the density of the groundwater in the aquifer to be constant and does not accounts for the effects of density variations and their implications but this is often not the case especially in coastal areas. It is in view of this that has necessitated this research work targeted at the same aquifer to investigate the influence of density variations on flow geometry in the area.

# CHAPTER THREE

# MATERILS AND METHODS

The methodology used in this research in order to achieve the objectives includes; desk study, acquisition of logistics, fieldwork and post field activities.

## 3.1 DESK STUDY

Desk study was conducted to obtain more information about the study area. The desk study entailed review of earlier publications (literature) on the geology, hydrogeology and topography of the study area. The review also centered on various publications which employed numerical techniques (finite difference and finite elements) and procedures to simulate impact of density variations on groundwater movement. Information such as groundwater flow rate and aquifer thickness of the shallow unconfined aquifer in the area was also acquired during the desk study and field visit.

## 3.2 ACQUSITION OF LOGISTICS

The materials used for the study were acquired before the main fieldwork. These materials include; base maps of the study area, ice chest for storing water samples, groundwater sampling bottles, Garmin Vista GPS and pH conductivity meter. The GPS was used to record locations where water samples were taking whilst the pH conductivity meter was helpful in taken measurement of total dissolve solids (TDS), as well as temperature, pH and electrical conductivity. The ground elevations of the wells were recorded using the GPS.

### 3.3 FIELDWORK

One week fieldwork was carried out in the study area. During this period, groundwater samples were taken from wells completed in the shallow unconfined aquifer in the area. The sampling was done following standard groundwater sampling techniques on the field. Groundwater samples taken were stored in an ice chest containing ice block. This was necessary to preserve the chemical parameters in the samples during transportation back to the laboratory.

As part of the fieldwork, groundwater physical parameters such as total dissolve solids (TDS), electrical conductivity (EC), pH and temperature of the groundwater were also measured using pH conductivity meter. A total of 50 wells were sample on the field and taken to the Ecological Laboratory at the Geography Department of University of Ghana for analysis.

After the main field exercise, several follow up field visits were undertaken back to the study area to monitor changes in the groundwater physical parameters in an interval of two weeks. The follow ups visits were necessary to gather more data to update the numerical model being setup.

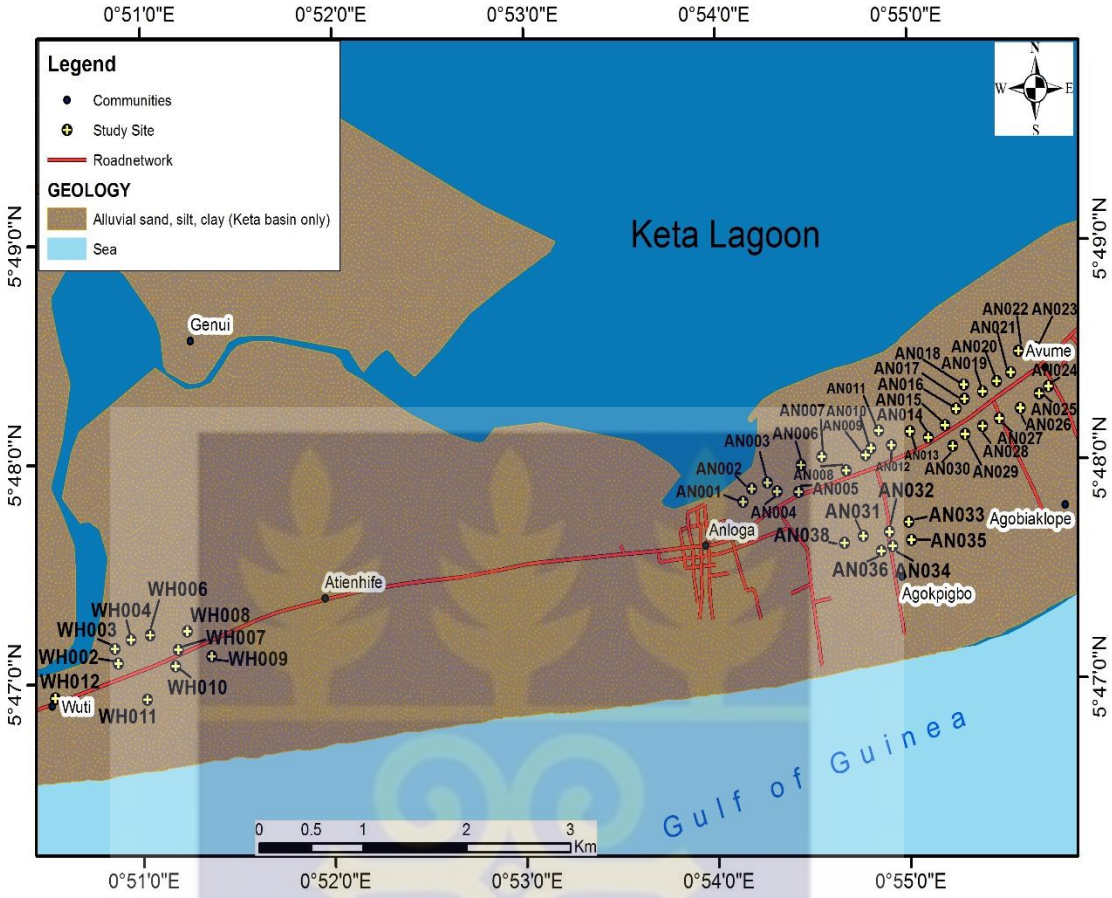


Figure 3.1: Distribution map showing sample locations in the study area.

### 3.4 SAMPLE ANALYSIS

The samples were analyzed using the Atomic Absorption Spectrophotometry (AAS) to obtain concentrations of elements such as chlorine ($Cl^-$), sodium ($Na^+$), magnesium ($Mg^{2+}$), potassium ($K^+$), calcium ($Ca^{2+}$) and sulphate ($SO_4^{2-}$). Atomic Absorption Spectrophotometry provides accurate quantitative analyses for metals in water, sediments, soils or rocks. The AAS analyzed the samples in solution form, so solid samples must be leached or dissolved prior to analysis.

Atomic absorption units have four basic parts: interchangeable lamps that emit light with element specific wavelengths, a sample aspirator, a flame or furnace apparatus for volatilizing the sample, and a photon detector. In order to analyze for any given element, a lamp is chosen that produces a wavelength of light that is absorbed by that element. Sample solutions are aspirated into the flame. If any ions of the given element are present in the flame, they will absorbed light produced by the lamp before it reaches the detector. The amount of light absorbed depends on the amount of the element present in the sample. Absorbance values for unknown samples are compared to calibration curves prepared by running known samples.

Figure 3.2: Atomic Absorption Spectrophotometry (AAS) used to analyze water samples.

### 3.5 GROUNDWATER MODELLING

A finite element code FEMWATER (Lin et al., 1997) in the Groundwater Modeling System (GMS) software was used for the simulation of variable density flow and scenario analysis in the study area. The GMS was selected for this study due to its numerous applications in groundwater studies and the different numerical codes available for solving hydrogeological problems. The software package incorporates the United States Geological Survey's Modular three dimensional finite difference groundwater flow code, MODFLOW-2000 (Harbaugh et al., 2000), the finite element code, FEMWATER (Lin et al., 1997), MT3DMS (Zheng and Wang, 1999), and several other solute transport codes for investigating groundwater and environmental problems. The type of numerical code selected therefore depends on factors such as the availability of data and the objectives of the study. There are several numerical codes available in the literature for the simulation of regional and local groundwater flow systems (Yidana and Chegbeleh, 2013). FEMWATER is based on the finite element approximation of the general equation that describes the three dimensional flow of groundwater of variable density and viscosity through a porous geologic material under both stead state and transient conditions.

Several visits to the field (study area) in an interval of two weeks for a period five months indicated that, total dissolve solids (TDS) and electrical conductivity (EC) measured in groundwater varied marginally. The finite element numerical codes in GMS was selected for this study due to its ability to simulate flow of varying density in saturated-unsaturated porous media. A FEMWATER code has the ability to accounts for variations in groundwater flow due to density difference. The essence of this study was to evaluate the impact of introducing density variations of groundwater due to variabilities in TDS of groundwater imposed by several intervening processes such as

the impact of the lagoon in the north/west and the Gulf of Guinea to the south of the domain, and solute inputs arising from the use of agricultural chemical and waste disposal.

Numerical codes are governed by mathematical equations, boundary conditions and initial conditions to achieve desired results in groundwater and environmental modeling. FEMWATER is a finite-element based numerical simulation model. In groundwater flow and transport, the flow equations are solved first to obtain the heads and velocity of flow. In the process of density-dependent flow such as salinity intrusion in coastal aquifers, the velocity of groundwater at any location at any time is a function of the concentration, which is obtained from the solution of the flow equation. The velocity of flow depends on the density of the water and density in turn, varies with the salinity concentration in space and time. The density dependence causes the coupling of the flow and transport equations, and the simultaneous solution of them induces high non-linearity in the density-dependent flow and transport as illustrated in Equations 3.1 and 3.2 (Lin et al., 1997).

$$\frac{\rho}{\rho_o} F \frac{\partial h}{\partial t} = \nabla . [K . \left(\nabla h + \frac{\rho}{\rho_o} \nabla z\right)] + \frac{\rho^*}{\rho_o} q \qquad \textbf{3.1}$$

$$F = \alpha' \frac{\theta}{n} + \beta' \theta + n \frac{dS}{dh} \qquad \textbf{3.2}$$

Where

**F**= storage coefficient

**h**= Pressure head

**t**= time

**K**= hydraulic conductivity tensor

**Z**= potential head

**q**= source and/ or sink

***p***= water density at chemical concentration C

$P_o$= referenced water density at zero chemical concentration

**p***= density of either injection fluid or withdraw of water

**θ**= moisture content

**α'**= modified compressibility of the medium

**β'**=modified compressibility of water

**n**= porosity of the medium

**S**= saturation

The hydraulic conductivity K is given as

$$K = \frac{\rho g}{\mu} k = \frac{(\frac{\rho}{\rho_o})}{(\frac{\mu}{\mu_o})} \frac{\rho_o}{\mu_o} K_s K_r = \frac{\rho/\rho_o}{\mu/\mu_o} K_{so} K_r \quad \textbf{3.3}$$

**μ**= dynamic viscosity of water at chemical concentration C

$\mu_o$= reference dynamic viscosity at zero chemical concentration,

**K**= permeability tensor,

$K_s$= saturated permeability tensor

$\mathbf{k_r}$ = relative permeability or relative hydraulic conductivity

$\mathbf{K_{so}}$ = referenced saturated hydraulic conductivity tensor.

The referenced value is usually taken at zero chemical concentration. The density and dynamic viscosity of water are functions of chemical concentration and are assumed to take the following form

$$\frac{\rho}{\rho_o} = a_1 + a_2 C + a_3 C^2 + a_4 C^3 \quad \textbf{3.4}$$

And

$$\frac{\mu}{\mu_o} = a_5 + a_6 C + a_7 C^2 + a_8 C^3 \quad \textbf{3.5}$$

Where $\mathbf{a_1}$, $\mathbf{a_2}$... $\mathbf{a_8}$ are the parameters used to define concentration dependence of water density and viscosity and C is the chemical concentration (Lin et al., 1997).

The Darcy velocity is calculated as follow

$$V = -K.\left(\frac{\rho}{\rho_o}\nabla h + \nabla Z\right) \quad \textbf{3.6}$$

The governing equations for transport are derived based on the continuity of mass and flux laws. The major processes are advection, dispersion/diffusion, adsorption, decay, biodegradation, and source/sink as illustrated in Equation 3.7.

$$\theta \frac{\partial c}{\partial t} F + \rho_b \frac{\partial S}{\partial t} + V.\nabla C - \nabla.(\theta D.\nabla C) = -\left(\alpha^1 \frac{\partial h}{\partial t} + \gamma\right)(\theta C + \rho_b S) - (\theta K_w.C + \rho_b K_s S) + m - \frac{\rho^*}{\rho} qC + (F\frac{\partial h}{\partial t} + \frac{\rho_o}{\rho} V.\nabla\left(\frac{\rho}{\rho_o} - \frac{\partial \theta}{\partial t}\right) C \quad \textbf{3.7}$$

Although not much FEMWATER publications are available, it is still considered as one of the best and tested numerical codes for simulating density dependent flow in

groundwater aquifers. It can predict hydrogeological system correctly within the limits of available data and field conceptualization (Anderson and Woessner, 2002).

### 3.5.1 Model Conceptualization and Formulation

The terrain was modeled as a single-layer unconfined aquifer based on available data and information from literature in the area. Different colors were used to distinguish materials of the upper and lower limits of the unconfined units as in Figure 3.3. The boundaries of the model domain in the study area were conceptualized as specified head boundaries and no flow boundaries. The north-western end of the domain is boarded by the Keta lagoon and was conceptualized as a specified head boundary and a head value assigned to the node at the upper left corner.

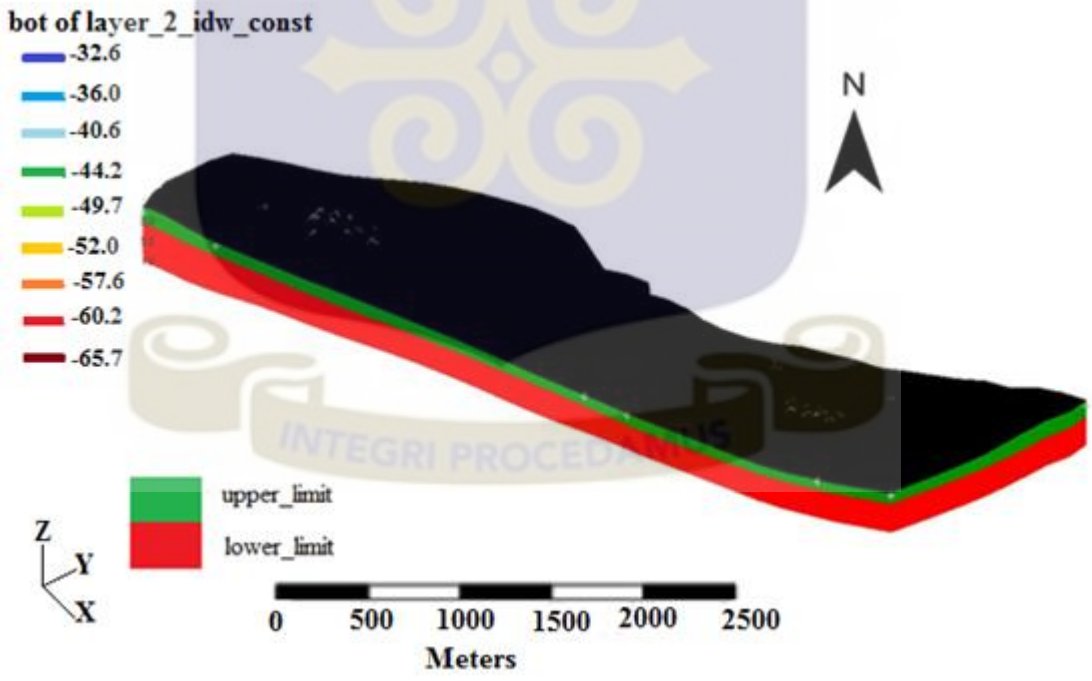


Figure 3.3: A map showing the spatial interpolation of aquifer limits in the study area

FEMWATER will compute values which vary linearly along the boundary based on the value assigned. The southern end of the model domain is boarded by the Gulf of Guinea (sea) and was conceptualized also as specified head boundary with constant head conditions. The constant head value is the same as the default value (zero) which coincided with sea level. The Western and Eastern ends of the model were conceptualized as no flow boundaries. The lower limit of the unit modeled was conceptualized as a confining layer whilst the top was conceptualized as unconfined to coincide with atmospheric conditions at the top. Geophysical profiles conducted by Banoeng-Yakubo et al. (2005) in the area suggest the presence of a low conductivity clay layer at the bottom of the shallow unconfined system under study. It was on the basis of this that the lower limits of the unit were conceptualized as a no-flow boundary. The contrast in hydraulic conductivity values between the loose unconfined material and the underlying clay layer is significant enough to justify this boundary condition (Yidana and Chegbeleh, 2013). The conceptualization was performed using the map tools in the Groundwater Modeling System, GMS, version 10.0.13 (Aquaveo, 2014).

Apart from the Gulf of Guinea and the Keta lagoon which borders the study area to the south and north respectively, there was no visible drainage (rivers and streams) system in the study area to be digitized and incorporated into the model. The study area is relatively a small coastal expanse which was divided into a number of zones to create coverage's for flux rate. The zonation was based on knowledge of previous research work in the area by Yidana and Chegbeleh, (2013), geology and topography of the area indicating where there may be possible high conductivities as well as recharge (flux rate) and discharge areas. For the coverage of the flux rate, polygons were created to simulate spatial variations in flux in the study area (Fig. 3.4).

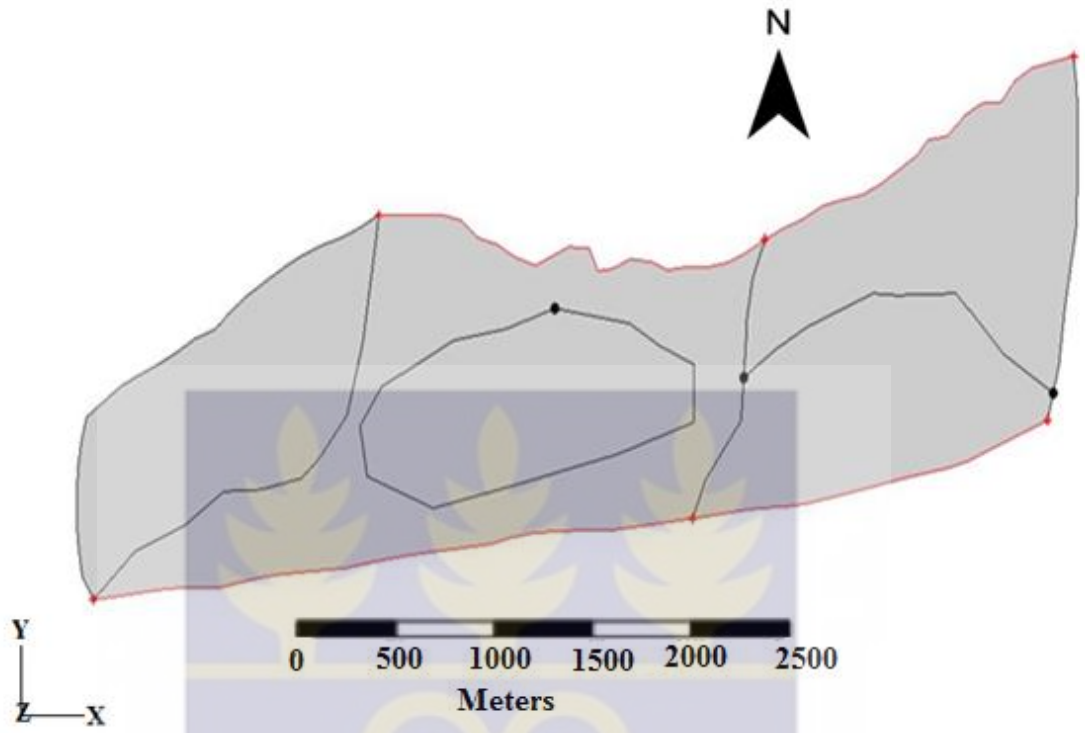


Figure 3.4: A digitized map of the coverage area showing polygons

Initial values were assigned to the polygons based on normal values associated with similar materials in literature; Yidana and Chegbeleh (2013). Surface runoff is virtually nonexistent in the area and much of the annual rainfall returns to the atmosphere through evapotranspiration and some go into the shallow unconfined aquifer system through vertical infiltration and percolation.

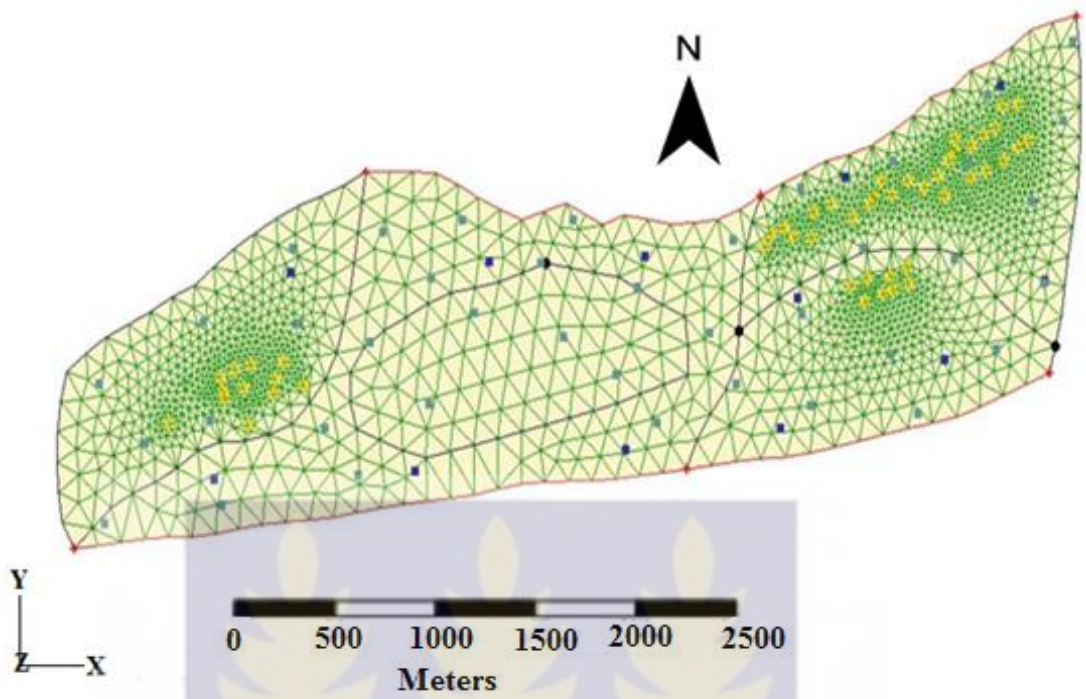


Figure 3.5: A map in plain view showing active mesh over the study domain

An observation coverage was created to accommodate the chloride concentration of 50 wells from the area for the purposes of calibration. A uniform two-dimension (2D) mesh system was automatically generated to overlay the domain (Fig. 3.5). The 2D mesh was then projected using the feature object in the conceptual model. Three Triangulated Irregular Network (TINs) were created; one for the top terrain, one for the bottom of the upper aquifer and one for the bottom lower aquifer. The TINs were later used to create 3D finite elements (Fig. 3.6) using horizons to 3D mesh command. A total of 51,030 elements were generated to simulate density-dependent flow.

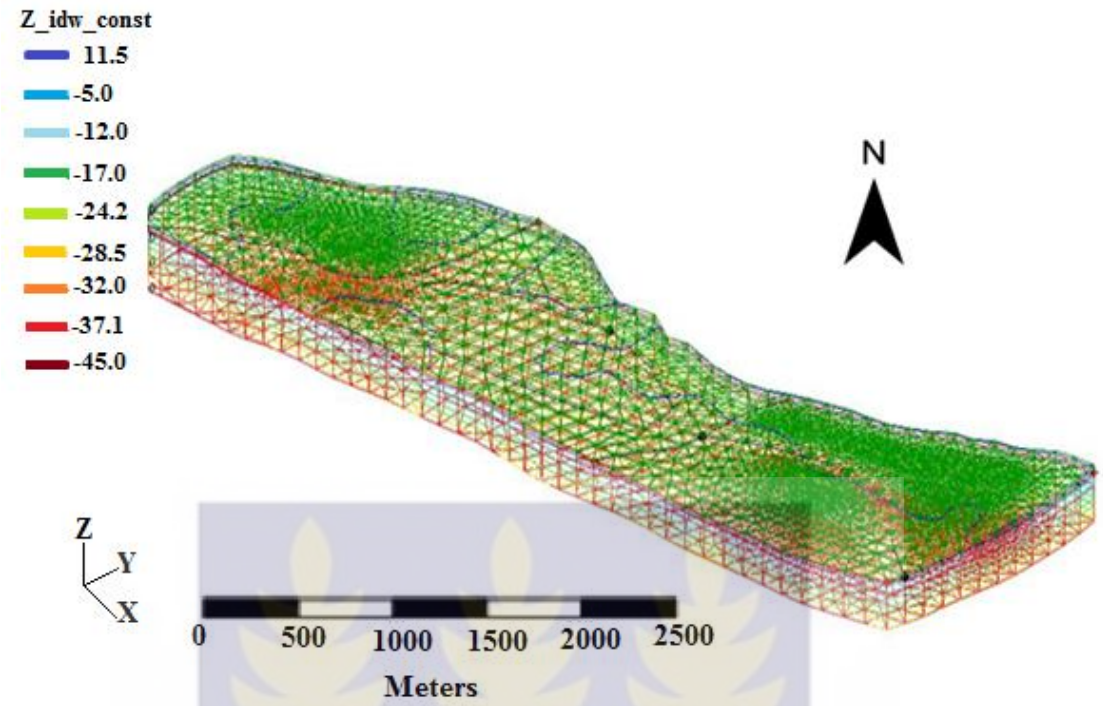


Figure 3.6: Map showing interpolate mesh over active domain

### 3.5.2 Numerical Simulation of Flow

The conceptual model was converted to numerical FEMWATER model to simulate for density-driven flow within GMS 10.0.13 in a transient state. Initial condition values for both pressure heads and concentrations were assigned to the numerical model to get it ready for simulation. Total dissolve solids (TDS) data was collected over a period of five months from the study area. The TDS data was used to initialize the numerical model with a maximum simulation time of 364 days and a constant time step of 14 days. Three solvers and stimulation types are available in FEMWATER run options command in GMS. The solver package available includes; pointwise iteration matrix solver preconditioned conjugated gradient method (polynomial) and preconditioned conjugate gradient method (incomplete Choleski). The simulation packages include; flow only (KMOD=10), transport only (KMOD=1) and coupled flow and transport (KMOD=11). Four quadrature are also available for numerical integration. They are

nodal/nodal quadrature, nodal/Gaussian quadrature, gaussian/nodal quadrature and gaussian/gaussian quadrature (Lin et al., 1997).

The choice of a solver is based on two main considerations: the ability of the solver to solve the differential equations for the problem being investigated, and the time it takes to complete solutions. Although the solution time varies from one computer to the next, for the same computer, one solver will solve the same equations faster than other solvers. In addition to these two criteria, the choice of a solver is determined by the memory space required by each solver since different solvers have different computer memory requirements. Every solver undertakes the solution of the differential groundwater flow equation through iterative procedures (Yidana et al., 2010).

In this study, coupled flow (i.e. flow and transport) and pointwise iteration matrix solver were, respectively, chosen to simulation density-dependent flow conditions in the domain. This solver is preferred in the study because it is more robust than the other two solvers. However, when the speed of convergence is too slow, one may wish to choose one of the other two solvers. The domain under study has a very large partially saturated region. The larger the unsaturated zone, the more difficult it is to get FEMWATER to converge. For these types of problems, the nodal/nodal option is a good choice for quadrature. It is not as accurate as the default option (Gaussian/Gaussian), but more stable (Lin et al., 1997).

.

### 3.5.3 Model Calibration

Calibrating a model is a process of altering or adjusting model parameters to reflect field conditions. These processes continue until the model replicate near or exact field conditions. It is only a calibrated model which can be used for hydrogeologic predictions and for characterizing hydraulic parameters. Unlike MODFLOW which support both manual and automatic calibrations, FEMWATER in the GMS currently support only the manual form of calibration. The model was calibrated against chloride concentrations and observation head data. Model parameters such as porosity, flux rate, moisture content curve and water capacity curves were varied continually and run each time until the compute heads matches that of the observation heads data. The calibrated target was set at $\pm 0.25\ m$, which means for each observation well, calibration was said to have been achieved whenever the observed and model computed heads were within $\pm 0.25\ m$ of each other.

### 3.5.4 Sensitivity Analysis

It is recommended that a sensitivity analysis be done after the calibration of every model. The purpose of sensitivity analysis is to measure the stability of the model in the face of subtle changes in some of the model parameters. It is done by making little variations in the key parameters and noting the effects on the calibrated model. When the calibrated model shows significant departure from the calibration after the slight changes in the key parameters, it is said to be unstable and can therefore not be relied upon to predict scenarios. Under such circumstance, the model will have to be recalibrated. Finite element code (FEMWATER) does not currently support automatic sensitivity analysis because there is no provision for it but it can be done manually.

### 3.5.5 Scenarios Analysis

The calibrated transient model was used to evaluate scenarios of groundwater abstractions in the study area. This has become necessary since rainfall patterns have become irregular due to climatic changes throughout the globe. Out of the 50 observations wells, 28 wells with available yields were used in this study (Table 3.1). The estimated yields were obtained from tube wells been pumped for irrigation farming in the area. These estimated yields were applied as the initial abstraction rates. In the first scenarios analyses, abstraction rates were increased by 10%, 25%, 30%, 50%, 100%, 200% and 300% whiles maintaining the flux rate, porosity and hydraulic conductivity of the aquifer unit at the calibrated rates. For the second scenario analyses, abstraction rates, flux rate, porosity and hydraulic conductivity were maintained whilst TDS concentrations were increased by 10%, 25%, 50% and 100% to reflect increasing surface activities in the area. The scenarios were determined somewhat arbitrarily to provide a preliminary test of the capacity of the system to contain probable stresses. This will also provide information regarding the tolerable limits for groundwater abstraction in the area.

Table 3.1: A table showing initial flow rate of 28 tube wells used for scenarios analyses

| Tube Wells | Northings | Easting | Initial flow rate (m3/d) |
|---|---|---|---|
| ANL_BH01 | 270010 | 642081 | -208 |
| ANL_BH02 | 270145 | 642166 | -600 |
| AHF_BH03 | 270281 | 642238 | -864 |
| AHF_BH04 | 270358 | 642421 | -864 |
| AHF_BH05 | 270530 | 642447 | -862 |
| AHF_BH06 | 270645 | 642122 | -864 |
| AHF_BH07 | 270530 | 642060 | -400 |
| ANS_BH08 | 270370 | 641938 | -130 |
| ANS_BH09 | 270171 | 641855 | -420 |
| ANC_BH10 | 270007 | 641792 | -660 |
| ANL_BH11 | 26840 | 641726 | -305 |
| ANL_BH12 | 269718 | 641625 | -608 |
| ANF_BH13 | 268849 | 640889 | -310 |
| ANF_BH14 | 269100 | 640910 | -230 |
| ANC_BH15 | 269289 | 640991 | -221 |
| WHU_BH16 | 269130 | 640788 | -810 |
| WHU_BH17 | 269313 | 640840 | -780 |
| WHU_BH18 | 269021 | 640751 | -701 |
| WHU_BH19 | 268820 | 640682 | -623 |
| WHU_BH20 | 268667 | 640823 | -550 |
| WHU_BH21 | 262327 | 640143 | -864 |
| WHU_BH22 | 262560 | 639928 | -211 |
| WHU_BH23 | 262212 | 639851 | -315 |
| ANF_BH24 | 261937 | 639571 | -295 |
| ANF_BH25 | 261050 | 639591 | -630 |
| AHF_BH26 | 268254 | 641481 | -660 |
| AHF_BH27 | 262238 | 639988 | -800 |
| AHF_BH28 | 267691 | 641175 | -864 |

# CHAPTER FOUR

# RESULTS AND DISCUSSION

## 4.1 TOTAL HYDRAULIC HEAD

The distribution of total hydraulic head in the study was obtained through a calibrated transient state simulation model. As illustrated by the time series plot (Figure 4.1a, b and c), there is a good match between the observed data and the model-computed data. This suggests that the transient model is reasonably representative of the hydrogeological conditions of the study area within the limits of the data used, and is therefore useful for fairly reliable predictions of the impacts of various scenarios of groundwater development and natural stresses on the system. It is also useful for assessing the position of the freshwater/saline water interface in the area. Figure 4.2 (a, b, c and d) contains the relationship between observed and model-computed hydraulic head data for the various individual stress periods in the terrain and indicates that even for the individual stress periods; there is reasonably a good match between the observed and model-computed hydraulic head data.

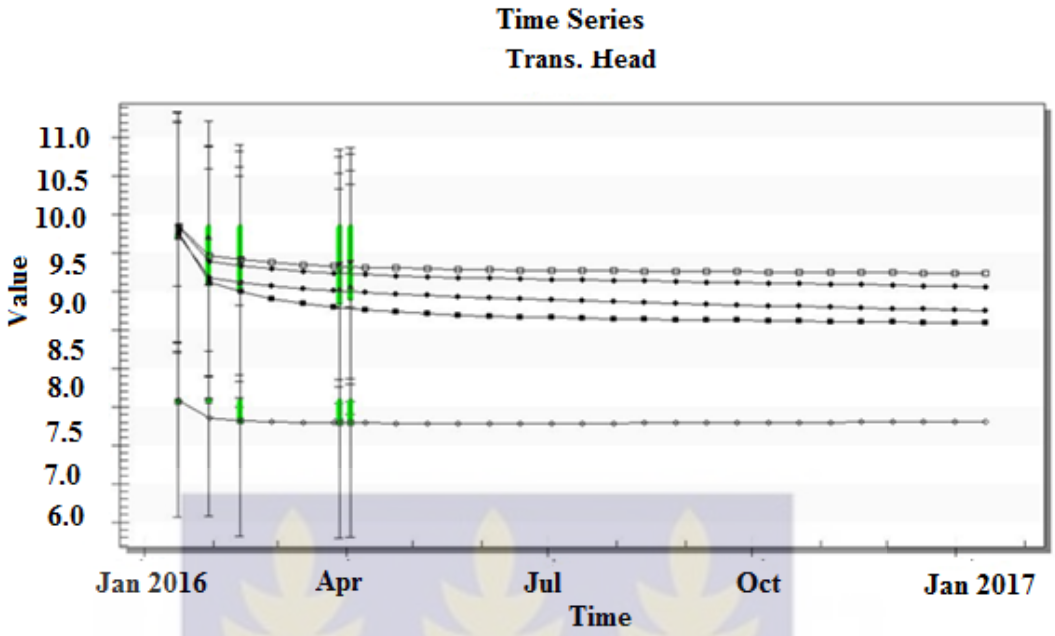


Figure 4.1a: A match between the models computed head and observed head for January 2016.

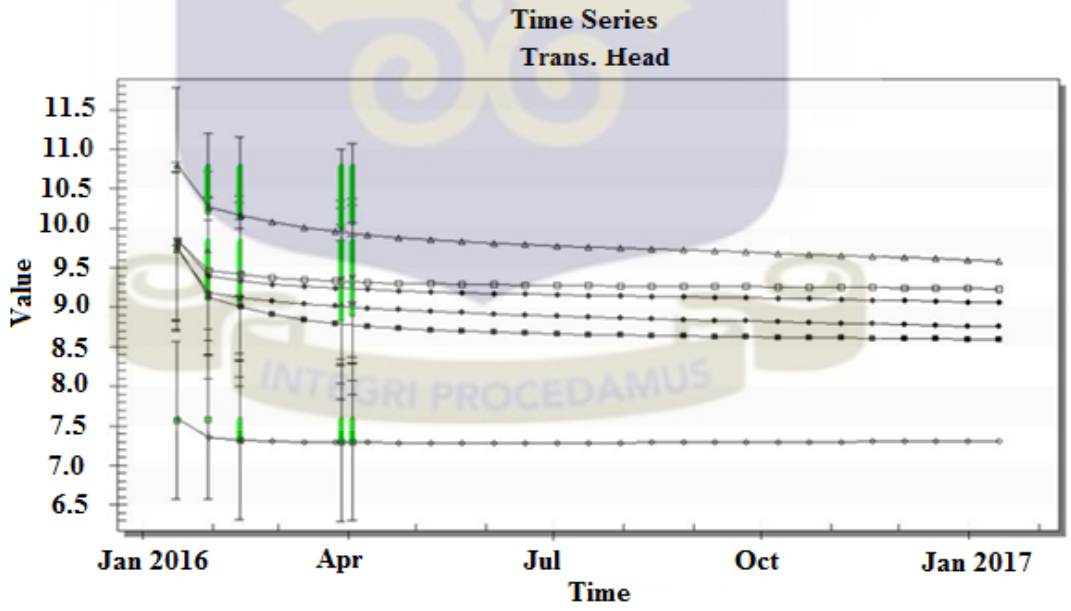


Figure 4.1b: A match between models computed head and observed head for February 2016.

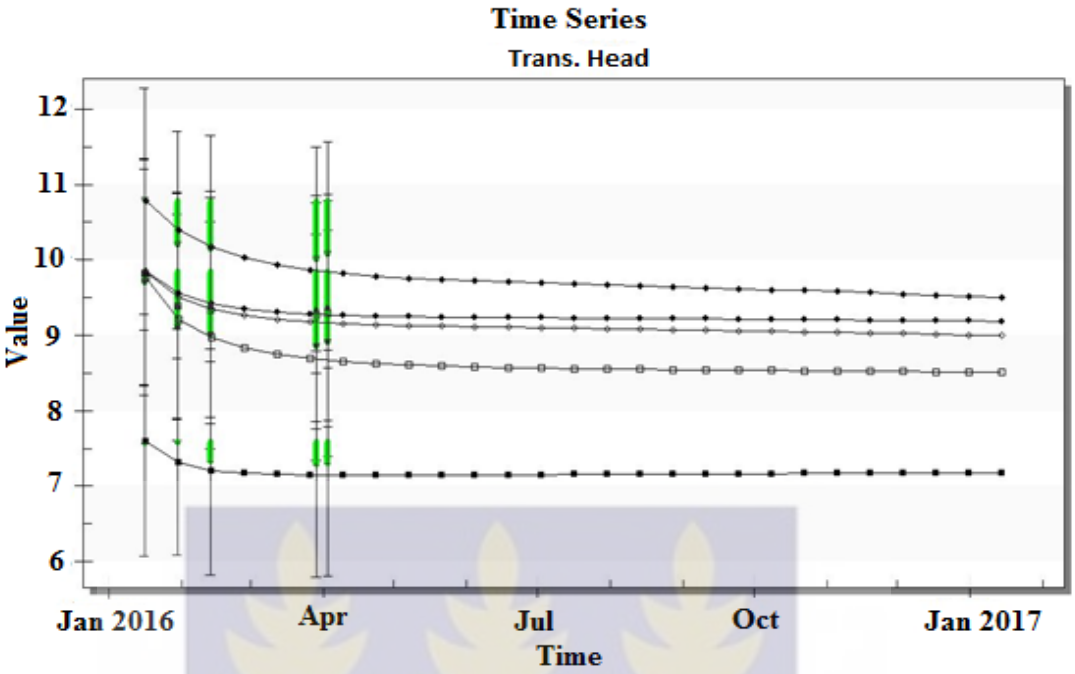


Figure 4.1c: A match between model computed head and observed head for April 2016

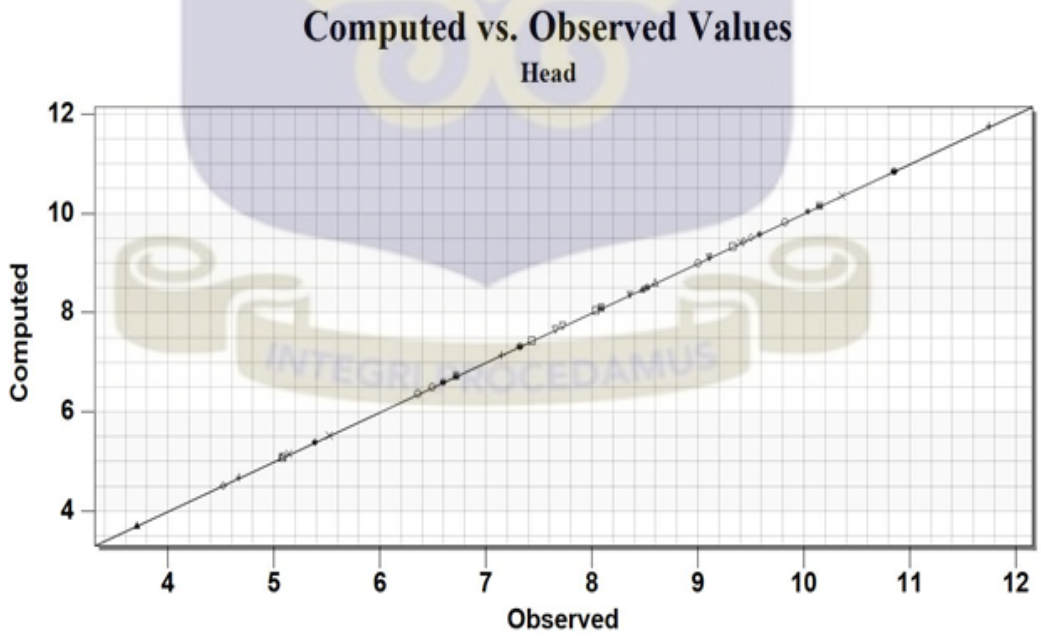


Figure 4.2a: A match between model computed head and observed head for January 2016.

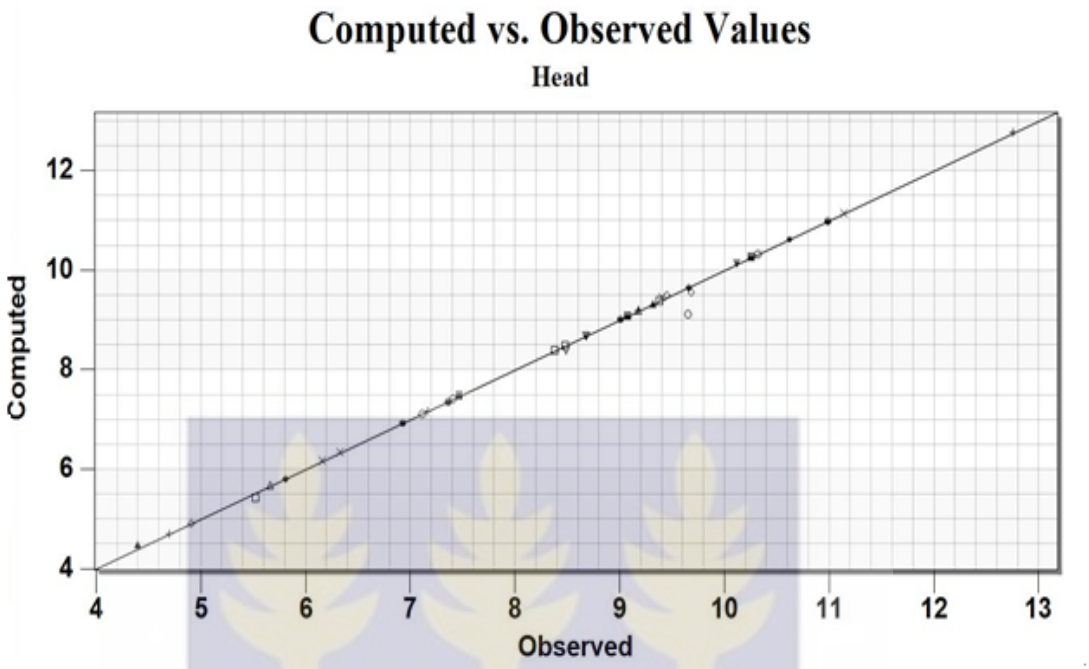


Figure 4.2b: A match between model computed head and observed head for February 2016.

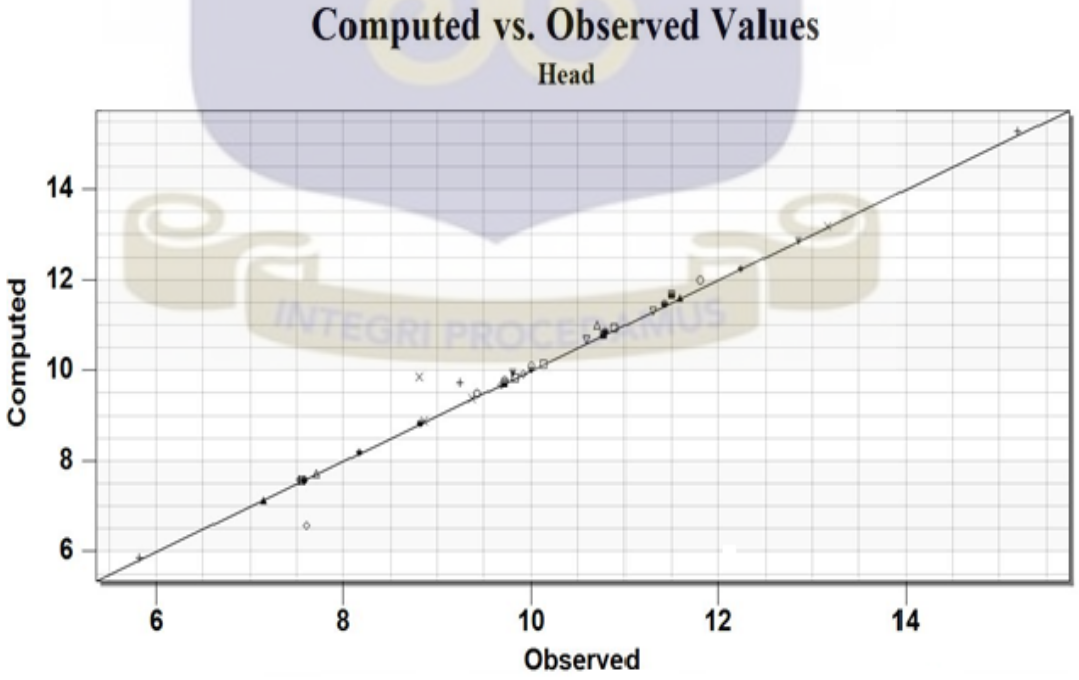


Figure 4.2c: A match between model computed head and observed head for March 2016

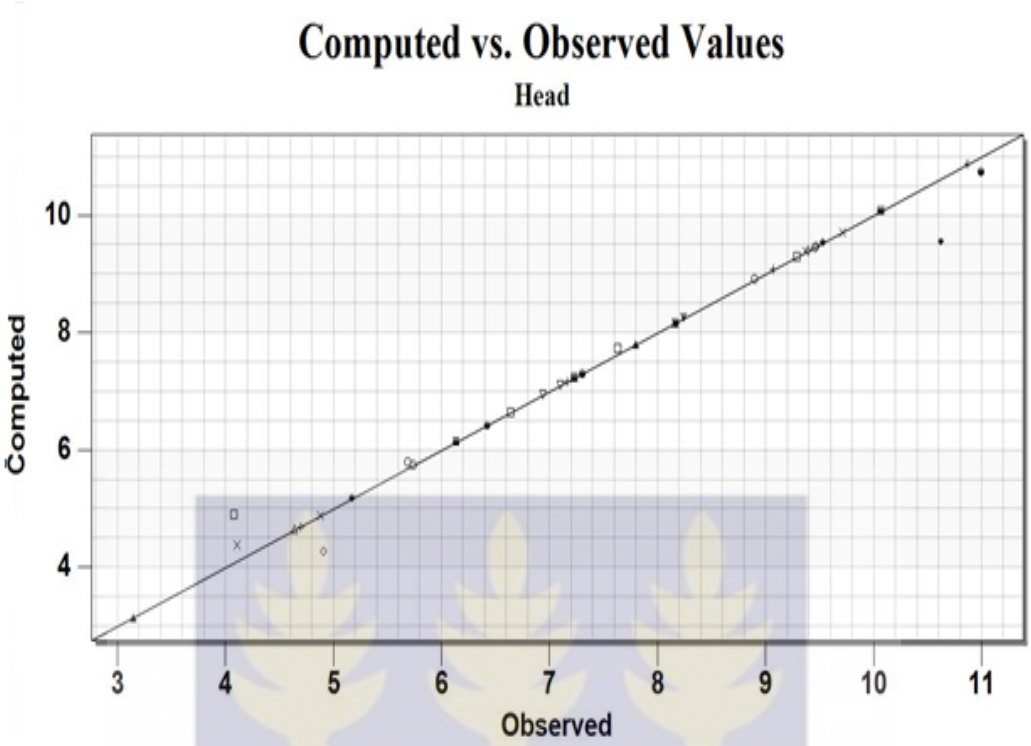


Figure 4.2d: A match between model computed head and observed head for April 2016.

The potential field as represented by the spatial variations in the hydraulic head is presented in Figure 4.3. High hydraulic heads are observed along the northern, northeast and western parts whilst low heads occur at the middle and south to southeastern portions of the terrain. This is in agreement with the findings of Yidana and Chegbeleh, (2013) who calibrated a steady state model over the terrain using a finite difference code, MODFLOW-2000 (Harbaugh et al., 2000). The two codes, finite element code, FEMWATER and finite difference code MODFLOW, therefore agrees in terms of the prediction of hydraulic potential field.

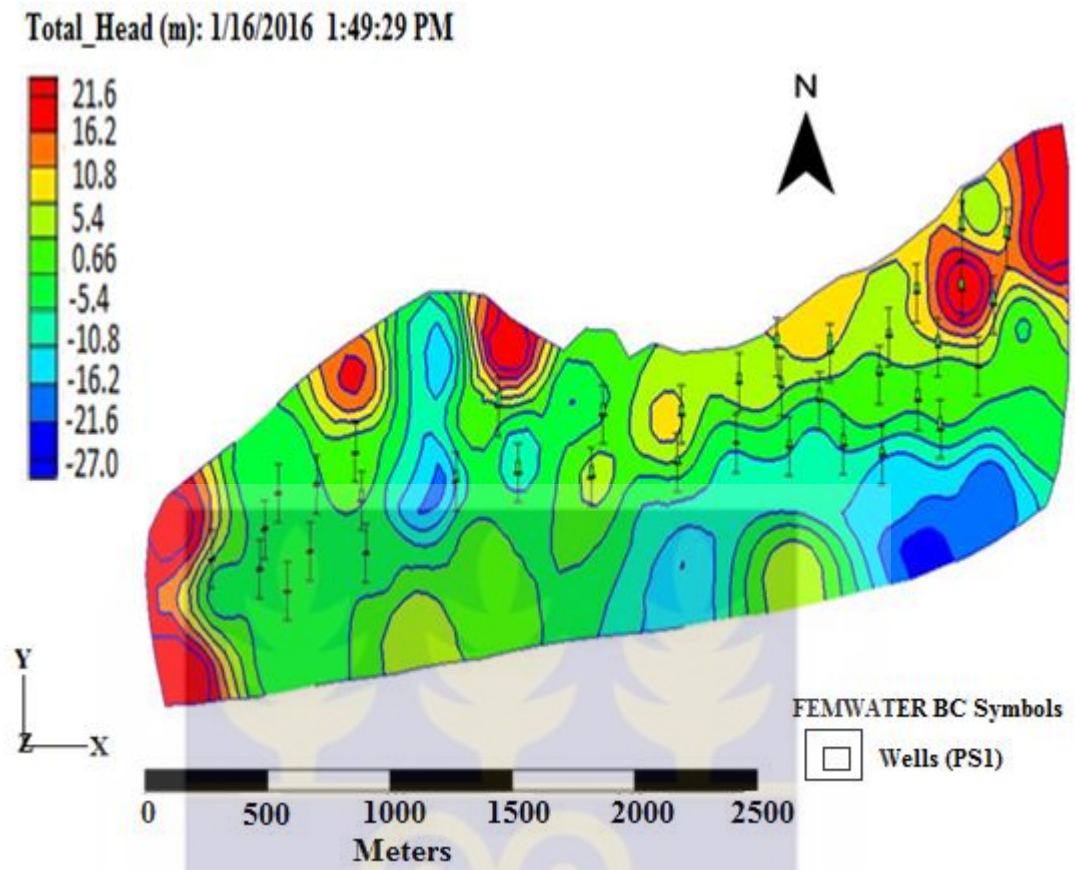


Figure 4.3: A model showing the distribution of hydraulic heads in the study area.

The flow patterns as predicted by the calibrated model are northwest southeast and south north flow patterns although there are some few cases of northeast southwest flow directions. The heads in the area generally ranges from -27 m to about 21 m. This suggests good fortunes of groundwater development for irrigation activities in the area (Yidana and Chegbeleh, 2013). Only a fraction of the study area shows very low levels of hydraulic heads which implies that a larger portion of the area has fairly high levels of groundwater as designated by the model. Considering the fact that the terrain is a coastal region, these relatively high levels are indications of huge volumes of groundwater hosted by the terrain and therefore can adequately support irrigation farming.

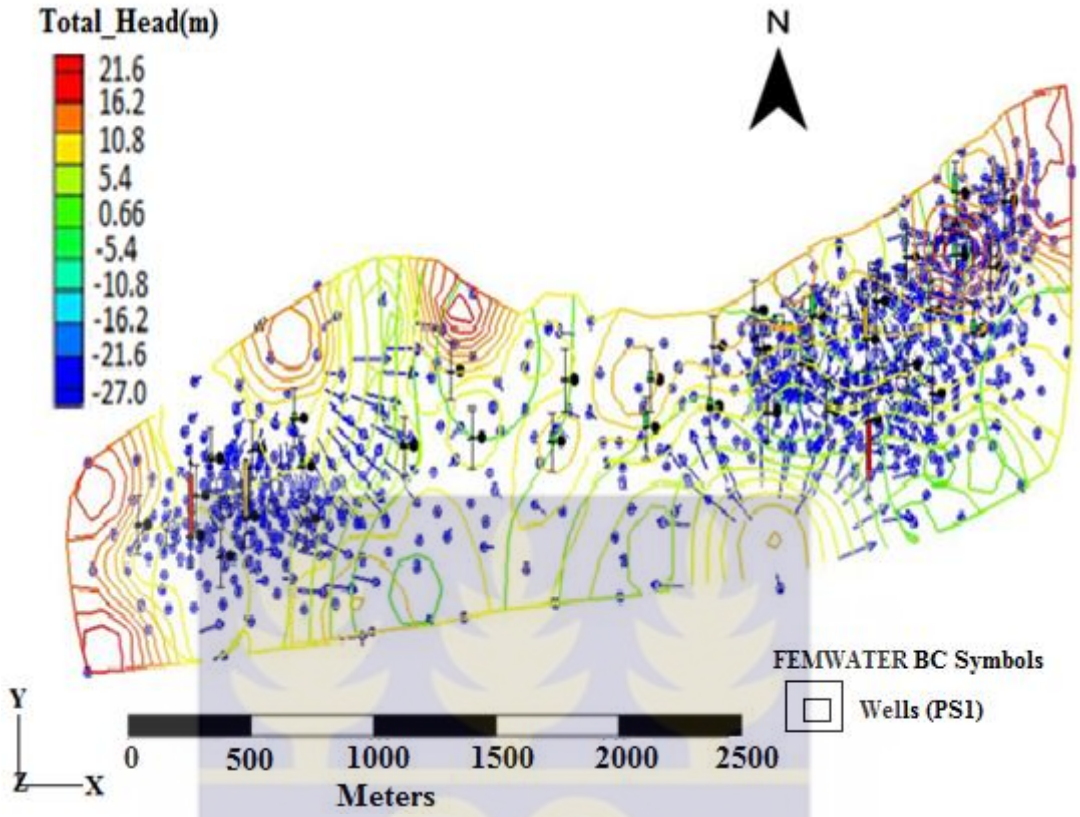


Figure 4.4: Linear contour map showing groundwater flow paths in the study area.

Proper and adequate management of the resource will therefore ensure sustainability of the irrigation activities since the majority of the residents in the area are into farming. The terrain is mostly flat lying and groundwater flow results from slight difference in hydraulic head in the area. There were no erosion channels observed within the area as at the time of this research emphasizing the flat nature of the terrain. This suggests that surface run-off is negligible in the area and almost all the water infiltrates into the shallow unconfined aquifer after a downpour. However, in the dry seasons, due to high evapotranspiration rates and excessive withdrawal for irrigation, the groundwater levels drop. The reduction in groundwater level has the potential of reversing groundwater flow paths and causing saline water intrusion when the declined becomes drastic considering the fact that the area is a coastal area. This could likely be the case in the study area as TDS and EC values measured were found to be very high in some sections

(see Appendix 1). The high TDS and EC values in the area can also be caused by chemicals applications to crops during farming. The intrusion of saline water increases the density of fresh groundwater and this in turn influences groundwater flow. The salinity in the freshwater aquifer in the area could result from either reversed underground flow of saline water from the ocean or due to chemical from irrigation activities.

Local flow systems are likely to be the most dominant flow systems in the terrain since the aquifer system is quite shallow (Yidana and Chegbeleh, 2013). According to Toth (1963), an aquifer system can comprise local, intermediate, and regional groundwater flow systems. In a local system of groundwater flow, recharge and discharge areas are next to each other. For intermediate groundwater flow system, recharge and discharge areas are parted by one or more topographic highs and lows. Regional groundwater flow system normally has recharge areas along groundwater divides, and discharge areas lie at the bottom of major drainage basins. Not all types of groundwater flow paths are present in every aquifer system. In this particular case, in the light of shallow depth and gentle relief, local flow systems are obvious.

## 4.2 GROUNDWATER FLOW RATE

The spatial distribution of groundwater flow rate in the locality of Whutti-Anloga part of the Keta strip was presented through a calibrated transient state model as in Figure 4.5. Groundwater velocities in the study area range between 0.93 m/d and 8.37 m/d with an average of 4.05 m/d. These nodal velocities are quite high compare to the general groundwater velocity within the subsurface or through a porous media as suggested by Alley et al. (1999). Groundwater velocity is directly related to the hydraulic conductivity in any given hydrogeologic system. This means that areas of high hydraulic conductivity should translate into areas of high velocities. However, a nodal velocity map produced for the shallow unconfined aquifer of the Keta Strip after a transient state simulation suggested otherwise and does not agreed entirely with the hydraulic conductivity field map produced for the same aquifer by Yidana and Chegbeleh (2013) using finite difference numerical code MODFLOW-2000 (Harbaugh et al., 2000).

Their work suggested the northern part of the terrain to have high hydraulic conductivity while the western part has low conductivity. This assessment does not reflect on the velocity map which identified the western part rather than the north of the domain to have high groundwater velocities. It can therefore be concluded that, the velocities of groundwater in the area does not necessarily depend on the hydraulic conductivity. Groundwater velocities in the area vary spatially and temporally and appeared to be influenced by the seasonal variations in TDS due to evaporative enrichment of residual groundwater since the shallow unconfined aquifer is prone to evaporating especially during the dry season (Fig. 4.7). Yidana and Chegbeleh, (2013) attributed the variations in hydraulic conductivity and by extension the flow rate to

varying clay content and heterogeneity of the aquifer materials in the area but this study largely found increasing density of the groundwater as the determinant of the flow rates (nodal velocities) rather than the hydraulic conductivity field of the area (Fig 4.7). The areas with high TDS (density) were observed to have low groundwater velocities and vice versa. Although the aquifer material appeared loose and porous in the area, it is the density of the groundwater which greatly influenced the nodal velocities. Aside the western end, the southwestern portion was also identified as an area with high groundwater velocities whilst the middle and southeastern parts were observed to have low velocities.

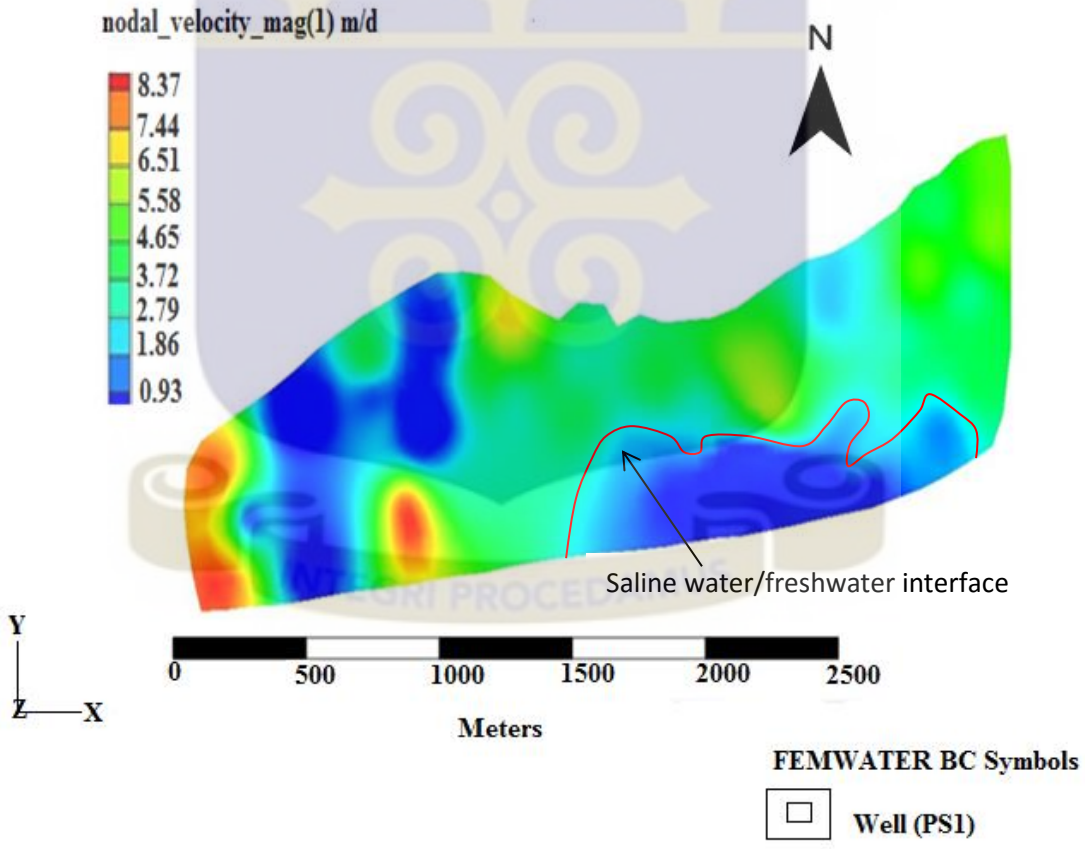


Figure 4.5: 2D map showing groundwater nodal velocities in the study area.

Some areas of high nodal velocities within the study domain coincided with areas of high hydraulic heads. The relatively high velocities in the area would facilitate rapid spread and dispersion of contaminants, especially if the contamination occurs at the western and southwestern part of the domain. Groundwater velocities in the area also appeared to be reducing as aquifer depth increases (Fig. 4.6). This observation is attributed to the effect of gravity due to increasing density of the groundwater and the presence of a low conductivity layer at the bottom of shallow aquifer as suggested by Banoeng-Yakubo et al., (2005) who conducted a geophysical profile in the area. The reduction in groundwater velocities with respect to depth in the area could not be associated to increasing compaction due to weight of overlying materials since the aquifer is quite shallow. Considering only hydraulic conductivity without fluid density variations in an attempt to predict groundwater flow rate in the area will therefore lead to some errors in the estimation of flow rates.

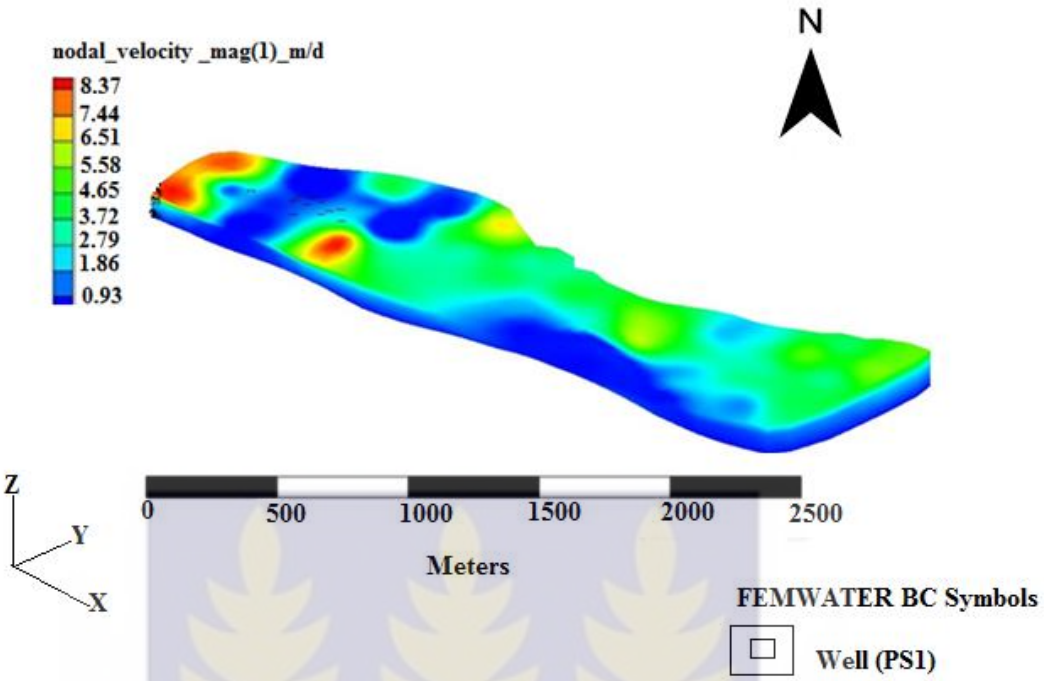


Figure4.6: 3D map showing the distribution of groundwater velocities in the study area in January 2016.

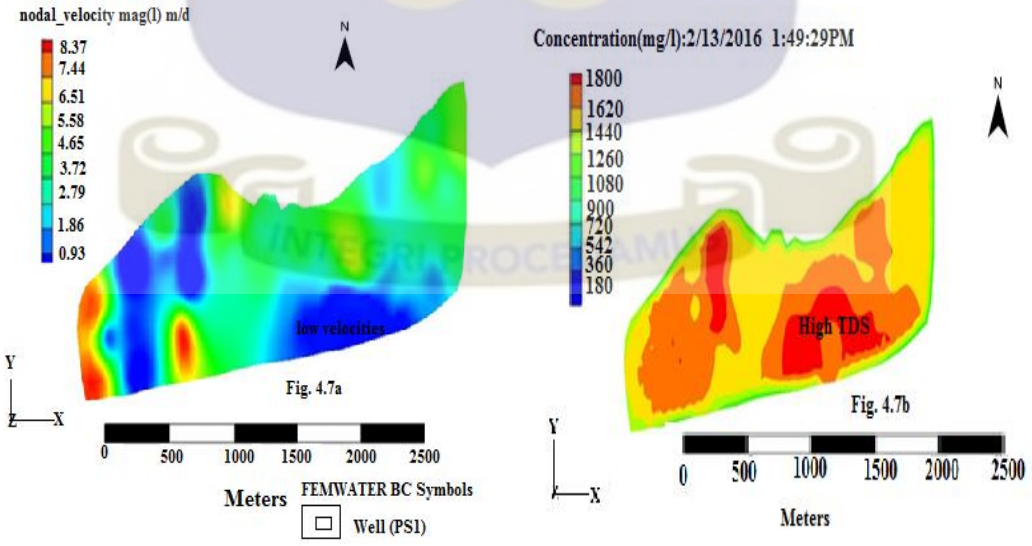


Figure 4.7: A comparison between groundwater velocity and TDS in the study.

The freshwater-saline water interface in the domain was monitored for the first five months of the year so as to observe the extent of movement. Although the time interval was relatively small, the changed in position of the interface could still be observed between the first and fifth month (Fig 4.8). The freshwater-saline water interface advanced further into the freshwater aquifer and the wedge became bigger and more distinct giving an indication of increasing salinity intrusion into the aquifer over time (Fig 4.8). The freshwater-saline water front in the area is affected by excessive abstractions of groundwater for irrigation causing a drastic decline of the water table and inducing seawater to flow into the aquifer. Different layers of the interface were also observed in figure 4.8b as the velocity front moved further towards the freshwater aquifer. This observation could be due to the variation in the velocity of the saline water due to different densities as it intrudes into the freshwater body in the domain. It also suggests, increasing in salinity closer to the boundary of sea (South) whilst the salinity reduces as you move away from the sea into the center of the domain.

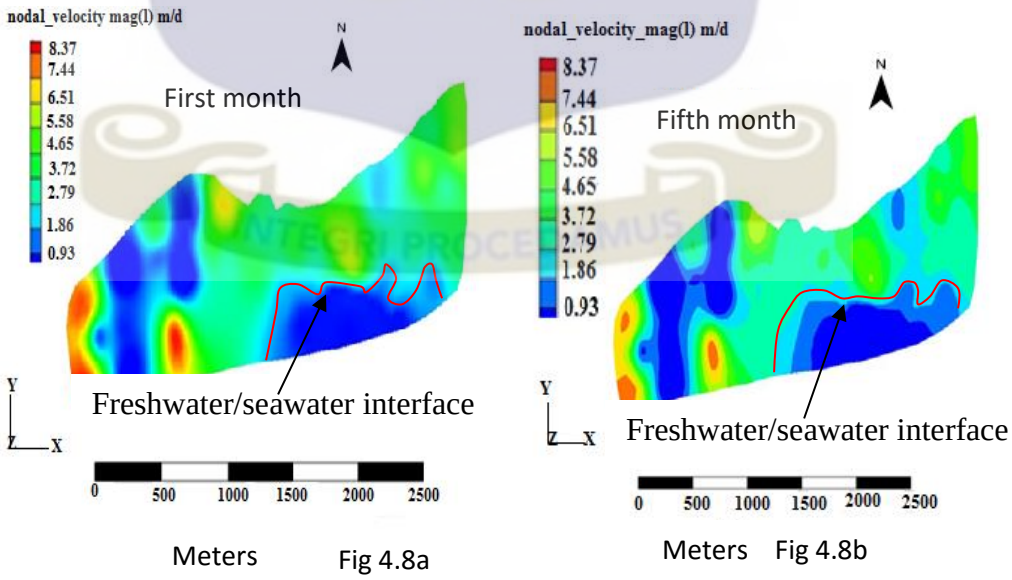


Figure 4.8: Change in position of the freshwater-saline water interface over time in the study area

Groundwater velocities in the study area also vary for the different stress periods shown by the calibrated transient models (Fig 4.6 and 4.9). Whilst the density of the groundwater consistently increased, the nodal velocity continuously got slower as showed by the maps of the different stress periods. Groundwater flow rate in the area was reduced as the water got denser causing the viscosity of the groundwater to increased and thereby decreasing the velocities. The denser groundwater settled at the bottom due to the effect of gravity whereas the lighter groundwater floats on top by buoyancy (Voss et al. 1991). The higher the viscosity of a fluid, the less susceptible it is to flow. Increased in salinity in the area could affect the hydraulic properties of the soil as well as crops production.

High salt content in the soil causes the dispersion of clay resulting in blockage of finer pore spaces and this subsequently leads to reduction in the hydraulic properties of the soil (Naderi et al., 2013). The blockage of the pore spaces also reduced the infiltration capacity of the soil and could cause flooding in an event of heavy down pour in the area. The increasing salinity also affects the geotechnical properties of the soil (Pathak and Pathak, 2016) and could impede infrastructural development in the area. In addition, increasing salinity would lead to crop yield losses. As the sanity of the water increases, the osmotic function of the plants is reversed causing the plants roots to rather loose water to the soil. The crops eventually die due to dehydration. The high salt content also reduces the variety of food crops that can be cultivated in the area since not all crops can survive in soil with high salinity level. This could result in scarcity of food as well as loss of jobs in the area since the soil will no longer be fertile for farming.

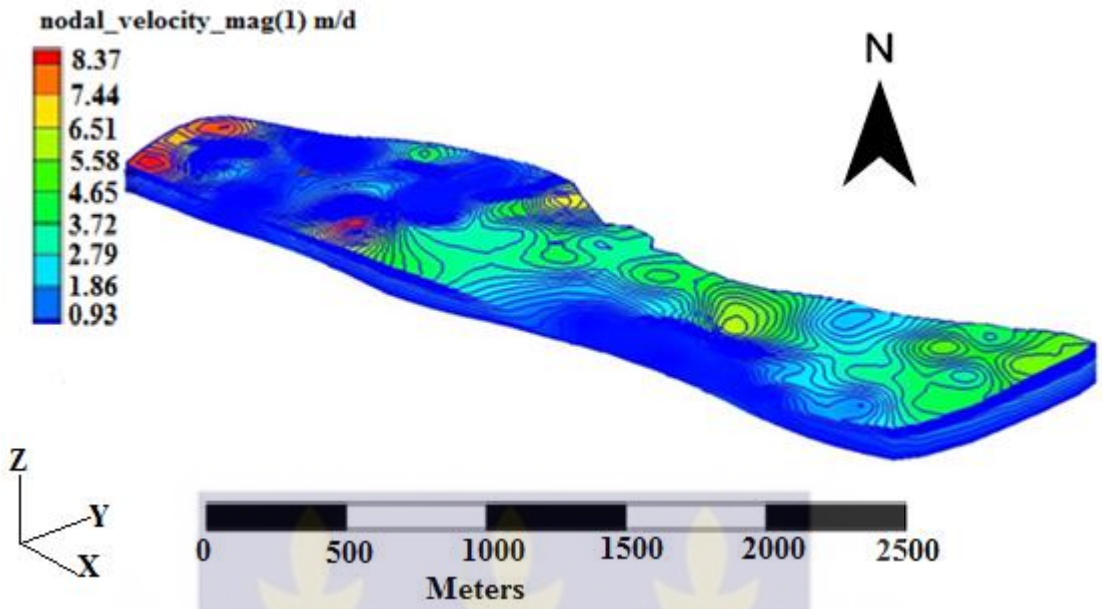


Figure 4.9: A 3D map showing spatial variations in nodal velocities for March 2016.

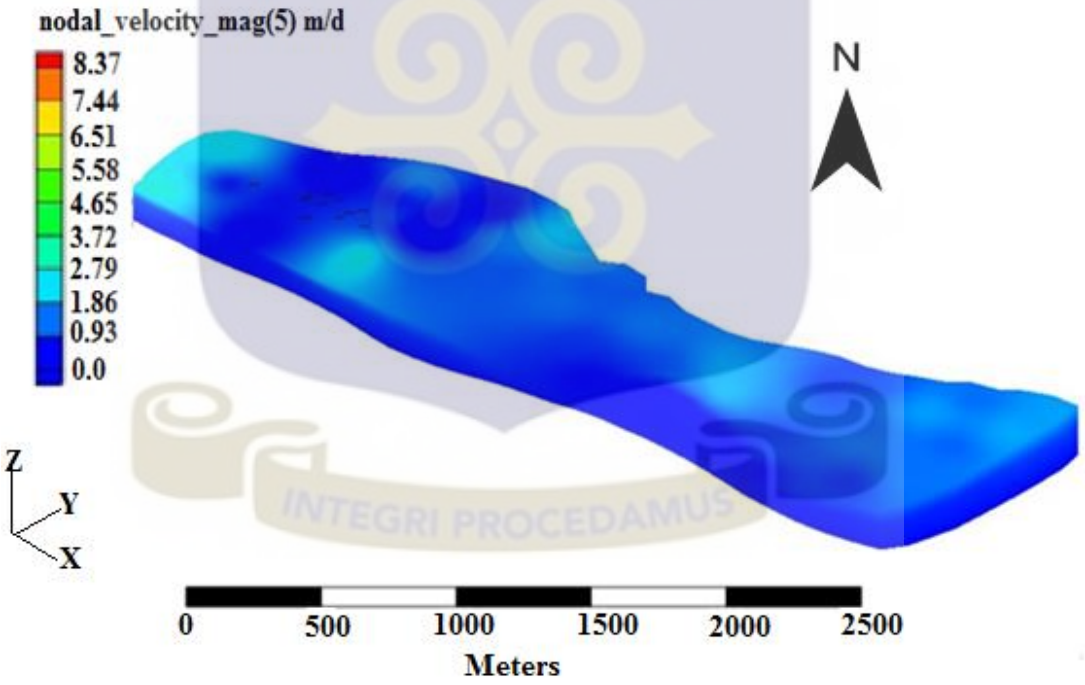


Figure 4.10: A 3D map showing variations in groundwater velocities for June 2016

## 4.3 TOTAL DISSOLVED SOLIDS AND GROUNDWATER DENSITY

In order to properly simulate density dependent flow, Total Dissolved Solids (TDS) measurements were taken for a period of five months and imported into the model for the different times. The calibrated model shows temporal and spatial variations in Total Dissolve Solids for the different stress periods throughout the domain. According to Essink (2001), the density of groundwater should be considered as a function of pressure, temperature and concentration of dissolved solids:

$$\rho = f(p, T, S) \quad (4.1)$$

Where:

$\rho$ = density ($kg/m^3$), p = pressure ($M\ L^{-1}\ T^{-2}$), T = temperature ($^oC$),

S = salinity or total dissolved solids (TDS) (mg/l).

Although pressure and temperature play a role on the density of groundwater, their effect is of minor significance compared to that of the impact of dissolved solids concentration within many hydrogeologic systems (Essink, 2001). Henceforth, the density of groundwater is often only related to the concentration of dissolved solids in the groundwater. The spatial distribution of TDS in the area was obtained after a calibrated transient state simulation. The TDS in the area ranges from 180 mg/l to 1800 mg/l with an average of 990 mg/l. High levels of TDS were observed at the northwest south southeast and middle portions of the study area whereas low TDS occur around the northeast and some sections in the middle of the domain (Fig. 4.12). The TDS concentration for the initial stress period (January 2016) was relatively lower and somehow uniform across the study area as presented in Figure 4.11.

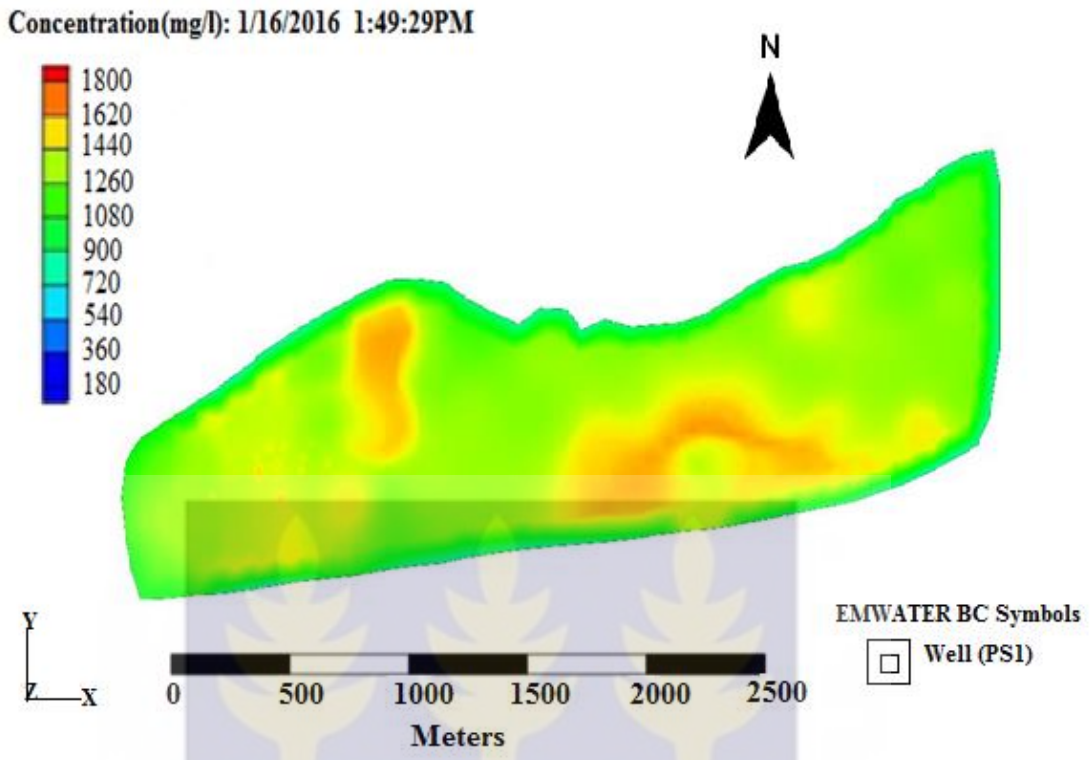


Figure 4.11: A map showing spatial distribution of TDS for January 2016

However, for successive stress periods the model shown distinctions in variation of TDS which follows an increasing pattern in terms of the distributions. The source of increasing groundwater salinity could be several: evaporative enrichment of residual water; seawater intrusion and the use of manure and related agricultural chemicals on the farms. Banoeng-Yakubo et al. (2005) observe significant temporal variations in groundwater salinity in the area. Generally, prior to the onset of the rains, there is an increasing trend in the TDS, arising largely from saline water intrusion and evaporative enrichment of the residual water. The variations in groundwater density have affected the flow geometry of groundwater in the area Figure 4.7. It is therefore important to incorporate the effect of density variations in groundwater modeling in order to account for groundwater flow in both horizontal and vertical directions and for more accurate predictions of flow rates. As the density of the water increases, gravity effect sets in

causing the groundwater to flow more vertical rather than lateral (Don et al., 1999 and Essink, 2001). This increasing vertical flow due to density influence coupled with the declining water table caused by over pumping and evapotranspiration activities reduces the availability of freshwater in wells in the area. Two major contaminant plumes (areas of high TDS) were identified as the source of TDS in the shallow aquifer after the study. The first plume was found migrating from the northwestern part of the domain which forms the boundary of the Keta lagoon. The second plume roved from the southern part which also forms the boundary of the ocean in the study area shown in Figure 4.12.

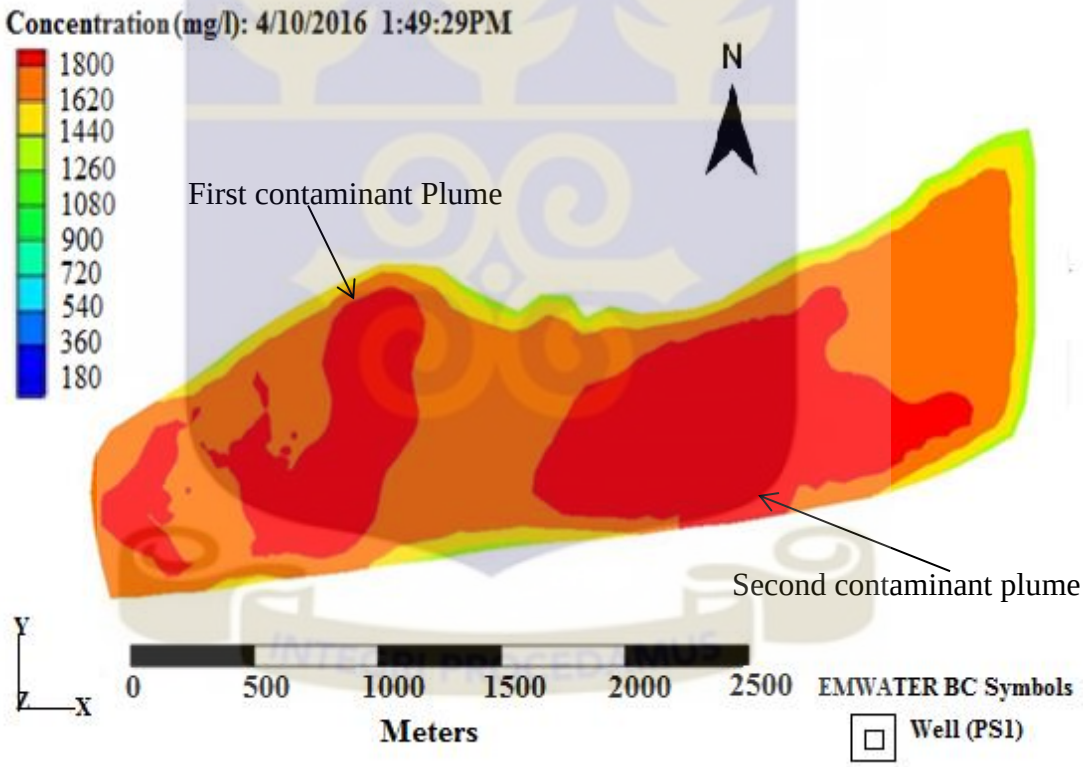


Figure 4.12: A map showing the main contaminant plumes in the study area

This suggests that the source of salinity in the aquifer is due to influx from both the lagoon and the ocean respectively. The suggestion is in agreement with Yidana et al. (2010) who used multivariate statistical and spatial analyses techniques to assess groundwater quality in the same aquifer and concluded that, the source of salinity in the aquifer was from seawater intrusion and weathering of minerals. Observing from maps of successive stress periods (Fig 4.12 to 4.18), the plumes began to spread (disperse) through the study domain. This dispersion is facilitated by the relatively high groundwater velocities in the aquifer with the flow patterns depicting that of the plume shape in the area. The rapid spread of this contaminant in the shallow aquifer could be catastrophic to farming activities in the area considering the fact that the source of water for these activities is from the shallow aquifer.

Continuous and haphazard pumping of groundwater for irrigation coupled with evapotranspiration activities in the study area has also resulted in drastic decline in the hydraulic head. The severe decline in hydraulic head facilitates up coning of the saline water wedge and further forces the wedge to move towards the freshwater aquifer. This phenomenon will subsequently elevate the TDS concentrations in the aquifer. In the major rainy season, however, the amount of salinity in the aquifer is reduced due to the direct recharge water from heavy down pour into the aquifer (Yidana and Chegbeleh, 2013). The infiltrated groundwater surges up the level of the water table in the unconfined aquifer and reverses the flow of the groundwater from the aquifer back to the sea which serves to reduce the salinity in the aquifer.

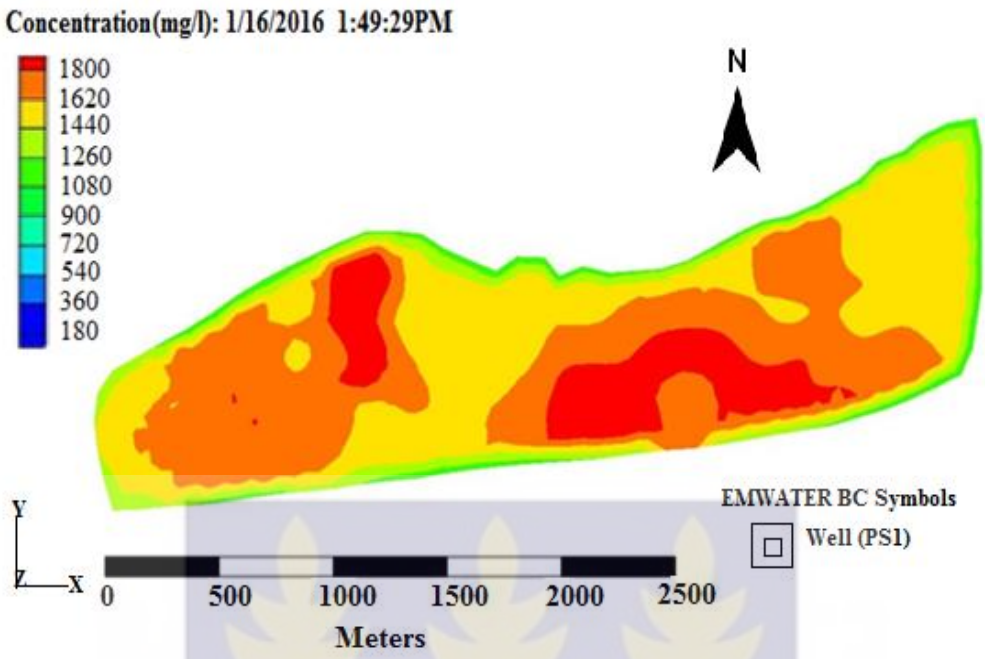


Figure 4.13: A 2D map showing spatial distribution of TDS for February 2016

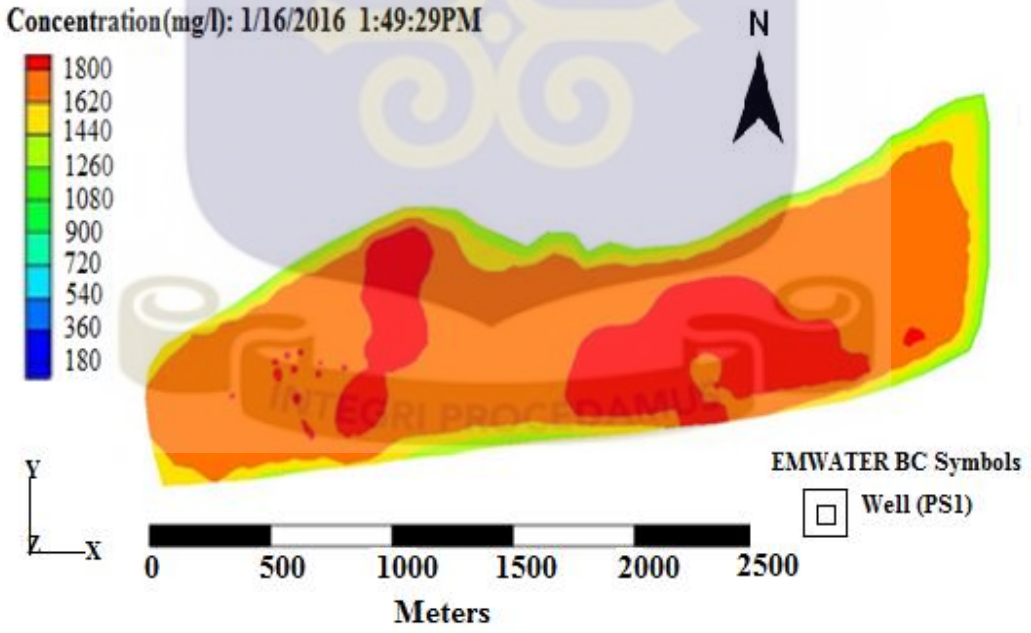


Figure 4.14: Spatial distribution of TDS concentration for April 2016 in 2D

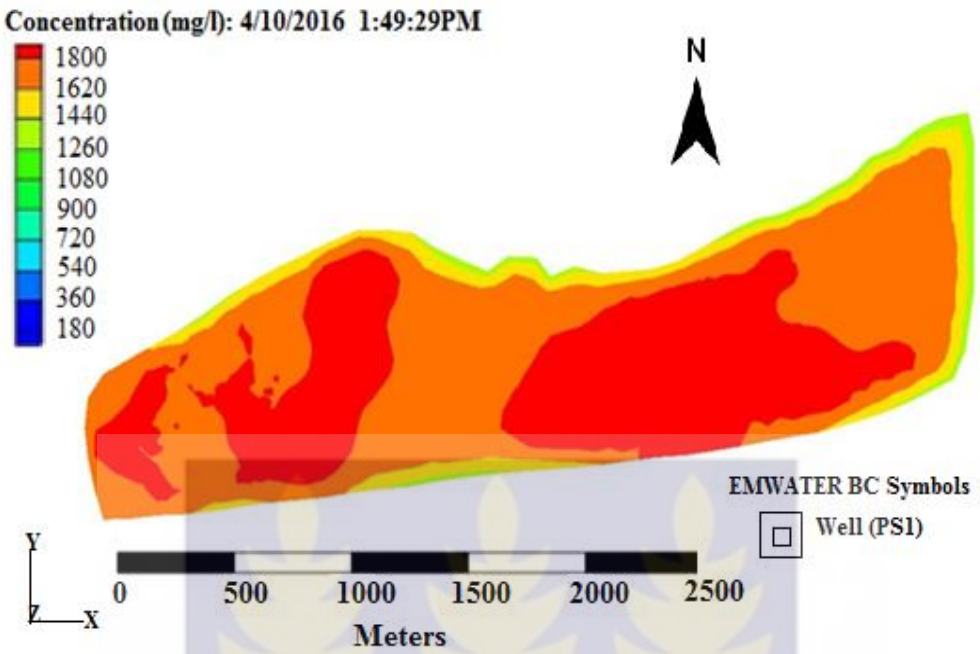


Figure 4.15: A spatial distribution of TDS concentration for June 2016

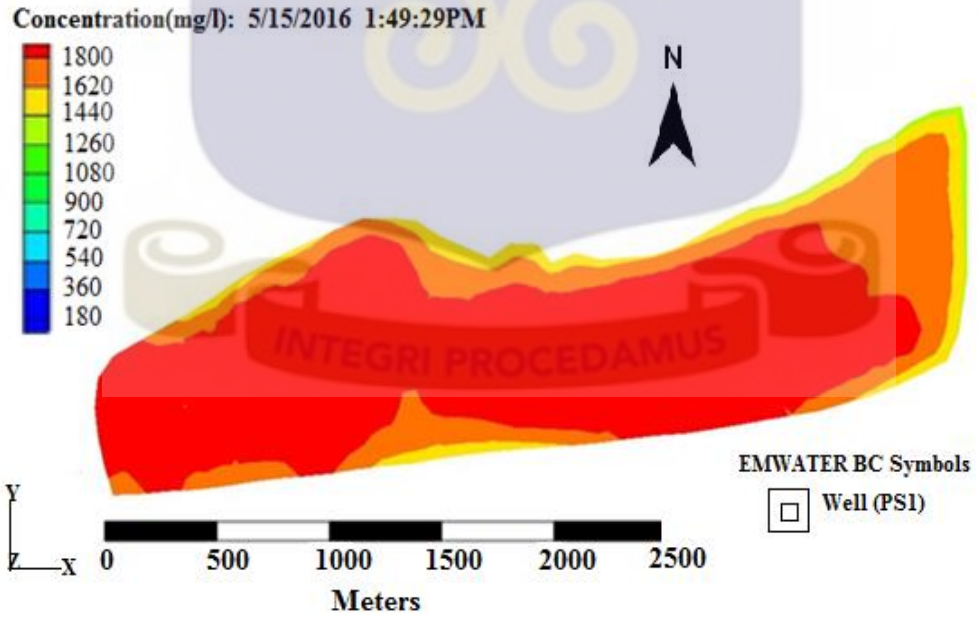


Figure 4.16: A map showing spatial distribution of TDS for January 2017

## 4.4 PRESSURE HEAD

The pressure head of groundwater measures the internal energy of the water due to pressure exerted on the aquifer (Bear, 1988). The pressure head of the study area was characterized for different stress periods (Fig. 4.19). The pressure head also known as static pressure heads appears uniform, generally low and fairly distributed throughout the study area except for some few cases within the study domain where pockets of high pressure heads occur. The generally low pressure heads in the area are an indication of the unconfined nature of the aquifer under study. The low level of the pressure head together with low elevations in the area accounts for the generally low hydraulic heads.

Groundwater pressure heads in the area range between -16 m and 24.2 m with an average pressure head of 4.1 m. The negative pressure head indicate unsaturated conditions and not necessarily dry conditions whiles positive pressure head infers saturated conditions. A greater percentage of the study area have a pressure head of negative which implies such areas are under saturated. High to average pressure heads occur at the northwest, middle and south portions of the study area with greater proportion having low pressure heads within the domain. Naturally, pressure head increases with depth below the water table (in the saturated zone) and decreases with height above the water table (in the unsaturated zone). A three-dimensional (3D) view of the model in the area shows that the pressure head increases with depth of the aquifer (Fig. 4.20). At deeper depth, the thickness and weight of the overburden increases causing the pressure exerted on the aquifer to also increase which in return causes the high-pressure head in the lower part of the unit.

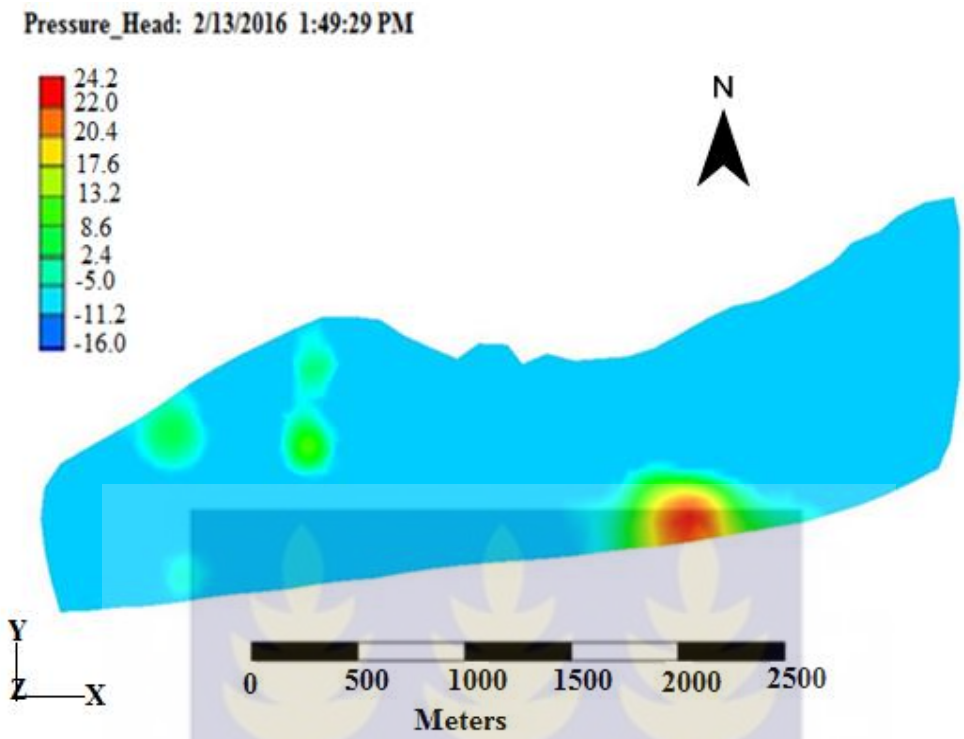


Figure 4.17: Distribution of pressure head in the study area.

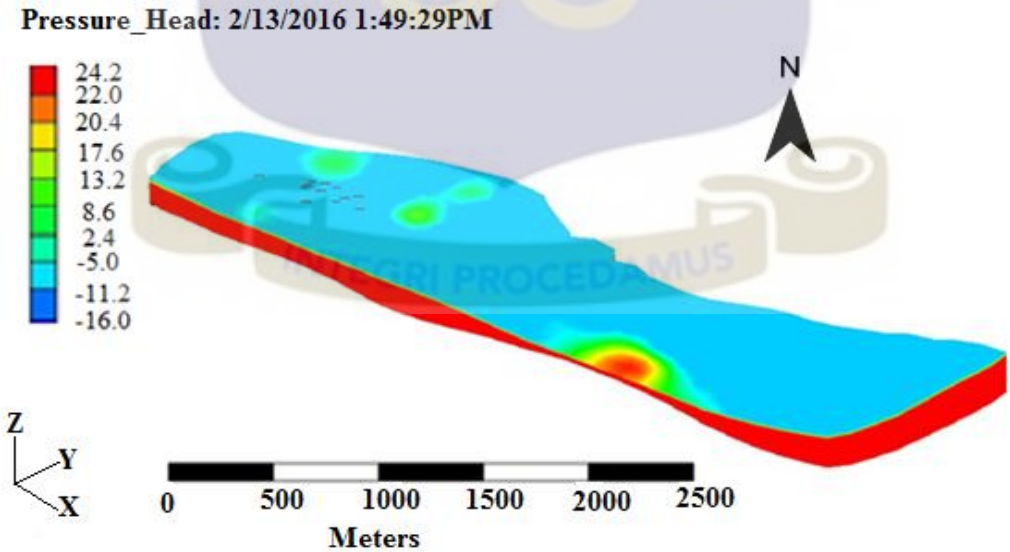


Figure 4.18: A map showing increased in pressure head with depth in the study area.

The pressure head at the top of the aquifer in the area varies in a decreasing fashion for the different stress periods. This is because pressure head of groundwater in an aquifer has an inverse relationship with both density and gravity according to the equation (Bear, 1988):

$$\Psi = \frac{P}{\gamma} = \frac{P}{\rho g} \qquad 4.2$$

Where Ψ = pressure head

P = fluid pressure

ϒ = specific weight

P = density of the fluid

g = acceleration due to gravity

The low-pressure heads in the area implies low hydraulic heads. When the hydraulic heads are reduced below the level of the seawater, inland migration of saline water occur (Davies and Peters, 1987 and Essink, 2001). The trend as observed serves to facilitate salinity intrusion in the area judging from the continue dropping in pressure heads which ultimately affects the hydraulic heads in the area. As groundwater density increases, the effect of gravity acting on the column of water also increases affecting the rate and patterns of flow of groundwater in the aquifer unit. The wells used in this research are completed in the unconfined aquifer and are shallower in depth, hence the vertical component of groundwater flow due to gravity will greatly reduce the availability of water in the wells.

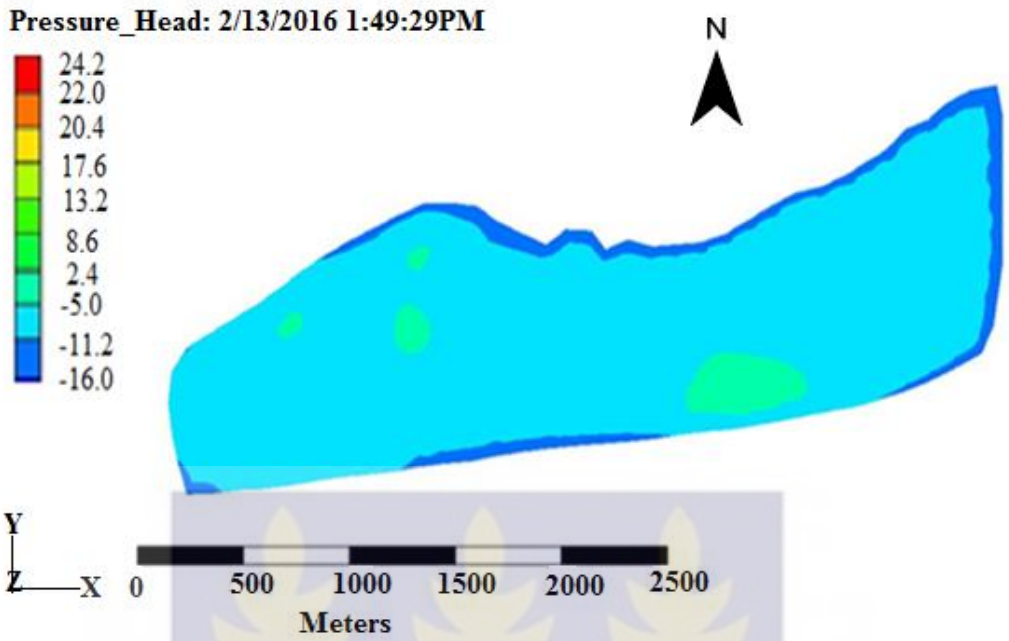


Figure 4.19: A maps showing decreasing pressure head in the study area for June 2016

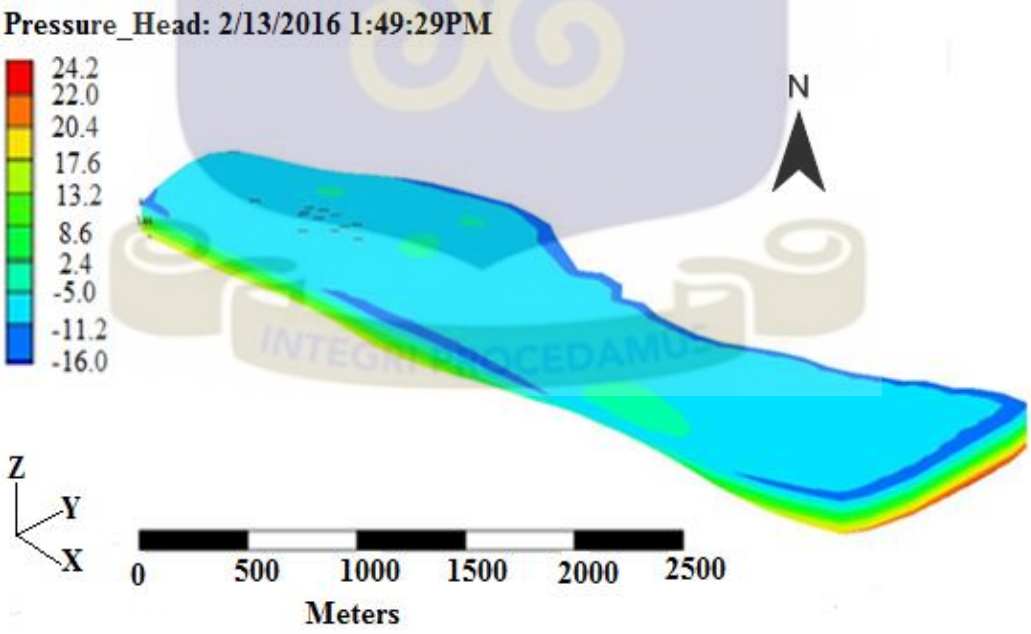


Figure 4.20: A map showing variations in pressure heads for June 2016

.

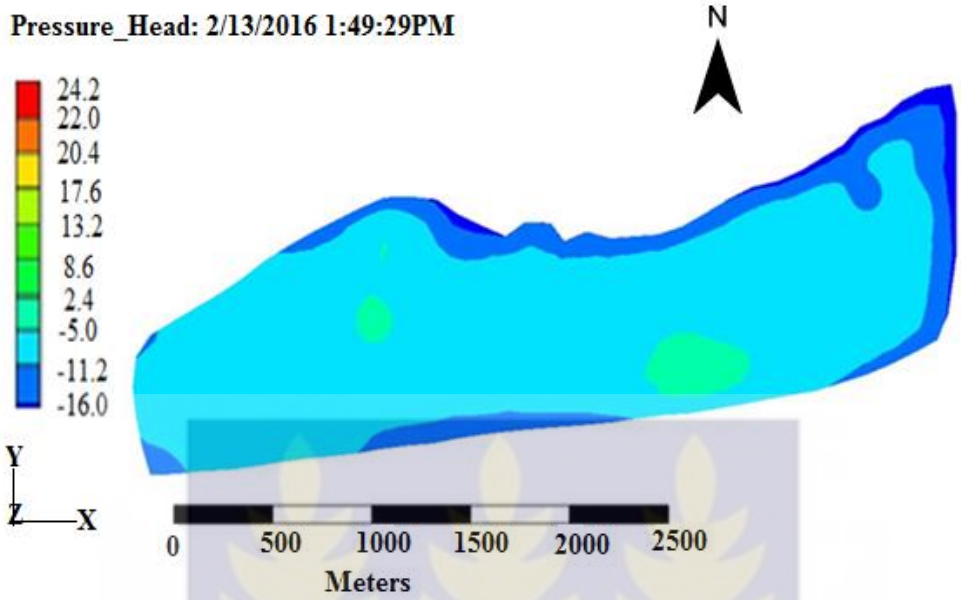


Figure 4.21: A map showing continuous decline in pressure head for January 2017

The pressure heads in the area is lowered over time and is caused by the continuous decline in total hydraulic head resulting from high groundwater abstractions for irrigation

## 4.6 SCENARIO ANALYSIS

It is expected that with the overwhelming interest in groundwater abstractions along the Keta strip for irrigation activities, scenarios analysis is carried out in order to advise farmers and policy makers on the management strategies to adopt in order to protect the resource and control the incidence of saline water intrusion in the area. The calibrated transient model was used to predict the effects of various scenarios of increasing groundwater abstraction and surface activities (TDS) on the total hydraulic head. Twenty-eight abstractions wells were created to reflect the groundwater usage in

the area and initial flow rates assigned to them. The flow rates assigned to wells were based on the yield of various pumping wells in the study area.

Table 4.1: A table showing initial flow rate for the scenarios analyses

| Tube Wells | Initial flow rate (m3/d) | Tube Wells | Initial Flow rate (m3/d) |
|---|---|---|---|
| ANL_BH01 | -208 | ANCC_BH15 | -221 |
| ANL_BH02 | -600 | WHU_BH16 | -810 |
| AHF_BH03 | -864 | WHU_BH17 | -780 |
| AHF_BH04 | -864 | WHU_BH18 | -701 |
| AHF_BH05 | -862 | WHU_BH19 | -623 |
| AHF_BH06 | -864 | WHU_BH20 | -550 |
| AHF_BH07 | -400 | WHU_BH21 | -864 |
| ANSHS_BH08 | -130 | WHU_BH22 | -211 |
| ANSHS_BH09 | -420 | WHU_BH23 | -315 |
| ANTC_BH10 | -660 | ANF_BH24 | -295 |
| ANL_BH11 | -305 | ANF_BH25 | -630 |
| ANL_BH12 | -608 | AHF_BH26 | -660 |
| ANHF_BH13 | -310 | AHF_BH27 | -800 |
| ANF_BH14 | -230 | AHF_BH28 | -864 |

For the first scenario, the flux rate, hydraulic conductivity and porosity were kept constant whiles abstraction increased by the following rates 10%, 25%, 30%, 50%, 100%, 200% and 300% to check the effects on the hydraulic head. The effects of these abstractions are presented in Table 4.2. This scenario was performed to address issues relating to increasing irrigation activities coupled with population rise in the area. Thus, the implication of this observation is that groundwater will progressively be mined from the aquifer if recharge remains constant whilst abstraction rates increases as a result of increasing irrigation due to population growth in the coming years.

Table 4.2: A table showing changes in total hydraulic heads of 28 wells used for the scenarios analyses of increasing abstraction rate up to 300%.

| **Well** | **W01** | **W02** | **W03** | **W04** | **W05** | **W06** | **W07** |
|---|---|---|---|---|---|---|---|
| **Initial** | 19.7258 | 12.8472 | 21.7651 | 20.5866 | 15.2689 | 18.173 | 21.5986 |
| **10%** | 19.5831 | 12.6055 | 19.622 | 20.2632 | 15.0221 | 18.627 | 20.3384 |
| **25%** | 19.066 | 11.8752 | 19.484 | 20.7979 | 14.7672 | 17.3624 | 19.8651 |
| **30%** | 15.0972 | 10.5011 | 18.1953 | 19.3431 | 14.4855 | 17.937 | 19.1022 |
| **50%** | 14.819 | 9.603 | 16.794 | 20.7113 | 13.5934 | 15.1258 | 17.4666 |
| **100%** | 9.2577 | 1.0028 | 10.444 | 19.6744 | 3.9975 | 12.7551 | 10.472 |
| **200%** | 5.2164 | 0 | 4.0003 | 20.0522 | 1.066 | 4.876 | 8.8213 |
| **300%** | 3.0018 | 0 | 1.3259 | 20.21 | 0 | 0.9499 | 5.4001 |
| **Wells** | **W08** | **W09** | **W10** | **W11** | **W12** | **W13** | **W14** |
| **Initial** | 21.821 | 17.5739 | 10.5763 | 12.8517 | 14.8646 | 21.3857 | 17.7188 |
| **10%** | 21.8701 | 17.3301 | 10.2509 | 12.4588 | 13.41 | 21.112 | 16.814 |
| **25%** | 21.428 | 16.8074 | 9.238 | 11.7445 | 13.4647 | 18.3103 | 15.962 |
| **30%** | 20.2113 | 16.3188 | 9.044 | 11.012 | 12.712 | 18.9446 | 14.4697 |
| **50%** | 18.0286 | 14.4061 | 7.004 | 10.107 | 12.6979 | 17.389 | 11.111 |
| **100%** | 13.9152 | 12.64 | 0 | 6.5763 | 7.329 | 1.6333 | 6.9281 |
| **200%** | 12.847 | 5.4027 | 0 | 3.0941 | 4.211 | 0 | 3.065 |
| **300%** | 4.5081 | 0 | 0 | 0 | 1.722 | 0 | 0 |
| **Well** | **W15** | **W16** | **W17** | **W18** | **W19** | **W20** | **W21** |
| **Initial** | 20.845 | 21.466 | 15.857 | 20.576 | 13.173 | 22.851 | 19.694 |
| **10%** | 20.203 | 21.054 | 15.362 | 20.052 | 12.8105 | 22.593 | 19.1574 |
| **25%** | 20.594 | 20.821 | 14.6601 | 16.61 | 12.321 | 21.189 | 18.7803 |
| **30%** | 17.0199 | 18.375 | 14.0078 | 14.992 | 11.9167 | 18.117 | 17.9904 |
| **50%** | 13.1574 | 18.746 | 11.252 | 13.155 | 10.6554 | 17.942 | 16.8105 |
| **100%** | 4.2549 | 4.311 | 6.601 | 12.35 | 3.021 | 13.022 | 8.3212 |
| **200%** | 0 | 1.563 | 1.299 | 0 | 1.277 | 4.5651 | 2.5837 |
| **300%** | 0 | 0.72 | 0 | 0 | 0.31 | 2.1574 | 0 |

Table 4.2 contd.

| Well | W022 | W023 | W024 | W025 | W026 | W027 | W028 |
|---|---|---|---|---|---|---|---|
| **Initial** | 20.173 | 18.122 | 11.521 | 19.694 | 15.817 | 21.626 | 17.5739 |
| **10%** | 20.085 | 18.307 | 12.1412 | 18.713 | 15.322 | 19.991 | 17.7049 |
| **25%** | 17.417 | 18.791 | 6.632 | 19.008 | 14.894 | 16.1351 | 16.3524 |
| **30%** | 19.075 | 16.1392 | 5.4028 | 15.412 | 12.513 | 15.827 | 16.176 |
| **50%** | 16.263 | 15.527 | 3.947 | 14.543 | 9.408 | 13.458 | 15.619 |
| **100%** | 3.364 | 12.705 | 1.606 | 6.204 | 4.0112 | 7.702 | 4.544 |
| **200%** | 1.01 | 12.203 | 0.081 | 2.7793 | 0 | 0.2611 | 2.886 |
| **300%** | 0 | 10.71 | 0 | 0.6152 | 0 | 0 | 2.294 |

There was no noticeable shift in the nature of the potential field when the current abstraction rate was increased up to about 50% in the existing pumping wells as presented in Table 4.2. However, increasing the abstraction rate above 100% causes a drastic reduction in the hydraulic heads in the domain. Over abstraction of water from the aquifer without allowing adequate time for the system to replenish can lead to depletion of the groundwater resource. When the initial rates assigned to the various wells were increased to 100% and above, the nodes in some of the wells run dried due to drastic decline in hydraulic heads. The consequence of this is that, the entire ecosystem stands the risk of being wiping-out and the livelihood of residence endangered if the abstraction rates are not regulated.

Another serious problem that could occur from excessive withdrawal of groundwater from the wells in the area is the up coning of saline water wedge. The study area is a coastal environment bordered by the Gulf of Guinea to south and the Keta lagoon to the north/west. The issues of saline water intruding into freshwater aquifers have become a serious problem throughout world in the wake adverse climatic changes causing the rise in oceanic water level.

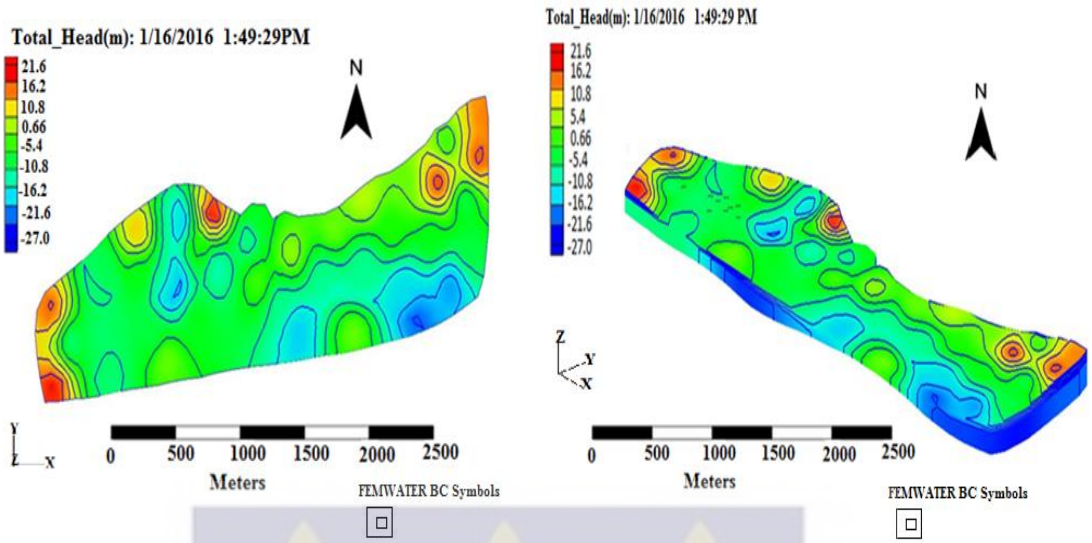


Fig. 4.22 A Fig 4.22 B

Figure 4.22: Maps showing spatial distribution of hydraulic heads after 10% increment in abstraction rate

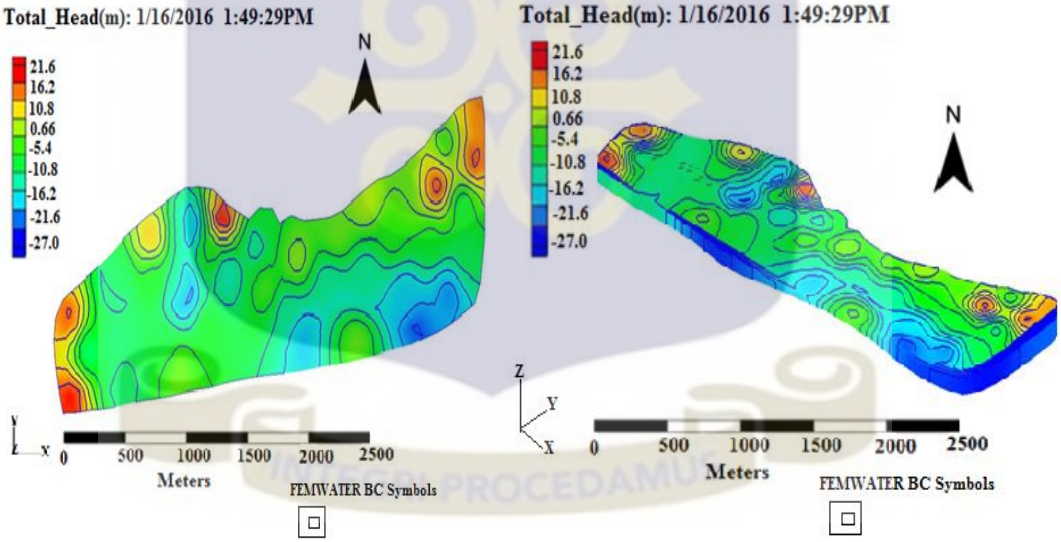


Fig 4.23 A Fig 4.23 B

Fig 4.23: Maps showing total hydraulic heads distribution after 25% increment in abstraction rate

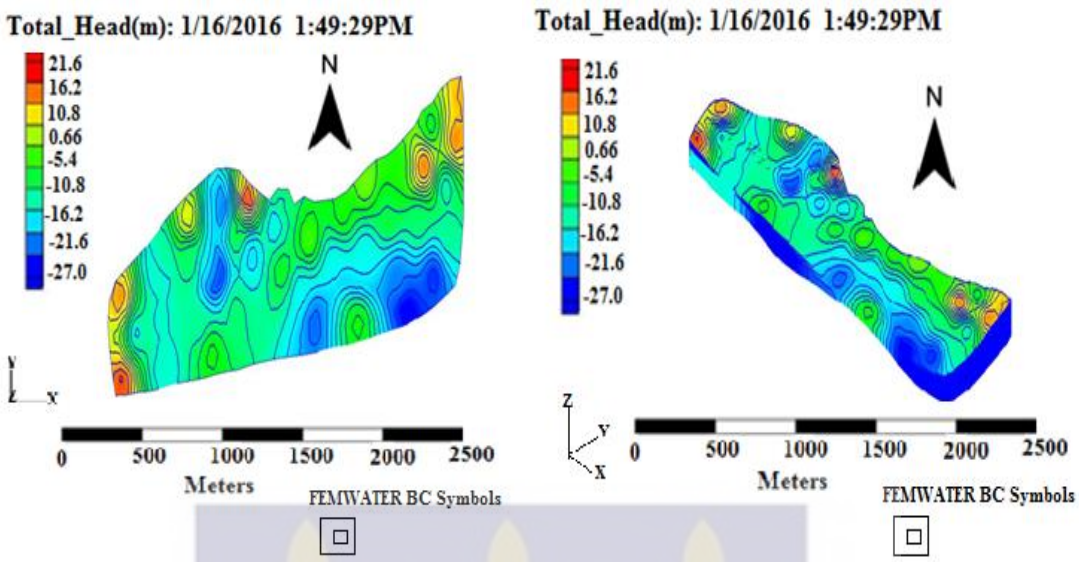


Fig 4.24 A Fig 4.24 B

Fig 4.24: Maps showing total hydraulic head distribution after 30% increment in abstraction rate

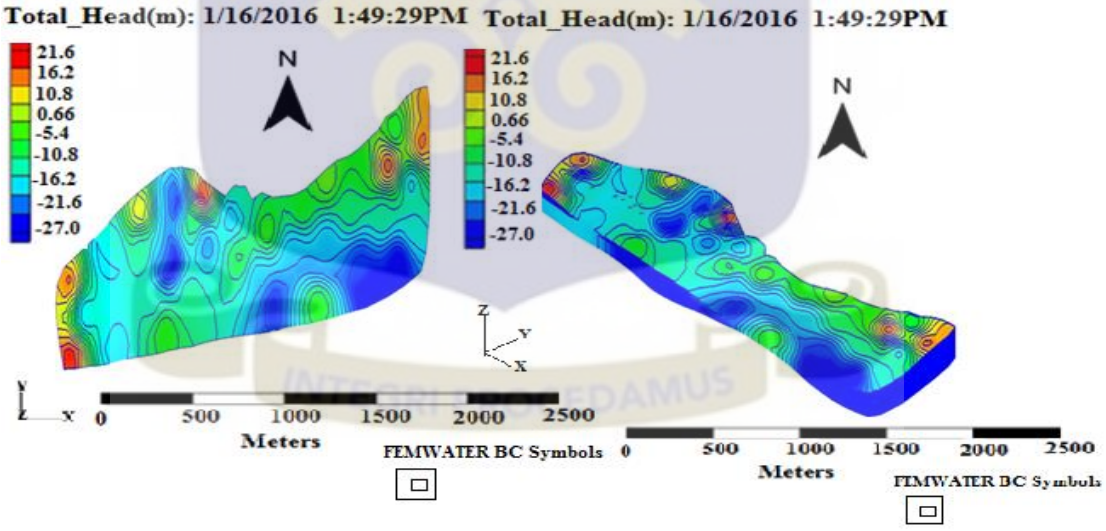


Fig 4.25 A Fig 4.25 B

Fig 4.25: Maps showing total hydraulic head distribution after 50% increment in abstraction rate

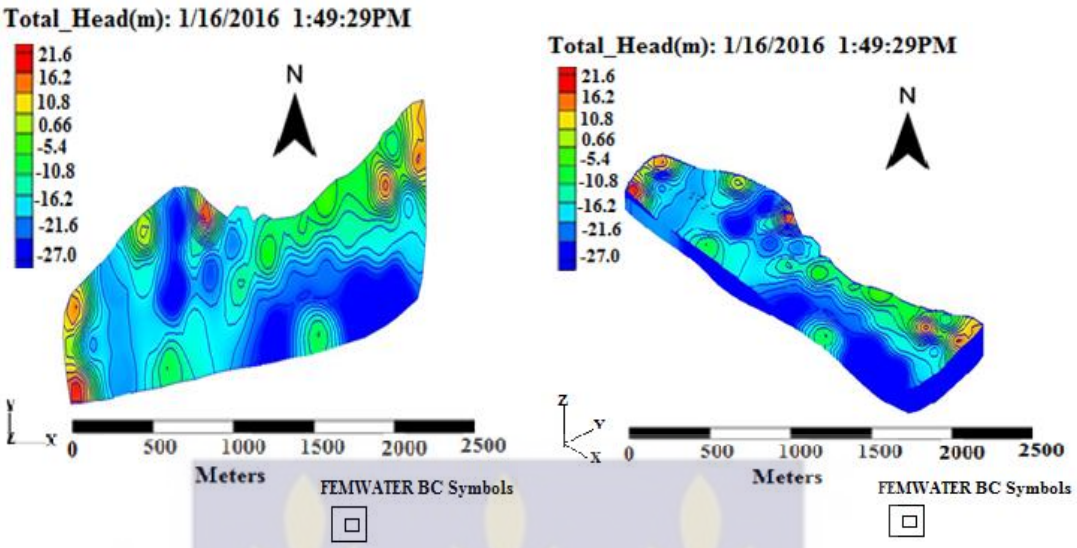


Fig 4.26 A Fig 4.26 B

Fig 4.26: Maps of total hydraulic head distribution after 100% increment in abstraction rate

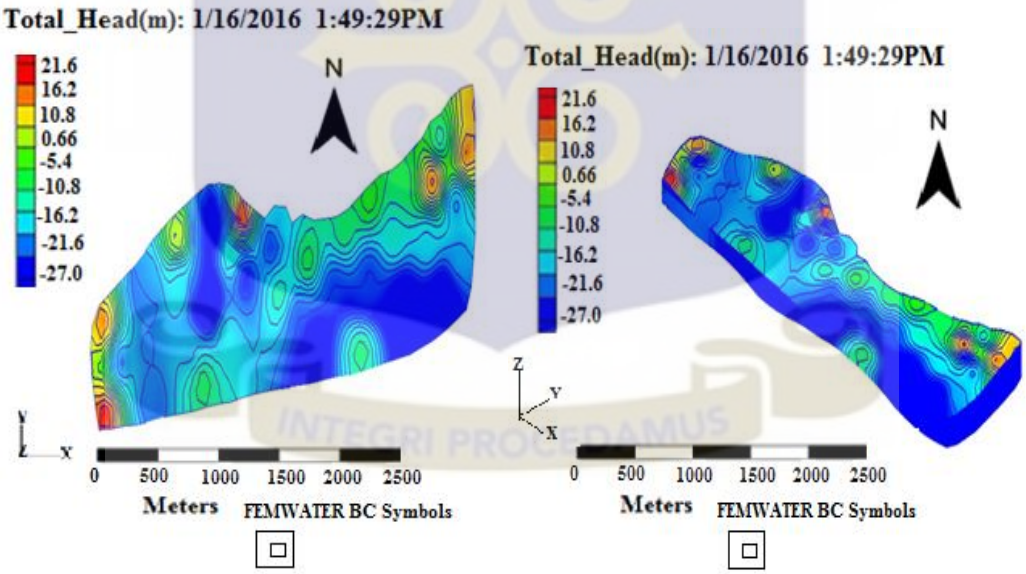


Fig 4.27 A Fig 4.27 B

Fig 4.27: Maps showing hydraulic head distribution after 200% increment in abstraction

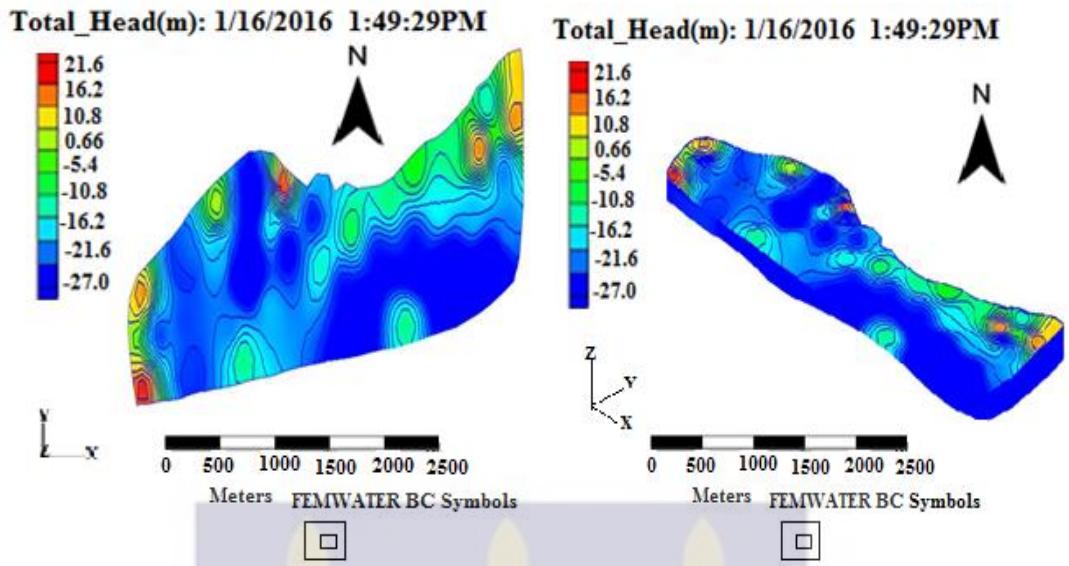


Fig 4.28 A Fig 4.28 B

Fig 4.28: Maps showing hydraulic head distribution after 300% increment in abstraction

For the second scenario, the flux rate, porosity and abstraction rates remain the same whilst TDS was increased by 10%, 25%, 50% and 100% based on increasing surface activities in the area. This was done to check the effects of increasing groundwater density on hydraulic head, pressure head and groundwater nodal velocities. The density of groundwater was increased by increasing TDS via surface activities. There were no obvious shifts in the nature of potential fields for initials stress period. However, subtle changes in total hydraulic heads along the boundaries of both the coastal and lagoon start to decrease after increasing surface activities up to 100% to reflect increase in TDS in the area (Fig 4.39). This observation suggests that the groundwater along those boundaries already have higher densities possibly due to the salinity intrusion and the increasing of TDS only serve to further increase the density causing the effect of gravity to become greater.

Table: 4.3 A Table showing changes in hydraulic heads of 30 wells for scenario of maintaining abstraction rates with increasing surface activities by 10%, 25%, 50% and 100%.

| **Well** | **W01** | **W02** | **W03** | **W04** | **W05** | **W06** | **W07** |
|---|---|---|---|---|---|---|---|
| Initial | 19.7258 | 12.8472 | 21.7651 | 10.5866 | 15.268 | 18.173 | 21.5986 |
| 10% | 19.7258 | 12.8469 | 21.7652 | 10.5573 | 15.268 | 18.172 | 21.5884 |
| 25% | 19.6451 | 12.7725 | 21.8253 | 10.4894 | 15.263 | 18.328 | 21.3499 |
| 50% | 19.6622 | 12.5881 | 21.8337 | 10.2767 | 15.405 | 18.112 | 21.3052 |
| 100% | 19.3752 | 12.4042 | 21.6225 | 9.8115 | 15.417 | 18.076 | 21.1211 |
| **Well** | **W08** | **W09** | **W10** | **W11** | **W12** | **W13** | **W14** |
| Initial | 21.821 | 17.5739 | 10.5763 | 12.8517 | 14.8646 | 22.3857 | 17.7188 |
| 10% | 21.822 | 17.5729 | 10.5763 | 12.8427 | 14.8644 | 22.3469 | 17.6694 |
| 25% | 21.821 | 17.5727 | 10.5761 | 12.8364 | 14.8377 | 22.3673 | 17.8305 |
| 50% | 21.753 | 17.5633 | 10.6214 | 12.6077 | 14.5333 | 22.1211 | 17.5227 |
| 100% | 21.508 | 17.3648 | 10.5425 | 12.6176 | 14.2062 | 22.3582 | 17.5053 |
| **Well** | **W15** | **W16** | **W17** | **W18** | **W19** | **W20** | **W21** |
| Initial | 22.845 | 14.466 | 16.857 | 20.576 | 13.173 | 22.851 | 19.694 |
| 10% | 22.845 | 14.456 | 16.752 | 20.577 | 13.442 | 22.793 | 19.657 |
| 25% | 22.833 | 14.384 | 18.663 | 20.419 | 13.461 | 22.774 | 19.582 |
| 50% | 22.769 | 14.389 | 18.724 | 20.509 | 13.709 | 22.583 | 19.704 |
| 100% | 22.466 | 14.107 | 18.495 | 19.811 | 13.813 | 22.499 | 19.683 |
| **Well** | **W22** | **W23** | **W24** | **W25** | **W26** | **W27** | **W28** |
| Initial | 22.173 | 18.122 | 11.521 | 19.694 | 15.817 | 21.626 | 17.574 |
| 10% | 22.166 | 18.122 | 11.572 | 19.675 | 15.817 | 19.648 | 17.483 |
| 25% | 21.864 | 18.353 | 11.488 | 19.581 | 15.777 | 20.594 | 16.647 |
| 50% | 22.172 | 18.157 | 11.483 | 19.361 | 18.321 | 20.214 | 15.633 |
| 100% | 22.005 | 18.208 | 10.722 | 19.442 | 18.267 | 20.111 | 15.486 |

The increasing effect of gravity on groundwater induces a vertical flow component due to density of the water and causes the pressure head to reduce (Davies and Peter, 1987). Pressure head being a component of the total hydraulic head then result in the lowering of groundwater head around those boundaries.

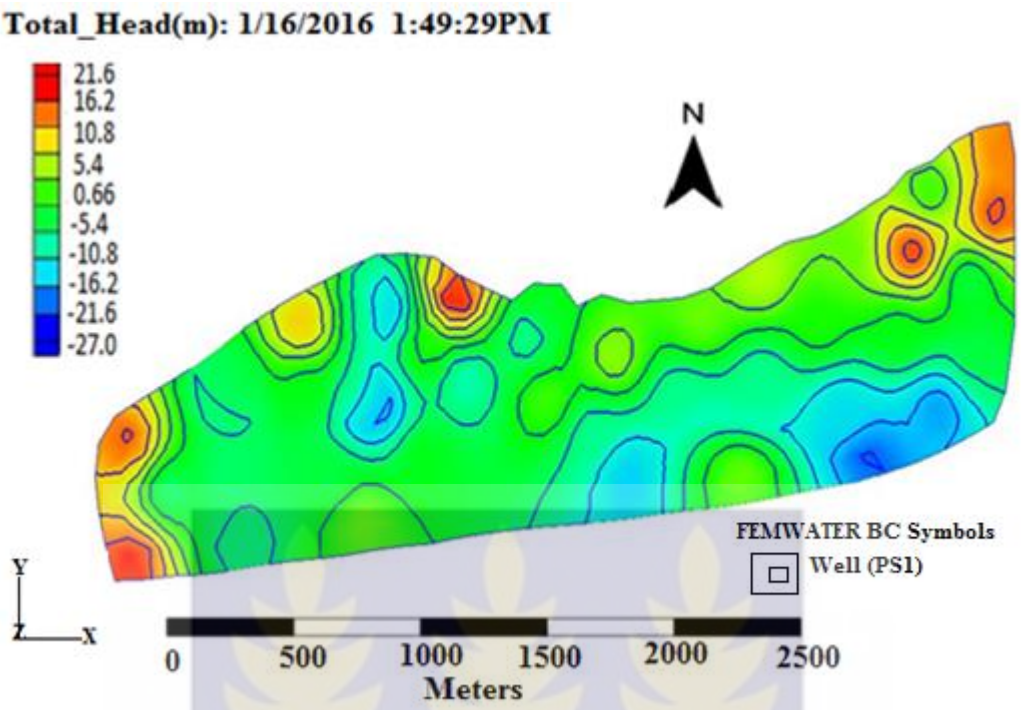


Figure 4.29: Total hydraulic head distribution after 10% in TDS

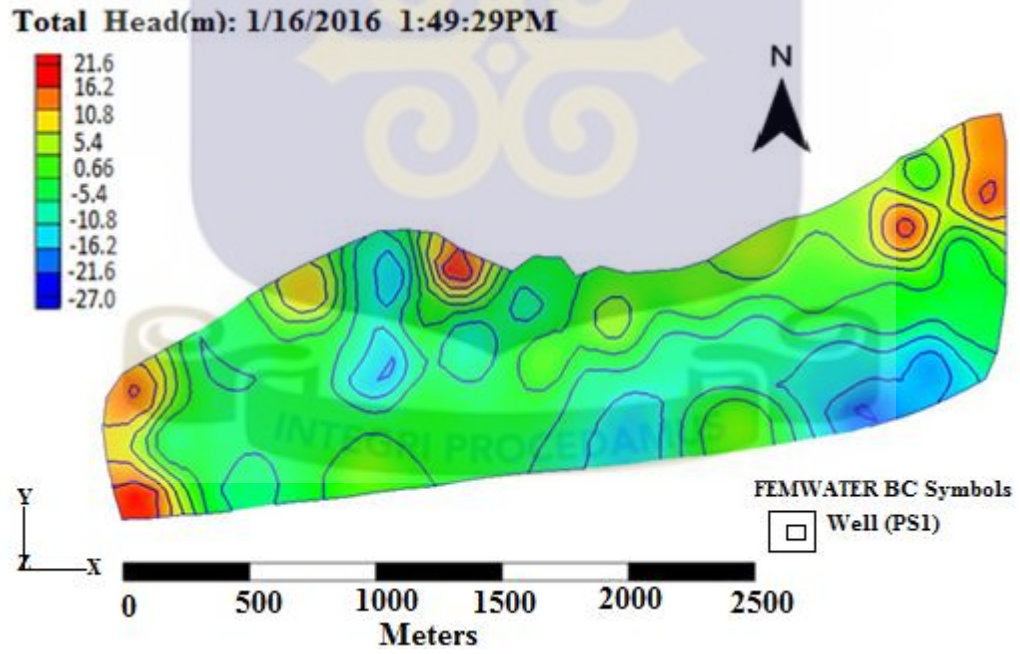


Figure: 4.30: Total head distribution after 25% increment in TDS

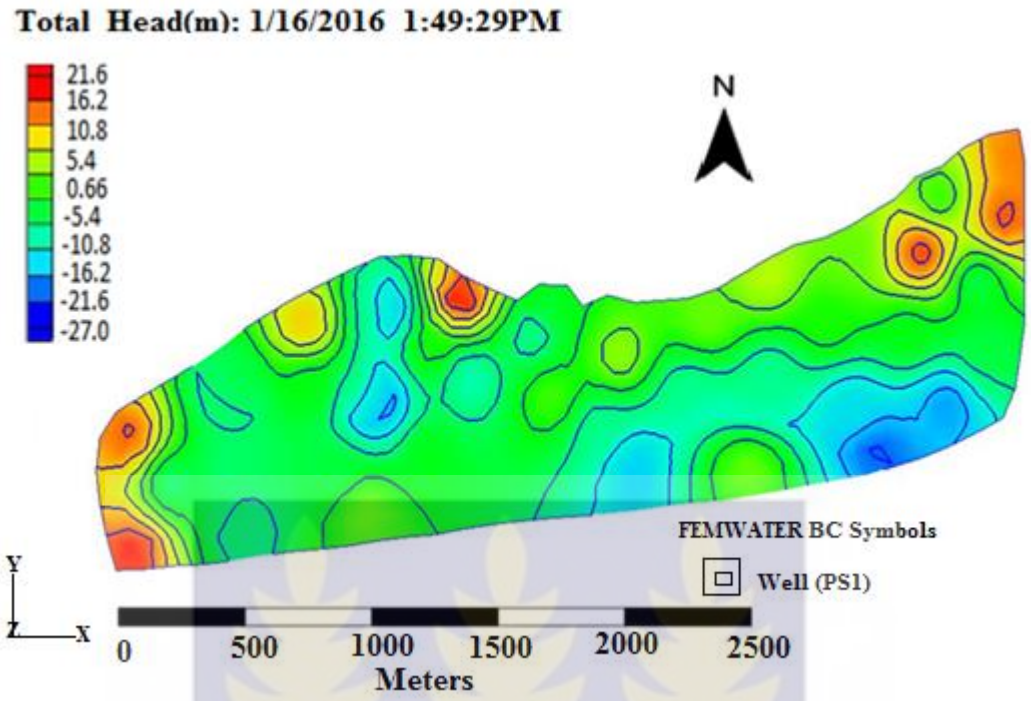


Figure: 4.31: Total head distribution after 50% increment in TDS

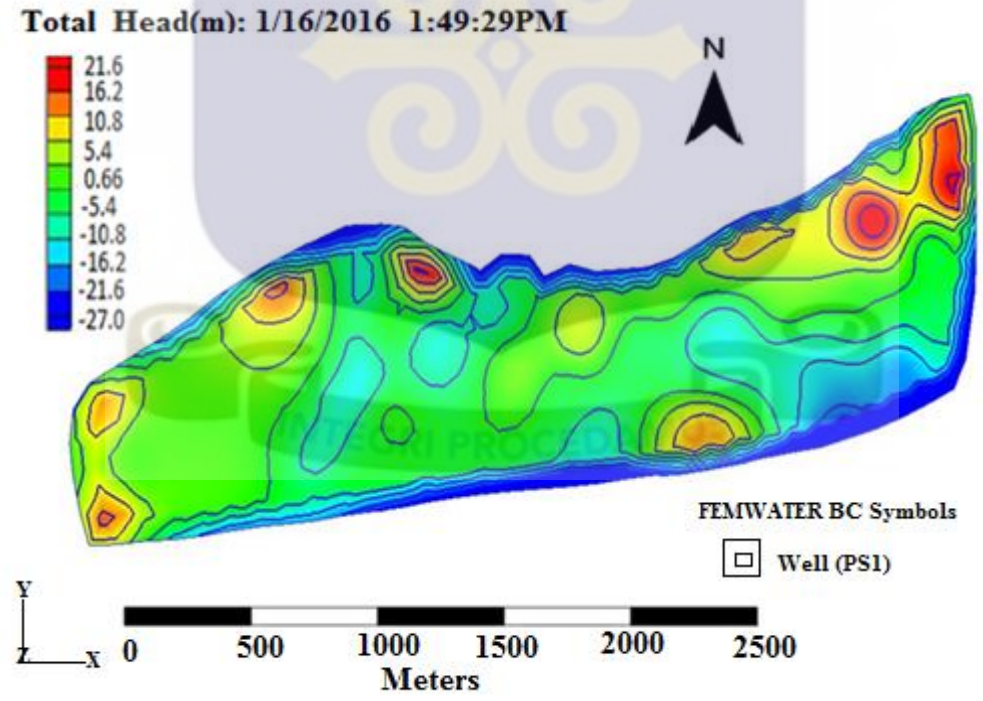


Figure 4.32: Total head distribution after 100% increment in TDS

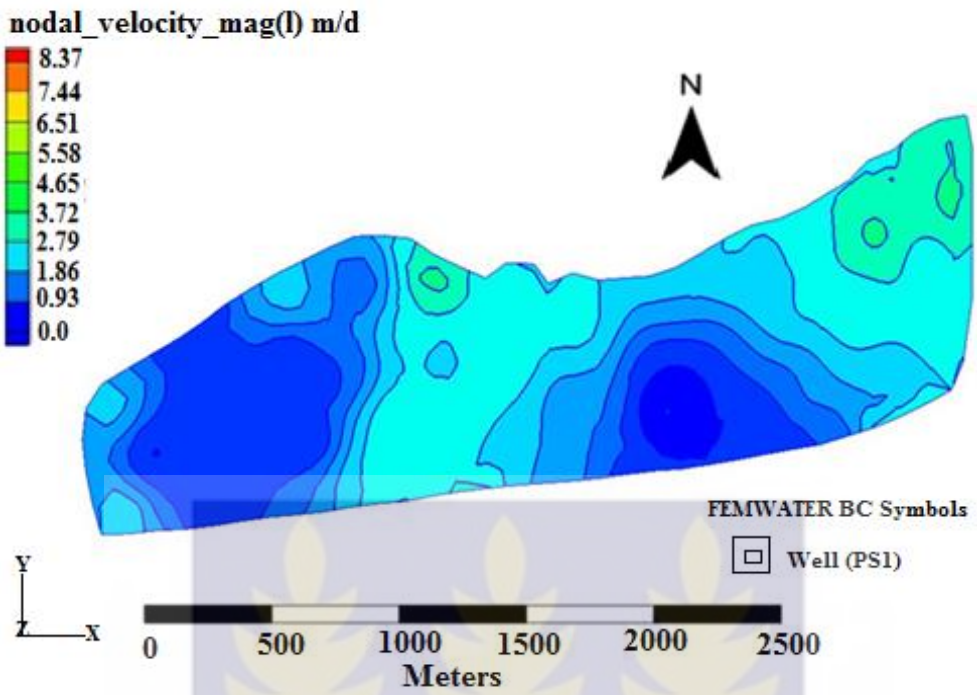


Figure 4.33: Nodal velocity distribution after 100% increment in TDS

There was general decreased in groundwater nodal velocity (figure 4.40) via the increasing surface activities in the area. Increase in TDS increases the density of the water which also makes the viscosity of the water high and reduces its mobility in the pore spaces.

# CHAPTER FIVE

# CONCLUSION AND RECOMMENDATIONS

## 5.1 CONCLUSIONS

A variable density transient groundwater numerical model has been calibrated for the unconfined aquifer system of the Keta Strip. The incorporation of density variations as induced by variations in the groundwater TDS, has presented a more realistic understanding of the general groundwater flow rate in the domain. The results suggest that the flow rate of groundwater in the area is influenced by the density of the water. The nodal velocities exhibit spatial variations dictated by variations in the groundwater TDS, suggesting that density is an important parameter which cannot be dispensed with when evaluating groundwater flow in coastal areas such as the Keta Basin. The spatial distribution of groundwater velocities ranges between 0.93 m/day to 8.37 m/day in the terrain. The highest velocity values were found in the northern, western and southwestern and parts of the study area and the lowest in the northwest and southeastern sections of the study area, and appear to be inversely related to the spatial pattern of distribution of the TDS.

The variations in groundwater velocities are likely attributed to both the variations in groundwater density and the variations in the clay content as well as the degree of sorting of sedimentary materials in the study area. The study found flow rates in the domain to be largely influenced by the density of the water in the aquifer. Local flow systems dominate the flow in the area in light of the shallow depth and unconfined nature of the aquifer. Groundwater velocities were also lower at areas characterized by high TDS giving an indication of the influence of density on the nodal velocities in the area.

TDS concentrations vary spatially throughout the study domain and also for the different stress periods. The TDS distribution in the area ranges between 180 mg/L to 1800 mg/L. The highest TDS values were observed at the northwestern, southern and middle parts of the study area whilst the lowest TDS occurred most at the northeastern sections of the area. It was also inferred from the maps of groundwater velocities that, the source of TDS in the shallow unconfined aquifer is mainly from the lagoon and the sea with little contributions from increasing surface activities. The concentration of TDS increases for different stress periods in the area progressively. For the first stress periods, TDS concentration was relatively low and uniform throughout the domain. This however was not the same for successive stress periods in the area. Whereas the TDS in the area increases for successive stress period, the nodal velocities reduce in same fashion, supporting the suggestion that the velocities in the area are influenced by the concentrations of TDS.

The pressure head produced by the transient state model ranges between -16.0 m to 24.2 m in the area. The generally low pressure heads in the area are an indication of the unconfined nature of the aquifer unit being studied. The pressure heads of the area appeared generally low and uniform for upper part of the unconfined unit with pockets of high pressure heads occurring at the southeastern and northwestern parts of the study area. The pressure heads however, was high at the lower limit which was found to be attributed to increasing pressure and compaction due to weight of overlying materials in the area. The low pressure head also characterized the generally low total hydraulic heads in the area.

The aquifer receives its recharge from direct precipitation with almost all the water infiltrating into the system due to the flat nature of the terrain. This was evident on the field with the fact that no run-off or soil erosion channels observed in the area. The unconfined aquifer holds huge volumes of water judging from the contour behavior of total hydraulic heads observed through scenario analysis. From the scenario analyses, increasing abstraction up to one hundred percent has no significant impact on the hydraulic heads. However when abstraction was increased beyond 100%, hydraulic heads in some of the mesh nodes were zero (dried).

## 5.2 RECOMMENDATIONS

- The research should be extended to cover the entire strip and the data collection (field visit) time interval should be increased to allow for clear observation of the concentration trend. At least data should be collected from months to a one-year interval.
- The use of chemicals by farmers in the area should be regulated to reduce the increasing incidence of TDS in the area.
- Subsurface dams should be constructed to safe-guard the aquifer from salinity intrusion and to ensure the availability of freshwater in the aquifer all year round.
- Farmers must be advice or educated on the dangers (effects) of excessive mining of the groundwater to reduce incidence of sea water intrusion.
- High groundwater recharge areas should be delineated and protected since the aquifer system heavily relies on direct precipitation.

# REFERENCES

Akpati, B. (1978.). Geological structure and evolution of the Keta Basin, Ghana,. West Africa. Geol. Soc. Am. , Bull. 89.

Alley W.M, Reilly T.E, and Franke O. L. (1999). Sustainability of Ground-Water Resources. U.S. Geological Survey Circular 1186.

Anderson, M. P., and Woessner, W. W. (2002). Applied Groundwater Modeling, Simulation of flow and Advective Transport. Academic Press, New York, NY, USA.

Annonymous. (unknown). Retrieved April 6, 2016, from gov: www.anrcatatalog.ucdavis.edu

Aquaveo. (2014). GMS Tutorial, FEMWATER: 3D finite element modelling.

Bakker M., Oude Essink G. H. P., and Langevin C. D. (2004). The rotating movement of three immescible fluids- a benchmark problem. J Hydrol, 287:270-8.

Banoeng-Yakubo B., Danso S., and Tumbulto J. (2005). Assessment of pollution status and vulnerability of water supply in Keta, Ghana. Final Report., 120.

Barlow P. M. , Voss I. C. , Thomas E . Reilly , and Leonard F . Konikow. (2006). The Handbook of Groundwater Engineering, Second Edition. DOI: 10.1201/9781420006001.ch23.

Basack S., Bhattacharya, A. K., Maity P. (2012). Hydrogeological investigation on saline water intrusion into a coasta aquifer of west Bengal, India. Proceedings of Indian Geotechnical Conference, Paper No. G701 13-15, 2012, Delhi.

Bear J. (1988). Dynamics of fluids in porous materials. Dover publications.

Bear J., and Alexander H., D., Cheng. (2010). Modeling groundwater flow and Contaminant Transport. Springer, 834pp.

Bear, J., A.H. Cheng, S. Sorek, D. Ouazar, and I. Herrers. (1999). Seawater Intrusion in Coastal Aquifer Concepts, Methods, and Practices. London, UK: Kluwer Academic Publishers.

Bithin D., Harikrishna V., Anirban D. (2009). Modeling and control of saltwater intrusion in a coastal aquiferof Andhra Pradesh, India. Journal of Hydro-environment Research, 3 148-159.

Chan Hee P. (2004). Saltwater Intrusion In Coastal Aquifer. Georgia Institute of Technology.

Cooper, H.H., Kohout, F.A., Henry, H.R. & Glover, R.E. (1964). Sea water in coastal aquifers, . U.S.G.S. Water Supply Paper, 1613-C, 84 pp.

Davies and Peters. (1987). Modeling areal, variable-density, ground-water flow using equivalent freshwater head—analysis of potentially significant errors. In Solving groundwater problems with models:. Proceedings of the National Water Well Association/International Groundwater Modeling Center Conference , (pp. 888-903).

Demirel, Z. (2003). The history and evaluation f saltwater intrusive into a coastal aquifer in mersin, Turkey. Journal of environmental management,, Vol. 70 : 275-282.

Deschaine L. M., Lillys T. P., and Pinter D. J. (2013). Groundwater remediation design using physics-based flow transport, and optimization technologies. Environmental Systems Research, DOI: 10.1186/2193-2697-2-6.

Dickson, and Benneh. (1995). A New Geography of Ghana. Longman, UK.

Diersch H.J.G. (2002). Finite Element Subsurface Flow&Transport Simulation system. WASY Institute for Water Resources Planning and Systems Research Ltd, 292 pp.

Don Vroblesky A., Michelle Lorah M., and James Oliveros P. (1999). Groundwater, surface water and sediment contamination in the O-field area, Aberdeen proving ground, Maryland and the possible effects seleected remedial on groundwater. U.S Geological Survey Department.

Elhassadi, A. (2007). Sea water intrusion in Derna located in the Green mountain region, Libya- a threatening recurrentphenomenon calling for desalination. Desalination,, Vol. 220 : 189-193.

Essink, G. H. (2001). Density dependent groundwater flow. Utrecht.

Fetter, C. (2001). Applied Hydrogeology. fourth ed. Prentice Hall, Upper Saddle River, New Jersey.

Freeze, and Cherry. (1979). Groundwater, . Prentice Hall, Englewood Cliffs, NJ, USA.

Gaalou N., Pliakas F., Kallioras A., Schuth C., and Marinos P. (2012). Simulation of Seawater Intrusion in Coastal Aquifers: Forty Five-YearsExploitation in an Eastern Coast Aquifer in NE Tunisia. The Open Hydrology Journal, 6, (Suppl 1-M6) 31-44.

Ghana Statisitical Service P. H.C. (2013). Regional Analytical Report,. Accra: GSS.

GHP, O. E. (2001). Improving fresh groundwater supply problems and solutions. Ocean Coast Management, 44:429–449.

Giada F., Valentina C., Vittorio D. F. ( 2013, ). Saltwater Intrusion in Coastal Aquifers: A Primary CaseStudy along the Adriatic Coast Investigated within a Probabilistic Framework. Water, 5, 1830-1847.

Glynn, P.D., and Plummer, L.N. (2005). Geochemistry and the understanding of ground-water systems. Hydrogeology Journal, v. 13, no. 1, p. 263-287.

Gounari C., Skordak K., Gounaris A., Kosmidis D., KaryotiI A. (2014). Seawater Intrusion and Nitrate Pollution in Coastal Aquifer of Almyros– Nea Anchialos Basin, Central Greece. Hellenic Agricultural Organization, General Directorate for Agricultural Research, Land Reclamation Institute, Sindos 57400, GREECE, V10 2224-3496.

Gorgij A. D., and Moghaddam A. A. (2012). Vulnerability Assessment of saltwater intrusion using simplified GAPDIT method: a case study of Azarshahr Plain Aquifer, East Azerbaijan, Iran. Arabian Journal of Geosciences.

Guiguer N. and Franz T. (1996). Visual Modflow version 2.00 - The Integrated Modeling Enviroment for MODFLOW and MODPATH, Waterloo. Hydrogeology software.

Harbaugh A., W., Banta E., R., Hill M., C., and McDonald M. G. (2000). MODFLOW-2000, The United States Geological Survey Modular Groundwater Model-User Guide to Modularization Concept and the Groundwater Flow Processes. U.S Geological Survey Open-File, 00-92.

Henry, H. R. (1960). Salt water Intrusion into Coastal Aquifers," . Intern. Assoc.

Hiscock, K. M. (2011). Groundwater in the 21st Century – Meeting the Challenges. University of East Anglia, Norwich, NR4 7TJ, UK: Springer Netherlands.

Hussein M.T. (2004). Hydrochemical evaluation of groundwater in the Blue Nile Basin, eastern Sudan, using conventional and multivariate techniques. Hydrogeoogyl Journal, 12:144–158.

Hutchings W. C., and David L. Tarbox. (2003). A Model of Seawater Intrusion in Surfacial and Confined Aquifers of Northeast Florida. The Second International Conference.

Huysmans, M., and Dassargues, A. (2006). Hydrogeological modeling of radionuclide transport in low permeability media: a comparison between Boom Clay and Ypresian Clay. Environ Geol, 5 (1): 122-131.

Javadi A. A., Sherif M. M., Abdl-Elhamid H. F. (2011). Finite element modelling of seawater intrusion in Adi Ham aquifer, UAE. Engineering Computations: international journal, pp. 484-503.

Jorgensen, N.O., and Banoeng-Yakubo, B.K. (2001). Environmental isotopes as a tool in groundwater investigations in the Keta Basin Ghana. Hydrogeology Journal, 9, 190–201.

Kohout, F. A. (1960). Flow pattern of fresh and salt water in the Biscayne aquifer of the Miami area, Florida. International Association of Scientific Hydrology, 52:. 440-448 .

Kortats B.K, Young E, and Mensah-Bonsu A. (2005). Potential impact of large scale abstraction on the quality of shallow groundwater for irrigation in the Keta Strip, Ghana. West African Journal of Applied Ecology, vol 8 No 1.

Kouzana, L., Mammou, A. B. and Felfoul, M. S. (2007). Seawater intrusion and associated processes : case of the Korba aquifer (Cap-Bon, Tunisia). C.R. Geoscience,, Vol. 341 : 21-35.

Lee, R. F. and Cheng L. (1974). A comparative study of lipids of water-striders from marine, estuarine, and freshwater environments; Halobates, Rheumatobates, Gerris (Heteroptera : Gerridae). Limnology and. Oceanography, 19: 958-965 .

Lin H. C. J., Richard D. R., Talbot C. A., Yeh G. T., Cheng J. R., Cheng H. P., and Jones N. L. (1997). FEMWATER: Three-Dimensional Finite Element Computer Model for Simulating Density-Dependent Flow and Transport in Variably Saturated Media. . U.S. Army Engineer Water Experiment Station Coastal and Hydraulics Laboratory. Technical Report , CHL-97-12.

Lookjan, A., Chalermyanont T. and Arrykul, S. (2009). Three-dimensional density-dependent seawater intrusion modeling for the hat yai basin. The 14th National convention on civil engineering, Suranaree University of Technology, Page: 1253-1259.

McDonald M.G., and Harbaugh A. W. (2003). The history of MODFLOW Groundwater. 41, 2: 280-283.

Meier P.M, Carrera J. and Sanchez-Villa, X. (2007). A evaluation of Jacob's method for the interpretation of pumping test in heterogeneous formations: . Water Resources Research, 34, p 1011-1025.

Milnes, E. and Renard, P. (2003). The problem of salt recycling and seawater intrusion in coastal irrigated plains : an example from the Kiti aquifer(Southern Cyprus). Journal of Hydrology,, Vol. 288 : 327-343.

Ministry of Local Goverments and Rural Development. (2016). ghanadistricts. Retrieved November 9, 2015, from ghana districts web site: http://www.ghanadistricts.com

Mondal, N., C., Singh V., P., and Sankaran S. (2011). Groundwater Flow Model for a Tannery Belt in Southern India. Journal of Water Resource and Protection, 3:pp 85-97. Doi: 10.4236/jwarp.2011.32010.

Mygatt. E. (2006). World's forest continue to shrink. Earth policy Institute Washington.

Naderi N.M, Kerimani M.R. and Gholam-Abbas B. (2013). Saltwater intrusion and groundwater resources management in coastal aquifers. European Journal of Enviromental Biology , 3(3): 80-94.

Narayan, K. A., Schleeberger, C. and Bristow, K. L. (2007). Modeling seawater intrusion in the Burdekin Delta irrigation area, North Queensland, Australia . Agricultural water management, Vol. 89 : 217-228 .

Nerquaye-Tetteh, B. (1993). Water resources of the Keta Basin. In: Proc. 19th WEDC Conf, Accra, pp. 102–108.

Pathak Y. and Pathak A. (2016). Effects of Saline water on Geotechnical properties of soil. International Journal of Innovation Research in Science Engineering anad Technology.

Pinder, G.F. and Cooper, H.H, Jr. (1970.). A numerical technique for calculating the transient position of the saltwater front. Water Resour. Res.,, 6(3), 875-882.

Post V. E. A. (2004). Groundwater Salinization Processes in the Coastal area of the Netherlands due to transgressions during the Holocene. Earh Science, VU-University of Amsterdam, 154pp.

Post V. E. A., Kooi, and Simmon C. T. (2007). Using hydraulic head measurement in variable-density groundwater flow analysis. Groundwater, 45(6). 664-71, doi.10.1111/j.1745=6584.2007.00339x.

Ralph C., H. (2012). Basic Ground-Water Hydrology. Virginia: U.S Geological Survey.

Redsaw S.C. K.R. (1979). Seepage and groundwater flow: Numerical analysis by analogue and digital methods:. New York, John Wiley and Sons, 339p.

Rouaida T., Moncef Z., Hamed B. D. (2007). Groundwater salinization of the Sfax superficial aquifer, Tunisia. Hydrogeology Journal, 15: 1341-1355.

Segol, G., G. F. Pinder, and W. G. Gray. (1976). Galerkin-Finite Element Technique for Calculating Transient Position of Saltwater Front. Water Resources Research, 11:343-347.

Sherif, M.M. and Kacimov, A. (2006). Modeling of groundwater in two selected coastal aquifers of UAE and Oman as a precursor for water resources

management . Final Report of collaboration Research Project (UAEU/SQU), October.

Sherif, M.M., Singh, V.P. and Amer, A.M. (1988). A two-dimensional finite element model fordispersion (2D-FED) in coastal aquifers. J. Hydrology, , Vol. 103, pp. 11-36.

Thomas E. Reilly, L. Niel Plummer, J. Phillips, Eurybiades Busenberg. (1994). The use of simulation and multiple environmental tracers to quantify groundwater flow in a shallow aquifer. Water Resource Research, DOI: 10.1029/93WR02655.

Todd, D.K., and Mays, L.W. (2005). Groundwater Hydrology. third ed. John Wiley & Sons Inc., Hoboken, NJ.

Toth J. (1963). A theoretical analysis of groundwater flow in small dranaige basin . Geophys. Res., , 68, 4795-4812.

Vacher, H. L. (1988). Dupuit-Ghyben-Herzberg analysis of strip-island lenses. . Geological Society of America Bulletin,, 100(4), 580-591.

Voss I. C. and Johan A. (1991). Some Aspects of Regional flow of variable density groundwater in crystalline basement rock of sweden. U.S. Geological Survey.

Weingchanda, P. (2010). Study of seawater intrusion and controlling methods using physical model simulation. Suranaree University of Technology.

Wilhelm S., Yoram R., Jones J. A. A. (2005). groundwater reservoir for a thirsty planet . Earth science for society foundation, Leiden Netherlands.

Yidana S. M., Alfa B., Banoeng-Yakubo B. and Addai M. O. (2012). Simulation of groundwater flow in a crystalline rock aquifer system in Southern Ghana_An evaluation of the effects of increased groundwater abstraction on the aquifer using a transient groundwater flow model. . Hydrogeological Processes, doi: 10.1002/hyp.9644.

Yidana S. M., Ophori D., Banoeng-Yakubo B., Samed A. A. (2008). Groundwater resources management in the Afram plain Area, Ghana. Journal of Civil Engineering, 12(5): pp. 339-347

Yidana S. M. (2010). Groundwater modeling and particle tracking for chemical transport in sorthern Voltain aquifer . Environ Earth Science, 63: 709-721.

Yidana S., M., and Chegbeleh L. P. (2013). The hydraulic conductivity field and groundwater flow in the unconfined aquifer system of the Keta Strip, Ghana. Journal of African Earth Sciences, 86 45–52.

Yidana, S.M., Banoeng-Yakubo, B., Akabzaa, T.M. (2010). Analysis of groundwater quality using multivariate and spatial analyses in the Ketabasin, Ghana. Africa Earth Science, 58, 220–234.

Ying Ru., Kenji Jinno., Tosao Hosokawa and Kei Nakagawa. (2001). Study on Effect of Subsurface Dam in Coastal Seawater Intrusion. First International Conference .

Zheng, C. and Wang P.P. (1999). MT3DMS: A Modular Three-Dimensional Multispecies Transport Model for Simulation of Advection, Dispersion and Chemical Reactions of Contaminants in Groundwater Systems;. U.S. Army

Engineer Research and Development Center, Vicksburg, MS, Report SERDP-99-1.

Zhoua., and Wenpeng Li. (2011). A review of regional groundwater flow modeling. Geoscience Frontiers, Pages 205–214.

# APPENDICES

Appendix 1: Data for first field visit; 16th January, 2016

| ID | UTM | | Z | SWL | H_H | TDS | EC | PH | TEM |
|---|---|---|---|---|---|---|---|---|---|
| WH001 | 261672 | 639814 | 11 | 1.8 | 9.2 | 267 | 522 | 8.73 | **29.1** |
| WH002 | 261660 | 639878 | 10 | 0.9 | 9.1 | 503 | 1045 | 8.33 | 27.7 |
| WH003 | 261628 | 640000 | 10 | 0.8 | 9.2 | 1289 | 2587 | 8.4 | 27.5 |
| WH004 | 261787 | 640077 | 11 | 1.2 | 9.8 | 2000 | 3999 | 8.3 | 27.3 |
| WH005 | 261885 | 639908 | 9 | 1.8 | 7.2 | 457 | 966 | 8.28 | 25.7 |
| WH006 | 261969 | 640113 | 12 | 1.58 | 10.42 | 1508 | 3068 | 8.14 | 27.6 |
| wh007 | 262238 | 639988 | 10 | 0.5 | 9.5 | 338 | 744 | 8.34 | 25.8 |
| WH008 | 262327 | 640143 | 12 | 1.6 | 10.4 | 2000 | 3999 | 8.87 | 27.5 |
| WH009 | 262560 | 639928 | 11 | 1.3 | 9.7 | 1528 | 3074 | 8.79 | 26.9 |
| WH010 | 262212 | 639851 | 12 | 1.9 | 10.1 | 579 | 1154 | 8.74 | 26.8 |
| WH011 | 261937 | 639571 | 9 | 1.3 | 7.7 | 412 | 834 | 8.2 | 27.7 |
| WH012 | 261050 | 639591 | 8 | 1.1 | 6.9 | 567 | 1139 | 8.6 | 26.9 |
| AN001 | 267691 | 641175 | 10 | 2.7 | 7.3 | 492 | 973 | 7.83 | 26.9 |
| AN002 | 267778 | 641286 | 13 | 2.06 | 10.94 | 1339 | 2688 | 8.69 | 27.4 |
| AN003 | 267928 | 641333 | 15 | 2.3 | 12.7 | 728 | 1456 | 8.66 | 27.8 |
| AN004 | 268023 | 641260 | 14 | 2.4 | 11.6 | 455 | 901 | 8.35 | 26.5 |
| AN005 | 268228 | 641254 | 12 | 1.1 | 10.9 | 521 | 1041 | 8.21 | 26.5 |
| AN006 | 268254 | 641481 | 14 | 0.7 | 13.3 | 413 | 824 | 8.44 | 28.1 |
| AN007 | 268455 | 641549 | 14 | 1.2 | 12.8 | 429 | 857 | 8.84 | 27.6 |
| AN008 | 268689 | 641431 | 11 | 1.2 | 9.8 | 612 | 1227 | 8.1 | 27.1 |
| AN009 | 268877 | 641558 | 9 | 1 | 8 | 398 | 797 | 8.9 | 28 |
| AN010 | 268931 | 641613 | 15 | 0.8 | 14.2 | 486 | 966 | 8.31 | 26.2 |
| AN011 | 269005 | 641763 | 4 | 1.3 | 2.7 | 712 | 1429 | 8.44 | 26.1 |
| AN012 | 269127 | 641638 | 9 | 2 | 7 | 396 | 793 | 8.2 | 25.4 |
| AN013 | 269306 | 641755 | 6 | 1.8 | 4.2 | 617 | 1222 | 8.33 | 27.3 |
| AN014 | 269481 | 641703 | 10 | 0.8 | 9.2 | 536 | 1079 | 8.38 | 26.3 |
| AN015 | 269644 | 641801 | 8 | 0.6 | 7.4 | 484 | 969 | 8.54 | 26.1 |
| AN016 | 269755 | 641940 | 12 | 0.4 | 11.6 | 581 | 1149 | 8.33 | 26.3 |
| AN017 | 269834 | 642023 | 18 | 1 | 17 | 273 | 545 | 8.29 | 26.6 |
| AN018 | 269829 | 642141 | 7 | 0.8 | 6.2 | 271 | 543 | 8.76 | 27.5 |
| AN019 | 270010 | 642081 | 9 | 0.6 | 8.4 | 522 | 1072 | 8.3 | 27.4 |
| AN020 | 270145 | 642166 | 12 | 1.4 | 10.6 | 461 | 933 | 8.43 | 26.2 |

NB: HH = Hydraulic Head, SWL = Static Water Level, Z= Elevation

Appendix 1: Data for first field visit; 16th January, 2016 (Cont'd)

| ID | UTM | | Z | SWL | H_H | TDS | EC | PH | TEMP |
|---|---|---|---|---|---|---|---|---|---|
| AN021 | 270281 | 642238 | 10 | 1.1 | 8.9 | 430 | 867 | 8.54 | 26.3 |
| AN022 | 270358 | 642421 | 9 | 1.4 | 7.6 | 723 | 1443 | 8.54 | 25.7 |
| AN023 | 270530 | 642447 | 10 | 1.2 | 8.8 | 607 | 1205 | 8.53 | 26.5 |
| AN024 | 270645 | 642122 | 9 | 2.1 | 6.9 | 245 | 489 | 8.55 | 26.3 |
| AN025 | 270530 | 642060 | 12 | 1.6 | 10.4 | 283 | 568 | 8.53 | 27.7 |
| AN026 | 270370 | 641938 | 11 | 2 | 9 | 204 | 404 | 8.95 | 29 |
| AN027 | 270171 | 641855 | 7 | 2 | 5 | 180 | 558 | 8.57 | 28.6 |
| AN028 | 270007 | 641792 | 11 | 1.6 | 9.4 | 677 | 1559 | 8.38 | 28 |
| AN029 | 268140 | 641726 | 12 | 2.4 | 9.6 | 619 | 1234 | 8.34 | 27.5 |
| AN030 | 269718 | 641625 | 12 | 2 | 10 | 466 | 925 | 8.51 | 29.4 |
| AN031 | 268849 | 640889 | 14 | 2.2 | 11.8 | 333 | 671 | 8.68 | 27.7 |
| AN032 | 269100 | 640910 | 17 | 2.1 | 14.9 | 513 | 1076 | 8.6 | 28.9 |
| AN033 | 269289 | 640991 | 9 | 2.2 | 6.8 | 511 | 1014 | 8.3 | 28 |
| AN034 | 269130 | 640788 | 21 | 2.4 | 18.6 | 433 | 863 | 8.81 | 29 |
| AN035 | 269313 | 640840 | 24 | 2 | 22 | 419 | 839 | 8.48 | 29.2 |
| AN036 | 269021 | 640751 | 22 | 2.2 | 19.8 | 420 | 927 | 8.43 | 29.3 |
| AN037 | 268820 | 640682 | 22 | 2 | 20 | 479 | 949 | 8.45 | 29.1 |
| AN038 | 268667 | 640823 | 15 | 2.7 | 12.3 | 366 | 737 | 8.41 | 29.2 |

Appendix 1: Data for Second field visit, 30th January, 2016

| ID | UTM | | TDS | EC | PH | TEM | Z | SWL | HH |
|---|---|---|---|---|---|---|---|---|---|
| WH001 | 261672 | 639814 | 305 | 612 | 8.8 | 29.9 | 11 | 1.32 | 9.68 |
| WH002 | 261660 | 639878 | 511 | 1047 | 9.1 | 29.2 | 10 | 0.74 | 9.26 |
| WH003 | 261628 | 640000 | 1868 | 2792 | 9.3 | 29.4 | 10 | 0.7 | 9.3 |
| WH004 | 261787 | 640077 | 1993 | 3994 | 8.5 | 28.4 | 12 | 0.74 | 11.26 |
| WH005 | 261885 | 639908 | 617 | 1238 | 8.3 | 30.1 | 8 | 0.96 | 7.04 |
| WH006 | 261969 | 640113 | 1520 | 3215 | 8.7 | 26.1 | 12 | 0.74 | 11.26 |
| wh007 | 262238 | 639988 | 377 | 769 | 8.8 | 27 | 11 | 0.9 | 10.1 |
| WH008 | 262327 | 640143 | 2000 | 3989 | 8.2 | 29.5 | 11 | 0.54 | 10.46 |
| WH009 | 262560 | 639928 | 1434 | 2843 | 9.5 | 29.7 | 7 | 0.9 | 6.1 |
| WH010 | 262212 | 639851 | 711 | 1482 | 9.0 | 29.4 | 10 | 1.26 | 8.74 |
| WH011 | 261937 | 639571 | 511 | 1002 | 8.9 | 29.3 | 10 | 1.2 | 8.8 |
| WH012 | 261050 | 639591 | 576 | 1098 | 8.5 | 26.7 | 6 | 0.9 | 5.1 |

Appendix 1: Data for second data visit; 30th January 2016 (Cont'd)

| ID | UTM | | TDS | EC | PH | TEM | Z | SWL | HH |
|---|---|---|---|---|---|---|---|---|---|
| AN001 | 267691 | 641175 | 478 | 964 | 8.7 | 29 | 14 | 0.63 | 13.37 |
| AN002 | 267778 | 641286 | 1474 | 2934 | 9.9 | 30.1 | 13 | 0.89 | 12.11 |
| AN003 | 267928 | 641333 | 704 | 1407 | 8.9 | 29.09 | 15 | 0.71 | 14.29 |
| AN004 | 268023 | 641260 | 507 | 1027 | 8.9 | 29.9 | 14 | 0.69 | 13.31 |
| AN005 | 268228 | 641254 | 574 | 1141 | 8.3 | 29.6 | 12 | 1.04 | 10.96 |
| AN006 | 268254 | 641481 | 398 | 796 | 9.5 | 30.3 | 13 | 0.87 | 12.13 |
| AN007 | 268455 | 641549 | 514 | 1018 | 9.3 | 30.5 | 14 | 1.23 | 12.77 |
| AN008 | 268689 | 641431 | 571 | 1148 | 8.8 | 30.2 | 11 | 1.31 | 9.69 |
| AN009 | 268877 | 641558 | 440 | 875 | 9.0 | 29.7 | 15 | 1.23 | 13.77 |
| AN010 | 268931 | 641613 | 487 | 966 | 8.5 | 29.7 | 18 | 1.4 | 16.6 |
| AN011 | 269005 | 641763 | 821 | 1639 | 8.6 | 28 | 4 | 1.2 | 2.8 |
| AN012 | 269127 | 641638 | 548 | 1077 | 9.1 | 29.8 | 13 | 0.86 | 12.14 |
| AN013 | 269306 | 641755 | 556 | 1112 | 8.6 | 29.4 | 7 | 1.11 | 5.89 |
| AN014 | 269481 | 641703 | 582 | 1173 | 8.8 | 29.4 | 4 | 0.92 | 3.08 |
| AN015 | 269644 | 641801 | 548 | 1077 | 9.1 | 29.8 | 13 | 0.86 | 12.14 |
| AN016 | 269755 | 641940 | 582 | 1173 | 8.8 | 29.4 | 12 | 0.92 | 11.08 |
| AN017 | 269834 | 642023 | 275 | 557 | 9.1 | 29.3 | 11 | 0.88 | 10.12 |
| AN018 | 269829 | 642141 | 292 | 586 | 9.3 | 28.9 | 12 | 1.1 | 10.9 |
| AN019 | 270010 | 642081 | 567 | 1127 | 8.5 | 29.1 | 11 | 1.14 | 9.86 |
| AN020 | 270145 | 642166 | 482 | 1526 | 9.3 | 29.2 | 11 | 1.8 | 9.2 |
| AN021 | 270281 | 642238 | 431 | 890 | 8.9 | 29.5 | 10 | 1.41 | 8.59 |
| AN022 | 270358 | 642421 | 638 | 1279 | 9.1 | 29.1 | 9 | 1.32 | 7.68 |
| AN023 | 270530 | 642447 | 670 | 1340 | 8.9 | 29 | 10 | 1.33 | 8.67 |
| AN024 | 270645 | 642122 | 246 | 507 | 8.9 | 30.3 | 11 | 1.97 | 9.03 |
| AN025 | 270530 | 642060 | 296 | 588 | 9.2 | 30.1 | 11 | 1.78 | 9.22 |
| AN026 | 270370 | 641938 | 227 | 447 | 8.7 | 30.2 | 11 | 2.07 | 8.93 |
| AN027 | 270171 | 641855 | 310 | 627 | 8.8 | 29.4 | 10 | 2.02 | 7.98 |
| AN028 | 270007 | 641792 | 700 | 1435 | 8.7 | 29.2 | 12 | 1.95 | 10.05 |
| AN029 | 26840 | 641726 | 690 | 1361 | 8.6 | 29.2 | 12 | 1.76 | 10.24 |
| AN030 | 269718 | 641625 | 528 | 1046 | 8.6 | 29.2 | 14 | 1.96 | 12.04 |
| AN031 | 268849 | 640889 | 401 | 812 | 8.7 | 29.23 | 11 | 1.52 | 10.2 |
| AN032 | 269100 | 640910 | 521 | 1110 | 8.8 | 29.4 | 15 | 2.3 | 12.7 |
| AN033 | 269289 | 640991 | 515 | 1015 | 9.0 | 28.1 | 9 | 1.91 | 7.09 |
| AN034 | 269130 | 640788 | 454 | 908 | 9.2 | 29.2 | 14 | 2.01 | 11.99 |
| AN035 | 269313 | 640840 | 432 | 861 | 9.4 | 29 | 13 | 2.21 | 10.79 |
| AN036 | 269021 | 640751 | 424 | 904 | 9.1 | 29.56 | 17 | 1.8 | 15.2 |
| AN037 | 268820 | 640682 | 501 | 1012 | 9.6 | 29.5 | 22 | 2.1 | 19.9 |
| AN038 | 268667 | 640823 | 387 | 814 | 8.8 | 29.21 | 15 | 1.8 | 13.2 |

Appendix 1: Data for third field visit, 13th February, 2016

| ID | UTM | | TDS | EC | PH | TEM | SWL | Z | H H |
|---|---|---|---|---|---|---|---|---|---|
| WH001 | 261672 | 639814 | 302 | 599 | 8.6 | 30 | 2 | 11 | 9 |
| WH002 | 261660 | 639878 | 510 | 1044 | 9.1 | 28.7 | 1.1 | 10 | 8.9 |
| WH003 | 261628 | 640000 | 1868 | 2800 | 9.4 | 29.2 | 0.65 | 10 | 9.35 |
| WH004 | 261787 | 640077 | 1795 | 3106 | 8.62 | 27.9 | 1.3 | 11 | 9.7 |
| WH005 | 261885 | 639908 | 623 | 1244 | 8.2 | 30.2 | 1 | 12 | 11 |
| WH006 | 261969 | 640113 | 1601 | 3300 | 8.7 | 26.2 | 0.71 | 7 | 6.29 |
| wh007 | 262238 | 639988 | 379 | 769 | 9.12 | 28.2 | 0.91 | 10 | 9.09 |
| WH008 | 262327 | 640143 | 2001 | 4002 | 8.34 | 29.5 | 0.62 | 11 | 10.4 |
| WH009 | 262560 | 639928 | 1446 | 2850 | 9.54 | 29.7 | 1.1 | 7 | 5.9 |
| WH010 | 262212 | 639851 | 718 | 1485 | 9.02 | 29.4 | 1.02 | 10 | 8.98 |
| WH011 | 261937 | 639571 | 511 | 1000 | 8.92 | 29.3 | 1 | 10 | 9 |
| WH012 | 261050 | 639591 | 552 | 1096 | 8.5 | 26.7 | 1 | 6 | 5 |
| AN001 | 267691 | 641175 | 479 | 964 | 8.73 | 29 | 0.81 | 14 | 13.2 |
| AN002 | 267778 | 641286 | 1478 | 2899 | 9.09 | 30.1 | 2.1 | 12 | 9.9 |
| AN003 | 267928 | 641333 | 715 | 1408 | 8.96 | 29.1 | 0.71 | 15 | 14.3 |
| AN004 | 268023 | 641260 | 507 | 1028 | 9 | 29.9 | 0.69 | 13 | 12.3 |
| AN005 | 268228 | 641254 | 581 | 1144 | 8.52 | 29.6 | 1.3 | 14 | 12.7 |
| AN006 | 268254 | 641481 | 399 | 795 | 9.4 | 30.3 | 0.62 | 13 | 12.4 |
| AN007 | 268455 | 641549 | 501 | 1019 | 9.31 | 30.5 | 1.31 | 14 | 12.7 |
| AN008 | 268689 | 641431 | 577 | 1151 | 8.64 | 30.2 | 1.31 | 11 | 9.69 |
| AN009 | 268877 | 641558 | 443 | 912 | 9.21 | 29.7 | 1.01 | 15 | 14 |
| AN010 | 268931 | 641613 | 478 | 965 | 8.54 | 29.7 | 0.84 | 18 | 17.2 |
| AN011 | 269005 | 641763 | 822 | 1638 | 8.6 | 28 | 1.1 | 4 | 2.9 |
| AN012 | 269127 | 641638 | 548 | 1079 | 9.16 | 29.8 | 0.76 | 13 | 12.2 |
| AN013 | 269306 | 641755 | 557 | 1111 | 8.68 | 29.4 | 0.96 | 7 | 6.04 |
| AN014 | 269481 | 641703 | 582 | 1175 | 8.83 | 29.4 | 0.93 | 4 | 3.07 |
| AN015 | 269644 | 641801 | 548 | 1076 | 9.16 | 29.8 | 0.63 | 13 | 12.4 |
| AN016 | 269755 | 641940 | 581 | 1173 | 8.83 | 29.4 | 0.54 | 12 | 11.5 |
| AN017 | 269834 | 642023 | 277 | 556 | 9.1 | 29.3 | 0.99 | 11 | 10 |
| AN018 | 269829 | 642141 | 292 | 587 | 9.03 | 28.9 | 1.4 | 12 | 10.6 |
| AN019 | 270010 | 642081 | 566 | 1128 | 8.56 | 29.1 | 0.87 | 11 | 10.1 |
| AN020 | 270145 | 642166 | 480 | 1524 | 9.3 | 29.2 | 0.89 | 11 | 10.1 |

Appendix 1: Data for third field visit, 13th February, 2016 (Cont'd)

| ID | UTM | | TDS | EC | PH | TEM | SWL | Z | H H |
|---|---|---|---|---|---|---|---|---|---|
| AN021 | 270281 | 642238 | 431 | 890 | 8.95 | 29.5 | 1 | 10 | 9 |
| AN022 | 270358 | 642421 | 639 | 1280 | 9.01 | 29.1 | 1.2 | 9 | 7.8 |
| AN023 | 270530 | 642447 | 680 | 1338 | 8.96 | 29 | 1.22 | 10 | 8.78 |
| AN024 | 270645 | 642122 | 251 | 504 | 8.93 | 30.2 | 2.1 | 11 | 8.9 |
| AN025 | 270530 | 642060 | 300 | 601 | 9.24 | 30 | 2.3 | 11 | 8.7 |
| AN026 | 270370 | 641938 | 302 | 450 | 9 | 29.6 | 0.94 | 11 | 10.1 |
| AN027 | 270171 | 641855 | 313 | 631 | 8.77 | 29.7 | 1.61 | 10 | 8.39 |
| AN028 | 270007 | 641792 | 710 | 1437 | 8.65 | 28.9 | 2.1 | 12 | 9.9 |
| AN029 | 26840 | 641726 | 701 | 1364 | 9 | 29.3 | 1.3 | 12 | 10.7 |
| AN030 | 269718 | 641625 | 592 | 1047 | 8.64 | 30.1 | 1.4 | 14 | 12.6 |
| AN031 | 268849 | 640889 | 411 | 804 | 8.92 | 28.9 | 1.82 | 11 | 9.18 |
| AN032 | 269100 | 640910 | 537 | 1111 | 8.79 | 29.6 | 2.1 | 15 | 12.9 |
| AN033 | 269289 | 640991 | 531 | 1015 | 9.21 | 27 | 1 | 9 | 8 |
| AN034 | 269130 | 640788 | 499 | 908 | 9.21 | 29.2 | 2.1 | 14 | 11.9 |
| AN035 | 269313 | 640840 | 437 | 864 | 9.4 | 29 | 2.1 | 13 | 10.9 |
| AN036 | 269021 | 640751 | 444 | 905 | 9.11 | 28.8 | 1.32 | 17 | 15.7 |
| AN037 | 268820 | 640682 | 513 | 1009 | 9.6 | 29 | 1.64 | 22 | 20.4 |
| AN038 | 268667 | 640823 | 30.11 | 2 | 15 | 13 | 2 | 15 | 8.81 |

Appendix 1: Data for fourth field visit, 4th March, 2016

| ID | UTM | | TDS | EC | PH | TEM | SWL | Z | HH |
|---|---|---|---|---|---|---|---|---|---|
| WH001 | 261672 | 639814 | 289 | 575 | 8.2 | 29.9 | 2.3 | 11 | 8.7 |
| WH002 | 261660 | 639878 | 520 | 1018 | 8.88 | 29.2 | 1.2 | 10 | 8.8 |
| WH003 | 261628 | 640000 | 801 | 1589 | 9.35 | 29.4 | 1 | 10 | 9 |
| WH004 | 261787 | 640077 | 198 | 3963 | 8.53 | 28.4 | 1.1 | 11 | 9.9 |
| WH005 | 261885 | 639908 | 633 | 1266 | 8.17 | 30.1 | 1.4 | 12 | 10.6 |
| WH006 | 261969 | 640113 | 1600 | 3202 | 8.7 | 26.1 | 2.4 | 7 | 4.6 |
| wh007 | 262238 | 639988 | 382 | 764 | 8.88 | 27 | 1.6 | 10 | 8.4 |
| WH008 | 262327 | 640143 | 2104 | 4207 | 8.27 | 29.5 | 1.4 | 11 | 9.6 |
| WH009 | 262560 | 639928 | 1445 | 2891 | 9.54 | 29.7 | 1.2 | 7 | 5.8 |
| WH010 | 262212 | 639851 | 684 | 1368 | 9.02 | 29.4 | 1.51 | 10 | 8.49 |
| WH011 | 261937 | 639571 | 511 | 1022 | 8.92 | 29.3 | 2.3 | 10 | 7.7 |
| WH012 | 261050 | 639591 | 560 | 1120 | 8.5 | 26.7 | 1.3 | 6 | 4.7 |

Appendix 1: Data for fourth field visit, 4th March, 2016 (cont'd)

| ID | UTM | | TDS | EC | PH | TEM | SWL | Z | HH |
|---|---|---|---|---|---|---|---|---|---|
| AN001 | 267691 | 641175 | 482 | 964 | 8.73 | 29 | 1.6 | 15 | 13.4 |
| AN002 | 267778 | 641286 | 1488 | 2976 | 9.09 | 30.1 | 1 | 12 | 11 |
| AN003 | 267928 | 641333 | 720 | 1440 | 8.96 | 29.09 | 1 | 15 | 14 |
| AN004 | 268023 | 641260 | 510 | 1020 | 8.91 | 29.9 | 1.91 | 13 | 11.0 |
| AN005 | 268228 | 641254 | 499 | 998 | 8.83 | 29.6 | 1.23 | 14 | 12.7 |
| AN006 | 268254 | 641481 | 397 | 794 | 9.05 | 30.3 | 0.7 | 13 | 12.3 |
| AN007 | 268455 | 641549 | 503 | 1006 | 9.36 | 30.5 | 1.2 | 14 | 12.8 |
| AN008 | 268689 | 641431 | 611 | 1222 | 8.86 | 30.2 | 1.2 | 11 | 9.8 |
| AN009 | 268877 | 641558 | 454 | 908 | 9.03 | 29.7 | 1 | 15 | 14 |
| AN010 | 268931 | 641613 | 486 | 972 | 8.54 | 29.7 | 0.8 | 18 | 17.2 |
| AN011 | 269005 | 641763 | 818 | 1636 | 8.6 | 28 | 1.3 | 4 | 2.7 |
| AN012 | 269127 | 641638 | 552 | 1104 | 9.16 | 29.8 | 2 | 13 | 11 |
| AN013 | 269306 | 641755 | 556 | 1112 | 8.68 | 29.4 | 1.8 | 7 | 5.2 |
| AN014 | 269481 | 641703 | 491 | 982 | 8.83 | 29.4 | 0.8 | 4 | 3.2 |
| AN015 | 269644 | 641801 | 568 | 1136 | 9.16 | 29.8 | 0.6 | 13 | 12.4 |
| AN016 | 269755 | 641940 | 557 | 1114 | 8.83 | 29.4 | 0.4 | 12 | 11.6 |
| AN017 | 269834 | 642023 | 588 | 1176 | 9.1 | 29.3 | 1 | 11 | 10 |
| AN018 | 269829 | 642141 | 587 | 1174 | 9.03 | 28.9 | 0.8 | 12 | 11.2 |
| AN019 | 270010 | 642081 | 601 | 1202 | 8.56 | 29.1 | 0.6 | 11 | 10.4 |
| AN020 | 270145 | 642166 | 452 | 904 | 9.3 | 29.2 | 1.4 | 11 | 9.6 |
| AN021 | 270281 | 642238 | 501 | 1002 | 8.95 | 29.5 | 1.1 | 10 | 8.9 |
| AN022 | 270358 | 642421 | 632 | 1264 | 9.01 | 29.1 | 1.4 | 9 | 7.6 |
| AN023 | 270530 | 642447 | 685 | 1370 | 8.96 | 29 | 1.2 | 10 | 8.8 |
| AN024 | 270645 | 642122 | 273 | 546 | 8.93 | 30.3 | 2.1 | 11 | 8.9 |
| AN025 | 270530 | 642060 | 310 | 620 | 9.24 | 30.1 | 1.6 | 11 | 9.4 |
| AN026 | 270370 | 641938 | 324 | 648 | 9 | 30.2 | 2 | 11 | 9 |
| AN027 | 270171 | 641855 | 317 | 634 | 8.89 | 29.4 | 2 | 10 | 8 |
| AN028 | 270007 | 641792 | 711 | 1422 | 8.72 | 29.2 | 1.6 | 12 | 10.4 |
| AN029 | 26840 | 641726 | 803 | 1311 | 8.62 | 29.2 | 2.4 | 12 | 9.6 |
| AN030 | 269718 | 641625 | 608 | 1002 | 8.64 | 29.2 | 2 | 14 | 12 |
| AN031 | 268849 | 640889 | 420 | 813 | 8.72 | 29.23 | 2.2 | 11 | 8.8 |
| AN032 | 269100 | 640910 | 541 | 1027 | 8.82 | 29.4 | 2.1 | 15 | 12.9 |
| AN033 | 269289 | 640991 | 531 | 999 | 9.01 | 28.1 | 2.2 | 9 | 6.8 |
| AN034 | 269130 | 640788 | 532 | 901 | 9.21 | 29.2 | 2.4 | 14 | 11.6 |
| AN035 | 269313 | 640840 | 443 | 823 | 9.4 | 29 | 2 | 13 | 11 |
| AN036 | 269021 | 640751 | 456 | 900 | 9.11 | 29.56 | 2.2 | 17 | 14.8 |
| AN037 | 268820 | 640682 | 518 | 921 | 9.6 | 29.5 | 2 | 22 | 20 |
| AN038 | 268667 | 640823 | 29.2 | 1.7 | 15 | 28 | 0.9 | 15 | 272 |

Appendix 1: Data for fifth field visit, 29th March, 2016

| ID | UTM | | TDS | EC | PH | TEM | SWL | Z | HH |
|---|---|---|---|---|---|---|---|---|---|
| WH001 | 261672 | 639814 | 301 | 602 | 8.5 | 30 | 1.9 | 11 | 9.1 |
| WH002 | 261660 | 639878 | 621 | 1240 | 8.9 | 30 | 0.9 | 10 | 9.1 |
| WH003 | 261628 | 640000 | 786 | 1574 | 9.25 | 29.1 | 1 | 10 | 9 |
| WH004 | 261787 | 640077 | 1669 | 3299 | 8.6 | 29 | 1.1 | 11 | 9.9 |
| WH005 | 261885 | 639908 | 634 | 1268 | 8.24 | 30 | 1.4 | 12 | 10.6 |
| WH006 | 261969 | 640113 | 1621 | 3241 | 8.86 | 28.2 | 2 | 7 | 5 |
| wh007 | 262238 | 639988 | 402 | 813 | 8.95 | 28 | 1.6 | 10 | 8.4 |
| WH008 | 262327 | 640143 | 2112 | 4224 | 8.34 | 30 | 1.4 | 11 | 9.6 |
| WH009 | 262560 | 639928 | 1447 | 2890 | 9.43 | 29.7 | 1.2 | 7 | 5.8 |
| WH010 | 262212 | 639851 | 686 | 1370 | 9.1 | 30.1 | 1.31 | 10 | 8.69 |
| WH011 | 261937 | 639571 | 512 | 1022 | 9.24 | 30.3 | 2.2 | 10 | 7.8 |
| WH012 | 261050 | 639591 | 560 | 1126 | 8.42 | 27 | 1.3 | 6 | 4.7 |
| AN001 | 267691 | 641175 | 480 | 963 | 8.81 | 30 | 1.6 | 15 | 13.4 |
| AN002 | 267778 | 641286 | 1488 | 2971 | 9.23 | 30.3 | 1 | 12 | 11 |
| AN003 | 267928 | 641333 | 724 | 1448 | 9 | 30.1 | 1 | 15 | 14 |
| AN004 | 268023 | 641260 | 513 | 1026 | 9 | 29.6 | 0.94 | 13 | 12.06 |
| AN005 | 268228 | 641254 | 523 | 1012 | 9.3 | 29 | 1.23 | 14 | 12.77 |
| AN006 | 268254 | 641481 | 399 | 801 | 8.97 | 28.4 | 0.7 | 13 | 12.3 |
| AN007 | 268455 | 641549 | 501 | 1003 | 9.01 | 30.1 | 1.2 | 14 | 12.8 |
| AN008 | 268689 | 641431 | 627 | 1224 | 9.23 | 28 | 1.2 | 11 | 9.8 |
| AN009 | 268877 | 641558 | 452 | 901 | 9.1 | 28 | 1 | 15 | 14 |
| AN010 | 268931 | 641613 | 488 | 973 | 7.99 | 29 | 0.8 | 18 | 17.2 |
| AN011 | 269005 | 641763 | 821 | 1644 | 8.61 | 29.4 | 1.3 | 4 | 2.7 |
| AN012 | 269127 | 641638 | 553 | 1105 | 9.3 | 27.3 | 2 | 13 | 11 |
| AN013 | 269306 | 641755 | 547 | 1094 | 8.72 | 30 | 1.8 | 7 | 5.2 |
| AN014 | 269481 | 641703 | 486 | 972 | 8.85 | 28.5 | 0.8 | 4 | 3.2 |
| AN015 | 269644 | 641801 | 570 | 1140 | 8.93 | 29.4 | 0.6 | 13 | 12.4 |
| AN016 | 269755 | 641940 | 557 | 1114 | 9.02 | 30.5 | 0.4 | 12 | 11.6 |
| AN017 | 269834 | 642023 | 586 | 1173 | 9.2 | 28 | 1 | 11 | 10 |
| AN018 | 269829 | 642141 | 585 | 1171 | 9.12 | 28 | 0.8 | 12 | 11.2 |
| AN019 | 270010 | 642081 | 600 | 1201 | 8.6 | 24 | 0.6 | 11 | 10.4 |
| AN020 | 270145 | 642166 | 451 | 902 | 8.92 | 29 | 1.4 | 11 | 9.6 |

Appendix 1: Data for fifth field visit, 29th March 2016 (cont'd)

| ID | UTM | | TDS | EC | PH | TEM | SWl | Z | HH |
|---|---|---|---|---|---|---|---|---|---|
| AN021 | 270281 | 642238 | 501 | 1005 | 911 | 28.1 | 1.1 | 10 | 8.9 |
| AN022 | 270358 | 642421 | 632 | 1263 | 9 | 28.3 | 1.4 | 9 | 7.6 |
| AN023 | 270530 | 642447 | 688 | 1376 | 9.21 | 29.1 | 1.2 | 10 | 8.8 |
| AN024 | 270645 | 642122 | 275 | 551 | 9 | 29.8 | 2.1 | 11 | 8.9 |
| AN025 | 270530 | 642060 | 311 | 611 | 8.85 | 27.8 | 1.6 | 11 | 9.4 |
| AN026 | 270370 | 641938 | 329 | 460 | 9.2 | 28.3 | 2 | 11 | 9 |
| AN027 | 270171 | 641855 | 321 | 623 | 8.94 | 29 | 2 | 10 | 8 |
| AN028 | 270007 | 641792 | 714 | 1425 | 8.81 | 30.1 | 1.6 | 12 | 10.4 |
| AN029 | 26840 | 641726 | 805 | 1301 | 8.7 | 30 | 2.4 | 12 | 9.6 |
| AN030 | 269718 | 641625 | 617 | 1001 | 8.56 | 29 | 2 | 14 | 12 |
| AN031 | 268849 | 640889 | 480 | 802 | 9.3 | 29 | 2.2 | 11 | 8.8 |
| AN032 | 269100 | 640910 | 550 | 1102 | 8.91 | 28.7 | 2.1 | 15 | 12.9 |
| AN033 | 269289 | 640991 | 536 | 1030 | 9.2 | 28.6 | 2.2 | 9 | 6.8 |
| AN034 | 269130 | 640788 | 546 | 921 | 8.89 | 28.3 | 2.4 | 14 | 11.6 |
| AN035 | 269313 | 640840 | 445 | 873 | 864 | 29 | 2 | 13 | 11 |
| AN036 | 269021 | 640751 | 555 | 913 | 9.53 | 28.8 | 2.2 | 17 | 14.8 |
| AN037 | 268820 | 640682 | 533 | 994 | 8.71 | 30 | 2 | 22 | 20 |
| AN038 | 268667 | 640823 | 436 | 820 | 8.71 | 29 | 1.3 | 15 | 13.7 |

Appendix 2: Laboratory Analyses

| Samples | UTM | | Cl (Mg/l) | Ca(Mg/l) | Mg(Mg/l) | Na(Mg/l) | K(Mg/l) | SO4 Mg/l |
|---|---|---|---|---|---|---|---|---|
| WH001 | 261672 | 639814 | 4.5106 | 7.894 | 13.3 | 36.9 | 15.41 | 52 |
| WH002 | 261660 | 639878 | 6.7659 | 8.577 | 19.57 | 68.37 | 10.31 | 74 |
| WH003 | 261628 | 640000 | 18.0424 | 7.862 | 649.3 | 198 | 12.47 | 66 |
| WH004 | 261787 | 640077 | 405.954 | 13.57 | 198.4 | 261 | 66.83 | 130 |
| WH005 | 261885 | 639908 | 5.6383 | 10.71 | 33.82 | 64.56 | 11.85 | 96 |
| WH006 | 261969 | 640113 | 24.8083 | 19.8 | 244.1 | 214.4 | 13.61 | 80 |
| WH007 | 262238 | 639988 | 5.6383 | 11.06 | 19.83 | 54.81 | 11.24 | 78 |
| WH008 | 262327 | 640143 | 47.3613 | 35.88 | 35.55 | 400.2 | 51.08 | 74 |
| WH009 | 262560 | 639928 | 29.3189 | 10.84 | 222.3 | 214.3 | 12.33 | 42 |
| WH010 | 262212 | 639851 | 9.0212 | 21.11 | 36.5 | 47.09 | 13.45 | 110 |
| WH011 | 261937 | 639571 | 6.7659 | 23.3 | 12.84 | 33.42 | 2.499 | 58 |
| WH012 | 261050 | 639591 | 7.8936 | 10.48 | 47.99 | 54.89 | 66.76 | 86 |

Appendix 2: Laboratory Analyses (cont'd)

| Samples | UTM | | Cl (Mg/l) | Ca(Mg/l) | Mg(Mg/l) | Na(Mg/l) | K(Mg/l) | SO4 Mg/l |
|---|---|---|---|---|---|---|---|---|
| AN001 | 267691 | 641175 | 6.7659 | 12.11 | 23.41 | 54.41 | 50.88 | 110 |
| AN002 | 267778 | 641286 | 39.1701 | 9.564 | 248.2 | 144.5 | 67.23 | 64 |
| AN003 | 267928 | 641333 | 10.1489 | 10.04 | 321.2 | 56.4 | 11.85 | 52 |
| AN004 | 268023 | 641260 | 5.6383 | 13.57 | 22.06 | 72.63 | 10.98 | 100 |
| AN005 | 268228 | 641254 | 6.7659 | 11.71 | 23.53 | 55.27 | 51.48 | 86 |
| AN006 | 268254 | 641481 | 5.6383 | 10.18 | 26.7 | 54.45 | 10.64 | 82 |
| AN007 | 268455 | 641549 | 5.6383 | 10.88 | 22.19 | 67.91 | 11.89 | 78 |
| AN008 | 268689 | 641431 | 6.7659 | 11.85 | 25.61 | 59.04 | 132.3 | 100 |
| AN009 | 268877 | 641558 | 5.6383 | 10.69 | 15 | 30.37 | 15.87 | 102 |
| AN010 | 268931 | 641613 | 5.6383 | 13.84 | 18.49 | 50.87 | 25.53 | 76 |
| AN011 | 269005 | 641763 | 7.8936 | 10.23 | 57.54 | 68.62 | 11.63 | 76 |
| AN012 | 269127 | 641638 | 5.6383 | 10.17 | 18.97 | 58.07 | 11.97 | 100 |
| AN013 | 269306 | 641755 | 7.8936 | 13.37 | 13.73 | 61.21 | 13.09 | 124 |
| AN014 | 269481 | 641703 | 6.7659 | 24.04 | 20.81 | 44.8 | 13.52 | 84 |
| AN015 | 269644 | 641801 | 5.6383 | 15.41 | 27.15 | 47.58 | 50.73 | 138 |
| AN016 | 269755 | 641940 | 7.8936 | 16.89 | 24.41 | 73.57 | 9.573 | 146 |
| AN017 | 269834 | 642023 | 5.6383 | 6.926 | 26.59 | 38.61 | 9.705 | 44 |
| AN018 | 269829 | 642141 | 6.7659 | 14.14 | 13.69 | 46.03 | 6.741 | 60 |
| AN019 | 270010 | 642081 | 5.6383 | 12.43 | 23.03 | 61.24 | 11.58 | 98 |
| AN020 | 270145 | 642166 | 6.7659 | 10.78 | 16.38 | 41.19 | 12.6 | 122 |
| AN021 | 270281 | 642238 | 5.6383 | 15.4 | 9.209 | 33.63 | 9.375 | 76 |
| AN022 | 270358 | 642421 | 10.1489 | 14.45 | 16.4 | 105 | 11.43 | 134 |
| AN023 | 270530 | 642447 | 10.1489 | 17.86 | 16.24 | 69.97 | 9.685 | 120 |
| AN024 | 270645 | 642122 | 3.383 | 11.41 | 7.168 | 29.41 | 9.897 | 68 |
| AN025 | 270530 | 642060 | 4.5106 | 13.42 | 8.346 | 25.43 | 10.55 | 66 |
| AN026 | 270370 | 641938 | 3.383 | 10.53 | 7.901 | 32.73 | 9.73 | 36 |
| AN027 | 270171 | 641855 | 4.5106 | 12.08 | 7.688 | 29.82 | 10.95 | 46 |
| AN028 | 270007 | 641792 | 10.1489 | 23.24 | 25.51 | 81.14 | 50.82 | 146 |
| AN029 | 26840 | 641726 | 9.0212 | 28.31 | 42.36 | 71.78 | 50.95 | 84 |
| AN030 | 269718 | 641625 | 5.6383 | 27.56 | 14.95 | 52.86 | 12.64 | 58 |
| AN031 | 268849 | 640889 | 5.6383 | 8.925 | 15.59 | 49.5 | 12.05 | 78 |
| AN032 | 269100 | 640910 | 7.8936 | 20.43 | 18.7 | 80.1 | 11.3 | 88 |
| AN033 | 269289 | 640991 | 6.7659 | 17.3 | 16.08 | 52.93 | 15.38 | 76 |
| AN034 | 269130 | 640788 | 6.7659 | 19.52 | 15.76 | 49.99 | 10.05 | 74 |
| AN035 | 269313 | 640840 | 5.6383 | 32.58 | 16.99 | 47.61 | 10.51 | 62 |
| AN036 | 269021 | 640751 | 4.5106 | 33.71 | 17.46 | 46.7 | 12.89 | 74 |
| AN037 | 268820 | 640682 | 7.8936 | 14.4 | 16.26 | 54.91 | 11.08 | 76 |
| AN038 | 268667 | 640823 | 4.5106 | 22.37 | 18.36 | 46.21 | 39.02 | 68 |